Hybrid Time and Time-Frequency Blind Source Separation Towards Ambient System Identification of Structures

by

Budhaditya Hazra

A thesis
presented to the University of Waterloo
in fulfillment of the
thesis requirement for the degree of
Doctor of Philosophy
in
Civil Engineering

Waterloo, Ontario, Canada, 2010

I hereby declare that I am the sole author of this thesis. This is a true copy of the thesis, including any required final revisions, as accepted by my examiners.

I understand that my thesis may be made electronically available to the public.

Abstract

Blind source separation methods such as independent component analysis (ICA) and second order blind identification (SOBI) have shown considerable potential in the area of ambient vibration system identification. The objective of these methods is to separate the modal responses, or sources, from the measured output responses, without the knowledge of excitation. Several frequency domain and time domain methods have been proposed and successfully implemented in the literature. Whereas frequency-domain methods pose several challenges typical of dealing with signals in the frequency-domain, popular time-domain methods such as NExT/ERA and SSI pose limitations in dealing with noise, low sensor density, modes having low energy content, or in dealing with systems having closely-spaced modes, such as those found in structures with passive energy dissipation devices, for example, tuned mass dampers.Motivated by these challenges, the current research focuses on developing methods to address the problem of separability of sources with low energy content, closely-spaced modes, and under-determined blind identification, that is, when the number of response measurements is less than the number of sources. These methods, requiring the time and frequency diversities of the measured outputs, are referred to as hybrid time and time-frequency source separation methods. The hybrid methods are classified into two categories. In the first one, the basic principles of modified SOBI are extended using the stationary wavelet transform (SWT) in order to improve the separability of sources, thereby improving the quality of identification. In the second category, empirical mode decomposition is employed to extract the intrinsic mode functions from measurements, followed by an estimation of the mode shape matrix using iterative and/or non iterative procedures within the framework of modified-SOBI. Both experimental and large-scale structural simulation results are included to demonstrate the applicability of these hybrid approaches to structural system identification problems.

Acknowledgements

First and foremost, I would like to express my sincere thanks and gratitude to my principal supervisor, Dr. Sriram Narasimhan, for his inspirational guidance and support. He has been a wonderful mentor and has provided me with the right attitude and impetus needed to complete this work on time. I would also like to thank my co-supervisor, Dr. Mahesh Pandey, for many useful discussions and encouragement during various stages of this work. My sincere thanks to Dr. Giovanni Cascante, Dr. Marianna Polak, Dr. Serhiy Yarusevych, and Dr. Carlos Ventura for serving on my thesis committee.

Special thanks to my colleagues Ayan Sadhu, Dr. Chandrika Prakash and Dr. Arindam Dey (University of Molise, Termoli, Italy) for their insightful comments and valuable suggestions from time-to-time. I would like to thank Aaron Roffel and Paul Paquet for acquiring field data, and making it available in a format that could be used in this research. The help and assistance provided by Arun Veeramany in the extraction of field data of the UCLA factor building, in a usable format, is thankfully acknowledged.

Special thanks are reserved for my parents Mrs. Kakali Hazra and Dr. Biren Hazra. My father's valuable advice on my early thesis drafts, and guidance in shaping up my academic career is gratefully acknowledged. I would also like to thank my father-in-law Mr. Sailen Banerjee and my mother-in-law Mrs. Namita Banerjee for their emotional support and encouragement.

Finally, I would like to thank my wife, Mitali, for her wonderful companionship. Without her unwavering emotional support, this work would have never crystallized. I would like to dedicate this work to her.

This study was funded in part by the Natural Sciences and Engineering Research Council of Canada (NSERC) and the UNENE IRC programs, which is gratefully acknowledged.

Dedication

Dedicated to my wife, Mitali, whose unstinted love and unflinching support made this work possible.

Contents

List of Tables

List of Figures

Chapter 1

Introduction

In the era of high performance flexible structures like Taipei 101, Burj Dubai, CN tower, and Guangzhou tower, estimation of dynamic properties of flexible structures, i.e., natural frequencies and damping, is of paramount importance. Its significance stems from the fact that such structures are liable to undergo changes over time, sustain damage, and/or get augmented by supplemental energy dissipation devices aimed at controlling their motions against wind or other disturbances. Extracting system information often needs to be accomplished without the knowledge of inputs, and is referred to as ambient system identification. The presence of measurement noise or supplemental energy dissipation devices like tuned mass dampers renders ambient system identification difficult. These difficulties are further compounded in situations where practically achievable sensor densities are governed by economics, and installation efforts. The aim of this research is to develop sophisticated system identification techniques that address these practical issues in an expedient manner.

Exclusive of the knowledge of inputs, extraction of system information from output measurements is known as ambient system identification. It differs from the traditional system identification in the sense that the latter requires the knowledge of both the input

and the output for complete identification. The system responses are assumed to be influenced by ambient conditions like wind, environmental conditions, traffic load etc. The importance of ambient system identification is evident because in many practical situations the excitation input is not easily observable. Civil engineering systems, typically, are very large and complicated, and the measurement of the input forces can be an arduous task (e. g., wind load). Outputs on the other hand can be measured relatively easily. Furthermore, for many structures, using forced vibration to induce response for system identification may be forbidden (due to concern of the owner(s) or structural damage likely to result). On the other hand, responses due to ambient vibration may be sufficient to perform system identification.

In view of the absence of unique solutions, extracting the parameters of an unknown system with no knowledge of inputs is a difficult mathematical problem. The mathematical statement of ambient system identification can be expressed as :

$$\mathbf{x} = \mathbf{A}\mathbf{s} \tag{1.1}$$

In the Eq. 1.1, $\mathbf{x}$ represents the output, or the system response, which is the only known quantity. $\mathbf{A}$ contains the system properties, and $\mathbf{s}$ contains the inputs or the sources, both of which are unknown. Such an equation yields infinite combinations of $\mathbf{A}$ and $\mathbf{s}$ that could result in the observed $\mathbf{x}$. Thus, unique determination of the system parameters, i.e., matrix $\mathbf{A}$ based on Eq. 1.1 is a formidable challenge.

Traditional ambient system identification methods are a wide class of methods operating in either the time or frequency domains. Time domain methods [45, 47, 46, 83] involve collection of impulse responses of finite chosen length and arranging them in matrix form, and then performing singular value decomposition to extract the system matrices. Frequency domain decomposition methods involve singular value decomposition (SVD) of the spectral density matrices evaluated at the PSD peaks. This reduces the matrix into a set of

auto-spectral density functions; each corresponding to a single degree of freedom system. A key feature of these methods is the pre-selection of model order that depicts the size of the state matrices or the number of identified modes. Application of these methods for accurate identification of modal parameters becomes difficult in situations when the input excitation is non-stationary, the structure is highly damped, and the measurements are noisy. Identification of modal parameters also becomes difficult in presence of closely spaced modes with high levels of damping in structures having supplemental devices such as those found with supplemental devices like tuned mass dampers.

Recent research in statistical signal processing has resulted in methods utilizing the concepts of information theory known as *blind source separation* (BSS). Unlike traditional methods, these methods do not require pre-selection of model order and have shown considerable potential in the area of structural system identification. BSS methods seek to determine the un-mixing matrix (i.e. the inverse of $\mathbf{A}$ matrix in Eq. 1.1) using the statistical information contained in the outputs. Two main tools to perform BSS have been studied in the literature: independent component analysis (ICA) [44], and second order blind identification (SOBI) [10]. Of these methods, those employing eigenvalue decomposition of the second order statistics of the output, known as second order blind identification, have shown significant promise in ambient system identification.

Ambient system identification with the aid of blind source separation techniques poses two major challenges. The first one is encountered if the energy content of some of the high-frequency modes is not large enough to facilitate their successful extraction. Such conditions are likely to arise in large real life structures, in which the higher modes of vibration may not have sufficient energy content. This issue is addressed in the proposed research by extending the basic principles of SOBI for static mixtures using the stationary wavelet transform (SWT) in order to enhance the separability of sources with low energy, thereby improving the quality of identification. The second issue is encountered when the

number of sensors is less than the number of identifiable modes. Physically, such situations arise in flexible structures that are instrumented with a relatively small number of sensors due to cost or other reasons. This problem is approached by combining the BSS techniques with a time-frequency decomposition known as empirical mode decomposition(EMD) in a hybrid manner. Finally, the hybrid approach is extended to the case of identification of structures with relatively large amount of damping, such as the case of structures equipped with tuned mass dampers.

1.1 Aims and Objectives

Having introduced the basic ideas of ambient system identification, blind source separation, and hybrid time and time-frequency domain methods, the broad-based objectives of the current research are summarized as follows:

1. Extend the concepts of SOBI to develop a new time-domain blind source separation method, geared towards the system identification of structures under ambient excitations.

2. Extend the above time domain method, to improve the separability of sources with low energy content, using a time-frequency approach.

3. Extend the time domain method for blind identification of full-scale structures for the under-determined case, that is, when the number of response measurements is less than the number of desired modes. The key idea is to develop a hybrid approach, where the output is first decomposed into mono harmonic components by utilizing empirical mode decomposition, and use these components as initial estimates of sources within the framework of BSS.

4. Application of a hybrid approach to identify structures with large amount of damping in the primary modes. Specifically, structures equipped with tuned mass dampers will be studied within the context of re-tuning in-service TMDs.

1.2 Organization of the thesis

This thesis contains 7 chapters. The second chapter presents a background on the methods of system identification, specifically related to modal identification. First, the traditional modal identification methods are reviewed, followed by the more recent ones which belong to the family of blind source separation (BSS) methods. During the course of relevant literature review, the basic demerits of the traditional modal identification methods are highlighted to illustrate the objectives of the proposed study.

The third chapter presents the theoretical development of a new method called modified cross-correlation method (MCC). This method extends the concept of SOBI to identify full-scale structures subjected to ambient excitations. Issues related to estimating damping and accounting for the measurement noise are addressed in the MCC method. The problem statement is presented first wherein the general problem of structural system identification is cast in a BSS framework. The formulation of SOBI and MCC methods is presented next, followed by the results of the numerical simulation of a simple three degree-of-freedom mass, spring, and dashpot system. Experimental results for a two-storey building model are presented next. Finally, the results of identification using the MCC method are presented for the case of a full-scale tower structure excited by both wind and earthquake forces.

The theoretical development of a new hybrid time and time-frequency source separation method called wavelet-based modified cross correlation method (WMCC) is introduced in the fourth chapter. WMCC extends the concept of MCC to improve the separability of sources with low energy content to identify full-scale structures subjected to ambient

excitations. The formulation of WMCC method is presented next, followed by the results of numerical simulation of a simple three degree-of-freedom mass, spring, and dashpot system. Finally, the results of identification are presented for the case of a real life structure, the *UCLA Factor Building*, using ambient vibration data, and also for recorded responses from the Parkfield earthquake.

A newly developed hybrid time and time-frequency domain blind identification method, to handle the under-determined blind identification of building structures, is introduced in the fifth chapter. The under-determined case is encountered when the number of sensors is less than the number of desired modes. This method is applied to a full-scale structure example to demonstrate its effectiveness. Key results and discussions are presented next.

The sixth chapter considers an application of the hybrid blind identification methods to retune an in-service TMD. Tuned mass dampers (TMD) are the oldest and most commonly used passive vibration control devices in flexible structures that work primarily by dissipating the vibrational energy through heat. De-tuning, resulting from several sources such as the alteration of the structural properties of the primary structure, deterioration of the TMD, in-correct design forecasts, etc., may lead to a significant deterioration in their performance. In order to re-tune the TMD, system identification of the primary structure while the TMD is in-service is often required. Retuning a TMD poses two major difficulties. The first major difficulty arises in the identification of the structure with TMD and due to relatively large amount of damping and the second one being the identification of the primary structure from the results of the identified structure with TMD. In this chapter, a brief idea of re-tuning is first introduced, followed by the details of the newly proposed identification method, MCC-EMD. The re-tuning algorithms are presented next, while the details of implementation, key results, and discussion are presented thereafter. Experimental results for a two-story bench-scale model with a TMD are presented, followed by important observations.

The main conclusions of the thesis are summarized in the seventh chapter along with the key accomplishments of the current research. Finally, recommendations for future research that could be possible extensions to this work are presented.

Chapter 2

Background and Literature Review

In this chapter a brief background of the literature in the area of structural modal identification is reviewed. First, the traditional methods are presented including the popular output-only modal identification methods, followed by the more recent ones belonging to the family of blind source separation (BSS) methods. Relevant literatures are reviewed and discussed, and the basic demerits of the traditional modal identification methods are highlighted to illustrate the need for the proposed study.

2.1 A Literature Review of the Traditional Methods of System Identification

The traditional methods of system identification are a wide class of methods, which were developed in early $1980's$ to address the problem of modal identification. These methods were mostly used for the identification of structural and mechanical systems with low damping. Initially, these methods were directed towards identification in noise free environments, later on, noise was also incorporated. There is a wealth of literature that exists

in this area [65]. Many researchers popularly referred system identification for structural and mechanical systems in 1970s and 1980s by names like modal analysis, modal identification, experimental modal analysis, operational modal analysis etc. A few extensively used methods are reviewed next.

Complex exponential (CE) algorithm based on Prony's method [65] is the first important single-input single-output (SISO) parametric modal identification method. Prony's method extracts periodic information from a uniformly sampled signal by building a series of damped complex exponentials, or sinusoids. This allows the estimation of frequency, amplitude, phase, and damping components of a signal. Extending the concept of Prony's method, ibrahim time domain (ITD) method [45] was the first modal identification method formulated for SISO systems. This method solved for eigenvalues and eigenvectors in one-step. The first multiple-input multiple-output modal identification method [75], polyreference complex exponential, was developed as an extension of the least squares complex exponential algorithm. The eigen system realization algorithm (ERA) [47] was developed based on the general state-space description for linear dynamic systems. A well-known unified matrix polynomial approach was proposed [3] covering a large number of major algorithms developed in the first two decades of modal identification in a common framework based on multiple-dimension auto-regression exogenous (ARX) model. Two important methods, natural excitation (NExT) [46] and stochastic sub-space iteration (SSI) [83, 84] which are the most popular methods in output only identification, are reviewed in detail in the following sections.

In the frequency domain, classical methods such as power spectral density peak picking were developed. However, PSD peak picking technique was found to be inaccurate, especially in mode shape and damping estimation. A new frequency domain modal identification operational technique, called frequency domain decomposition (FDD), was developed to resolve the difficulties encountered in peak picking, while retaining the advantages of

the classical pick picking method [90]. The classical FDD was extended [13] to identify symmetrical structures with closely-spaced modes. This method was based on singular value decomposition of spectral density matrix at the PSD peaks to yield auto-spectral density functions, each of which represents a single degree of freedom system. A method to estimate damping using the extended frequency domain decomposition was proposed subsequently [12]. There are a number of other frequency-domain methods in the literature, and a complete review of these methods is available in standard texts for this purpose [65].

Recent trends in system identification has witnessed a shift towards time-domain identification techniques. Time domain methods do not suffer from resolution issues as the frequency domain methods do. In this context, three most popular methods in structural identification literature, ERA, SSI and ITD, are reviewed here followed by a brief review of the FDD.

2.1.1 Eigen-System Realization Algorithm

The eigensystem realization algorithm [ERA] is a time domain technique [47] for modal parameter identification and model reduction for dynamical systems from input-output data. The algorithm is a basic extension of the system realization theory. ERA estimates the system information contained in the mathematical model of the dynamic system expressed in discrete state space form (see APPENDIX A). The starting point of the ERA is the collection of impulse response functions. Impulse response is defined as the response of a structure subjected to unit impulse input. The response of the structure in discrete time domain to a unit pulse is called pulse response, or markov parameters [48]. The markov parameters contain system information, and is a function system matrices (APPENDIX B). The ERA uses the discretized pulse response h to form a matrix known as the Hankel matrix:

$$\mathbf{H}(k-1) = \begin{bmatrix} h(k) & h(k+1) & : & h(k+c) \\ h(k+1) & h(k+2) & : & h(k+c+1) \\ .. & .. & : & .. \\ h(k+r) & h(k+r+1) & : & h(k+c+r) \end{bmatrix} \tag{2.1}$$

Substituting $k = 1$ in Eq. 2.1 and replacing the markov parameters (see APPENDIX A) yields,

$$\mathbf{H}(0) = \begin{bmatrix} \mathbf{C}\bar{\mathbf{B}} & \mathbf{C}\bar{\mathbf{A}}\bar{\mathbf{B}} & .. & \mathbf{C}\bar{\mathbf{A}}^{c-1}\bar{\mathbf{B}} \\ \mathbf{C}\bar{\mathbf{A}}\bar{\mathbf{B}} & \mathbf{C}\bar{\mathbf{A}}^{2}\bar{\mathbf{B}} & .. & \mathbf{C}\bar{\mathbf{A}}^{c}\bar{\mathbf{B}} \\ : & : & : & : \\ \mathbf{C}\bar{\mathbf{A}}^{r-1}\bar{\mathbf{B}} & \mathbf{C}\bar{\mathbf{A}}^{r}\bar{\mathbf{B}} & .. & \mathbf{C}\bar{\mathbf{A}}^{r+c-2}\bar{\mathbf{B}} \end{bmatrix} = \mathbf{PQ} \tag{2.2}$$

where the matrices $\mathbf{P}$ and $\mathbf{Q}$ are given by :

$$\begin{aligned} \mathbf{P} &= \begin{bmatrix} \mathbf{C} & \mathbf{C}\bar{\mathbf{A}} & \mathbf{C}\bar{\mathbf{A}}^{2} & ... & ... & \mathbf{C}\bar{\mathbf{A}}^{r-1} \end{bmatrix}^{T} \\ \mathbf{Q} &= \begin{bmatrix} \bar{\mathbf{B}} & \bar{\mathbf{A}}\bar{\mathbf{B}} & \bar{\mathbf{A}}^{2}\bar{\mathbf{B}} & ... & ... & \mathbf{A}^{c-1}\bar{\mathbf{B}} \end{bmatrix} \end{aligned} \tag{2.3}$$

Performing singular value decomposition of $\mathbf{H}(0)$ yields,

$$\mathbf{H}(0) = \mathbf{R}\mathbf{\Psi}\mathbf{S}^{T} \tag{2.4}$$

Where $\mathbf{\Psi}$ is a diagonal matrix with the singular values in the diagonal, and the matrices $\mathbf{R}$ and $\mathbf{S}$ are square and unitary. The matrices $\mathbf{\Psi}_N, \mathbf{R}_N$ and $\mathbf{S}_N$ are obtained eliminating the rows and columns corresponding to small singular values produced by computational modes. Since $\mathbf{\Psi}$ is a diagonal matrix, Eq. 2.4 can be expressed as:

$$\mathbf{H}(0) = \left(\mathbf{R}_N \mathbf{\Psi}_N^{\frac{1}{2}}\right)\left(\mathbf{\Psi}_N^{\frac{1}{2}} \mathbf{S}_N^{T}\right) \tag{2.5}$$

Using the discrete-time state space form (see APPENDIX A) of the equation and the Markov parameters, Eq. 2.1 becomes:

$$\mathbf{H}\left(k-1\right)=\mathbf{P}\bar{\mathbf{A}}^{k-1}\mathbf{Q}=\left[\begin{array}{c}\mathbf{C}\\ \mathbf{C}\bar{\mathbf{A}}\\ :\\ \mathbf{C}\bar{\mathbf{A}}^{P-1}\end{array}\right]\bar{\mathbf{A}}^{k-1}\left[\begin{array}{cccc}\bar{\mathbf{A}}\mathbf{x}(0) & \bar{\mathbf{A}}^{2}\mathbf{x}(0) & ..... & \bar{\mathbf{A}}^{r}\mathbf{x}(0)\end{array}\right] \tag{2.6}$$

Where $\bar{\mathbf{A}}$ and $\mathbf{C}$ are, respectively, the system and output matrices of a discrete state space realization of the linear system, and $\mathbf{x}\left(0\right)$ is the vector of initial conditions of the structure. From Eq. 2.5:

$$\begin{aligned}\mathbf{P}&=\mathbf{R}_{N}\boldsymbol{\Psi}_{N}^{1/2}\\ \mathbf{Q}&=\boldsymbol{\Psi}_{N}^{1/2}\,\mathbf{S}_{N}^{T}\end{aligned} \tag{2.7}$$

For $k=2$

$$\mathbf{H}\left(1\right)=\mathbf{P}\bar{\mathbf{A}}\mathbf{Q} \tag{2.8}$$

Combining Eqs. 2.6, 2.7, and 2.8, the system and the output matrices can be found :

$$\begin{aligned}\bar{\mathbf{A}}&=\boldsymbol{\Psi}_{\mathbf{N}}^{-1/2}\,\mathbf{R}_{\mathbf{N}}^{\mathbf{T}}\,\mathbf{H}\left(\mathbf{1}\right)\,\mathbf{S}_{\mathbf{N}}\boldsymbol{\Psi}_{\mathbf{N}}^{-1/2}\\ \mathbf{C}&=\left[\begin{array}{cc}\mathbf{I} & \mathbf{0}\end{array}\right]\mathbf{R}_{N}\boldsymbol{\Psi}_{N}^{-1/2}\end{aligned} \tag{2.9}$$

Where $\mathbf{I}$ is an identity matrix and $\mathbf{0}$ is a zero matrix, both of proper dimensions for the necessary matrix products. The natural frequencies and the mode shapes are obtained from the $\bar{\mathbf{A}}$ and $\mathbf{C}$ matrices. The natural frequencies $\boldsymbol{\Omega}$ and $\boldsymbol{\zeta}$ are obtained obtained from the eigenvalues $\boldsymbol{\Lambda}$ of the state matrix $\bar{\mathbf{A}}$, according to [48]:

$$\begin{aligned} \boldsymbol{\Omega} &= \frac{|\boldsymbol{\Lambda}'|}{2\pi} \\ \boldsymbol{\zeta} &= -\frac{100 \times real(\boldsymbol{\Lambda}')}{|\boldsymbol{\Lambda}'|} \end{aligned} \tag{2.10}$$

where $\boldsymbol{\Lambda}' = \frac{\log(\boldsymbol{\Lambda})}{t_s}$ and $\boldsymbol{\Lambda}'$ is the eigenvalue of the continuous time state space matrix $\mathbf{A}$ and t_s the sampling rate.

2.1.2 Natural Excitation Technique (NExT)

ERA is a well-established method for lightly damped systems, and is extensively used for advanced control and identification of civil structures. The method, however, is limited by the need to obtain free or impulse responses (experimentally, or otherwise) from the structures, which is not always feasible in civil engineering applications due to size, safety concerns, and the constant presence of ambient vibration. To overcome this limitation, a new method [46] demonstrated that, when forced vibration data is available from tests conducted with certain types of excitation, the cross-correlation functions between the response measurements and a single reference measurement satisfies the homogeneous differential equation of motion of the linear system and, therefore, can be treated as free responses (h). NExT has been used extensively for numerical and experimental analysis showing that, even in the case of band-limited ambient vibrations with questionable stationarity, free responses can be obtained reliably with sufficient frequency content to detect the dominant modes of vibration.

The equations of motion for an n degree of freedom, time invariant, linear system described by :

$$\mathbf{M}\ddot{\mathbf{x}}(t) + \mathbf{C}\dot{\mathbf{x}}(t) + \mathbf{K}\mathbf{x}(t) = \mathbf{F}(t) \tag{2.11}$$

where $\mathbf{M}$, $\mathbf{C}$, and $\mathbf{K}$ matrices are $n \times n$ matrices defining the mass, damping, and stiffness of the structure, $\mathbf{x}(t)$ and $\mathbf{F}(t)$ are $n \times 1$ stochastic vectors describing the displacement

and excitation, respectively. Post multiplying Eq. 2.11 by the displacement of any of the degrees of freedom measured $X_i(s)$ (referred to as the reference signal), and taking the expected value of each side yields:

$$\mathbf{M}R_{\ddot{\mathbf{x}}\mathbf{x}_i}(t,s) + \mathbf{C}R_{\dot{\mathbf{x}}\mathbf{x}_i}(t,s) + \mathbf{K}R_{\mathbf{x}\mathbf{x}_i}(t,s) = R_{\mathbf{F}\mathbf{x}_i}(t,s) \tag{2.12}$$

Where $R(.)$ denotes the vector of correlation functions and s denotes a different time instant. For weakly stationary processes, it can be shown that [11]:

$$\dot{R}_{\mathbf{x}\mathbf{x}_i}(\tau) = R_{\dot{\mathbf{x}}\mathbf{x}_i}(\tau) = -R_{\mathbf{x}\dot{\mathbf{x}}_i}(\tau) \tag{2.13}$$

where $(\tau) = t - s$ .Assuming that the displacement, velocity and acceleration processes are weakly stationary and uncorrelated with future disturbances (*i.e.*, $R_{\mathbf{FX}}(t,s) = 0$),and taking the fourth derivative of Eq. 2.11 we obtain [11]:

$$\mathbf{M}\ddot{R}_{\ddot{\mathbf{x}}\ddot{\mathbf{x}}_i}(\tau) + \mathbf{C}\dot{R}_{\ddot{\mathbf{x}}\ddot{\mathbf{x}}_i}(\tau) + \mathbf{K}R_{\ddot{\mathbf{x}}\ddot{\mathbf{x}}_i}(\tau) = 0 \tag{2.14}$$

Eq. 2.14 shows that the cross-correlation function of the responses of the structure with a reference signal satisfies the homogeneous equation of motion and can be treated as free responses. Once the free responses are obtained, the identification proceeds using ERA exactly in the same manner described in the previous section.

2.1.3 Stochastic Subspace Iteration Technique

Stochastic Subspace Identification method, developed in the early to mid 1990′s [83, 84], provided a powerful means of output only system Identification. The two general assumptions made in output-only modal analysis are that the underlying physical system behaves linearly, and is time-invariant. One of the typical parametric model structures to use in

output-only modal analysis of linear and time-invariant physical systems is the stochastic state space system.

$$\begin{aligned} \mathbf{x}_{t+1} &= \mathbf{A}\mathbf{x}_t + \mathbf{w}_t \\ \mathbf{y}_t &= \mathbf{C}\mathbf{x}_t + \mathbf{v}_t \end{aligned} \tag{2.15}$$

The first part of this model structure is the state equation depicting the model of the dynamic behavior of the physical system. The second equation is the observation or output equation, as this equation controls the part of the dynamic system that can be observed in the output. The measured system response $\mathbf{y}_t$ is generated by two stochastic processes $\mathbf{w}_t$ and $\mathbf{v}_t$ .These are called the process noise and the measurement noise, respectively. The process noise is the input that drives the system dynamics whereas the measurement noise is the direct disturbance added to the system response.

The dynamics of the physical system is modeled by the $n \times n$ state matrix $\mathbf{A}$. Given an $n \times 1$ input vector $\mathbf{w}_t$, this matrix transforms the state of the system, described by the $n \times 1$ state vector $\mathbf{x}_t$, to a new state $\mathbf{x}_{t+1}$. The dimension n of the state vector $\mathbf{x}_t$ is called the state space dimension. The observable part of the system dynamics is extracted from the state vector by forward multiplication of the $p \times n$ observation matrix $\mathbf{C}$. The $p \times 1$ system response vector $\mathbf{y}_t$ is a mixture of the observable part of the state and some noise modeled by the measurement noise $\mathbf{v}_t$.

Properties of stochastic state space systems

The state space model according to Eq. 2.15 is only applicable for linear systems that are not time-varying. However, this is not the only restriction. The only way to obtain an optimal estimate of a state space model based on measured system response is to ensure that the system response is a realization of a Gaussian distributed stochastic process with

zero mean. In other words, in the applied stochastic framework, the system response is modeled by a stochastic process $\mathbf{y}_t$ defined as:

$$E\left[\mathbf{y}_t\right] = 0$$
$$E\left[\mathbf{y}_{t+i}\,\mathbf{y}_i^T\right] = \mathbf{\Lambda}_i \tag{2.16}$$

Since the system response of the linear state space model is a Gaussian stochastic process it implies that $\mathbf{x}_t$,$\mathbf{w}_t$ and $\mathbf{v}_t$ all are Gaussian stochastic processes as well. $\mathbf{w}_t$ and $\mathbf{v}_t$ are assumed to be correlated zero-mean Gaussian white noise processes, defined by their covariance matrices as :

$$E = \left[\left[\begin{array}{c} \mathbf{w}_t \\ \mathbf{v}_t \end{array}\right] \left[\begin{array}{cc} \mathbf{w}_{i+k}^T & \mathbf{v}_{i+k}^T \end{array}\right]\right] = \left[\begin{array}{cc} \mathbf{Q} & \mathbf{S} \\ \mathbf{S^T} & \mathbf{R} \end{array}\right] \delta\left(k\right) \tag{2.17}$$

The Gaussian stochastic process describing the state $\mathbf{x}_t$ is also zero-mean and is completely described by its covariance function.

$$E\left[\mathbf{x_{t+i}}\mathbf{x_i^T}\right] = \sum_i \tag{2.18}$$

The cross covariance matrix between input and output is defined by the relation:

$$E\left[\mathbf{x_{t+i}}\mathbf{y_i^T}\right] = \mathbf{G} \tag{2.19}$$

At this stage, it is useful to define an extended observability matrix $\mathbf{\Gamma}_i$, which is extensively used in the linear prediction, and expressed as:

$$\mathbf{\Gamma}_i = \begin{bmatrix} \mathbf{C} \\ \mathbf{CA} \\ - \\ - \\ \mathbf{CA}^{i-2} \\ \mathbf{CA}^{i-1} \end{bmatrix} \tag{2.20}$$

In a similar manner, a reverse extended controllability matrix $\mathbf{\Delta}_i$ is defined as:

$$\mathbf{\Delta}_i = \begin{bmatrix} \mathbf{A}^{i-1}\mathbf{G} & \mathbf{A}^{i-2}\mathbf{G} & ..... & \mathbf{AG} & \mathbf{G} \end{bmatrix} \tag{2.21}$$

Optimal prediction

One of the most important parts of estimation is the ability to predict the measurements optimally. An optimal predictor is defined as a predictor that results in a minimum mean square error between the predicted and measured system response. If the system response can be predicted optimally, it implies that a model can be estimated in an optimal sense.

The state vector $\mathbf{x}_t$ completely describes the system dynamics at time t. It is assumed that the measurements $\mathbf{y}_t$ are available from some initial time $k = 0$ to $k = t-1$. Vectorially, it can be written as:

$$\mathbf{y}_{\mathbf{0}}^{t-1} = \begin{bmatrix} y_0 \\ y_1 \\ - \\ - \\ y_{t-2} \\ y_{t-1} \end{bmatrix} \tag{2.22}$$

In the Gaussian case, the optimal predictor of $\mathbf{x}_t$ is then given by the conditional mean according as:

$$\hat{\mathbf{x}}_t = E\left\lfloor \mathbf{x}_t \middle| \mathbf{y}_0^{t-1} \right\rfloor \tag{2.23}$$

The difference between $\hat{\mathbf{x}}_t$ and $\mathbf{x}_t$ is called the state prediction error $\boldsymbol{\gamma}_t$ and is defined as

$$\boldsymbol{\gamma}_t = \hat{\mathbf{x}}_t - \mathbf{x}_t \tag{2.24}$$

In order to predict the system response a similar conditional mean can be formulated for $\mathbf{y}_t$.

$$\begin{aligned} \hat{\mathbf{y}}_t &= E\left\lfloor \mathbf{x}_t \middle| \mathbf{y}_{\mathbf{0}}^{t-1} \right\rfloor \\ &= \mathbf{C}\hat{\mathbf{x}}_t \end{aligned} \tag{2.25}$$

The two predictors according to Eq. 2.23 and Eq. 2.25 are related through the so-called *Kalman filter* for linear and time-invariant systems [79].

$$\begin{aligned} \hat{\mathbf{x}}_{t+1} &= \mathbf{A}\hat{\mathbf{x}}_t + \mathbf{K}_t\mathbf{e}_t \\ \mathbf{e}_t &= \mathbf{y}_t - \mathbf{C}\hat{\mathbf{x}}_t \end{aligned} \tag{2.26}$$

The matrix $\mathbf{K}_t$ is called the non-steady state Kalman gain and $\mathbf{e}_t$ is called the innovation which is a zero-mean Gaussian white noise process. Defining the non-steady-state covariance matrix of the predicted state vector $\hat{\mathbf{x}}_t$ as $\mathbf{P}_t$, the Kalman gain $\mathbf{K}_t$ is calculated from

$$\begin{aligned} \mathbf{K}_t &= \left(\mathbf{G} - \mathbf{A}\mathbf{P}_T\mathbf{C}^T\right)\left(\boldsymbol{\Lambda}_0 - \mathbf{C}\mathbf{P}_T\mathbf{C}^T\right)^{-1} \\ \mathbf{P}_{t+1} &= \mathbf{A}\mathbf{P}_t\mathbf{A}^T + \left(\mathbf{G} - \mathbf{A}\mathbf{P}_t\mathbf{C}^T\right)\left(\boldsymbol{\Lambda}_0 - \mathbf{C}\mathbf{P}_t\mathbf{C}^T\right)^{-1}\left(\mathbf{G} - \mathbf{A}\mathbf{P}_t\mathbf{C}^T\right) \end{aligned} \tag{2.27}$$

The last of these equations is called the Ricatti equation. The Kalman filter predicts the state $\hat{\mathbf{x}}_{t+1}$ based on the previous predicated state $\hat{\mathbf{x}}_t$ and the measurement $\mathbf{y}_t$.

The Identification Framework

The fundamental problem to solve in the stochastic subspace identification technique is to extract the predicted state from the measured data. The state space system in Eq. 2.15 is considered and conditional expectation on both sides of the equations is taken to yield:

$$\begin{aligned} E\left\lfloor \mathbf{x}_{t+1} \middle| \mathbf{y}_0^t \right\rfloor &= \mathbf{A}E\left\lfloor \mathbf{x}_t \middle| \mathbf{y}_0^{t-1} \right\rfloor + E\left\lfloor \mathbf{w}_{t+1} \middle| \mathbf{y}_0^{t-1} \right\rfloor \\ E\left\lfloor \mathbf{y}_t \middle| \mathbf{y}_0^{t-1} \right\rfloor &= \mathbf{C}E\left\lfloor \mathbf{x}_t \middle| \mathbf{y}_0^{t-1} \right\rfloor + E\left\lfloor \mathbf{v}_t \middle| \mathbf{y}_0^{t-1} \right\rfloor \end{aligned} \tag{2.28}$$

Assuming that a recursion is started at time step q, and substituting Eq. 2.28 recursively into itself i times, followed by the insertion of Eq. 2.15 in Eq. 2.28, the following set of equations are obtained :

$$\begin{bmatrix} \hat{\mathbf{y}}_q \\ \hat{\mathbf{y}}_{q+1} \\ \vdots \\ \vdots \\ \hat{\mathbf{y}}_{q+i-1} \end{bmatrix} = \begin{bmatrix} \mathbf{C} \\ \mathbf{CA} \\ \vdots \\ \vdots \\ \mathbf{CA}^{i-1} \end{bmatrix} \hat{\mathbf{x}}_q \Leftrightarrow \hat{\mathbf{o}}_q = \mathbf{\Gamma}_i \hat{\mathbf{x}}_q \tag{2.29}$$

Denoting the left hand side of the Eq. 2.29 as $\hat{\mathbf{o}}_q$, it can be inferred from the equation that if $\mathbf{\Gamma}_i$ and $\mathbf{o}_q$ can be estimated for several values of q, then the predicted states can be estimated for several values of q as well.

At this stage let the following two matrices $\mathbf{O}_i$ and $\mathbf{Y}_p$ be defined as under:

$$\mathbf{O}_i = \begin{bmatrix} \hat{y}_i & \hat{y}_{i+1} & .. & .. & \hat{y}_{i+j-1} \\ \hat{y}_{i+1} & \hat{y}_{i+2} & .. & .. & \hat{y}_{i+j} \\ .. & .. & .. & .. & .. \\ .. & .. & .. & .. & .. \\ \hat{y}_{2i-1} & \hat{y}_{2i} & .. & .. & \hat{y}_{2i+j-2} \end{bmatrix} \quad , \quad \mathbf{Y}_p = \begin{bmatrix} y_0 & y_1 & .. & .. & y_{j-1} \\ y_1 & y_2 & .. & .. & y_j \\ .. & .. & .. & .. & .. \\ .. & .. & .. & .. & .. \\ y_{i-1} & y_1 & .. & .. & y_{i+j-2} \end{bmatrix} \tag{2.30}$$

The index p in Eq. 2.30 signifies that the matrix contains system response of the past compared to the system response to be predicted. Since the system response is assumed stationary, Eq. 2.29 can easily be extended to yield

$$\hat{\mathbf{X}}_i = \mathbf{\Gamma}_i^{-1} \hat{\mathbf{O}}_i \tag{2.31}$$

Where $\hat{\mathbf{X}}_i$ is a bank of predicted states, defined as: $\hat{\mathbf{X}}_i = [\hat{\mathbf{x}}_i, \hat{\mathbf{x}}_{i+1}, ..., \hat{\mathbf{x}}_{i+j-1}]$

The matrix $\hat{\mathbf{O}}_i$ only depends on system response and system response covariance, and can therefore be estimated directly from the measured system response. In order to estimate $\mathbf{A}$ and $\mathbf{C}$, it is necessary to estimate the extended observability matrix $\mathbf{\Gamma}_i$. The only input is the matrix $\mathbf{O}_i$, i.e., only information related to the system response. The underlying system that generates the measured response is unknown, which means that we do not know the state space dimension of underlying system. The outer dimension of $\mathbf{O}_i$ and therefore also of $\mathbf{\Gamma}_i \hat{\mathbf{X}}_i$ is, $ip \times j$. The inner dimension is exactly the state space dimension of the underlying system.

Therefore, to find $\mathbf{\Gamma}_i$ first task is to determine this dimension. This is done by using singular value decomposition of $\mathbf{O}_i$, pre and post multiplied by the weight matrices $\mathbf{W}_1$ and $\mathbf{W}_2$, which are user-defined. Taking the SVD of the resulting product yields :

$$\begin{aligned}\mathbf{W}_1\mathbf{O}_i\mathbf{W}_2 &= \begin{bmatrix} \mathbf{U}_1 & \mathbf{U}_2 \end{bmatrix} \begin{bmatrix} \mathbf{S}_1 & 0 \\ 0 & 0 \end{bmatrix} \begin{bmatrix} \mathbf{V}_1^T \\ \mathbf{V}_2^T \end{bmatrix} \\ &= \mathbf{U}_1\mathbf{S}_1\mathbf{V}_1^T \\ &= \mathbf{W}_1\mathbf{\Gamma}_i\hat{\mathbf{X}}_i\mathbf{W}_2\end{aligned} \tag{2.32}$$

Assuming that $\mathbf{W}_1$ has full rank and that the rank of $\mathbf{W}_2$ is equal to the rank of $\mathbf{Y}_P\mathbf{W}_2$ the dimension of the inner product $\mathbf{\Gamma}_i\hat{\mathbf{X}}_i$ is equal to the number of non-zero singular values, i.e. number of diagonal elements of $\mathbf{S}_1$ From Eq. 2.32 $\mathbf{\Gamma}_i$ is given by :

$$\mathbf{\Gamma}_i = \mathbf{W}_1^{-1}\mathbf{U}_1\mathbf{S}_1^{1/2}\mathbf{T} \tag{2.33}$$

The non singular $n \times n$ matrix $\mathbf{T}$ represents an arbitrary similarity transform. This means that the extended observability matrix has been determined, except for an arbitrary similarity transformation.

2.1.4 Ibrahim Time Domain method (ITD)

The ITD algorithm [45] uses the time response of several outputs in order to find model parameters. In the standard ITD method, at least $2N$ response locations need to be measured to identify a model of order N.

The starting point of this method is the premise that the cross correlation function of the responses at the i^{th} and j^{th} locations can be represented by the response of the structure at a location i due to an impulse at location j. This can be expressed as the product of a constant term modulated by an exponential time function. Expressing the cross correlation function x_{ij} at time $k\Delta t$ as x_k, one can write:

$$x_k = x\left(k\Delta t\right) = \sum_{r=1}^{2N} a_r e^{S_r(k\Delta t)} \tag{2.34}$$

Where $S_r = \omega_r\varsigma_r + i\omega_r\sqrt{(1-\varsigma_r^2)}$and ω_r , ς_r are the r^{th} modal natural frequency and damping ratio respectively. Denoting $L + 2N - 1$ as L^* and $2N - 1$ as N^* and re-writing Eq. 2.34 for different starting time samples (i.e. shifted for different starting times), gives:

$$\mathbf{X} = \mathbf{A}\mathbf{\Lambda} \tag{2.35}$$

where $\mathbf{X}$, $\mathbf{A}$ and $\mathbf{\Lambda}$ are given by the following Equations :

$$\mathbf{X} = \begin{bmatrix} x_1 & x_2 & : & x_L \\ x_2 & x_3 & : & x_{L+1} \\ : & : & : & : \\ x_{2N} & x_{2N+1} & : & x_{L^*} \end{bmatrix};\ \mathbf{A} = \begin{bmatrix} a_1 & a_2 & : & a_{2N} \\ a_1 e^{S_1\Delta t} & a_2 e^{S_2\Delta t} & : & a_{2N} e^{S_{2N}\Delta t} \\ : & : & : & : \\ a_1 e^{S_{1(N^*)}\Delta t} & a_2 e^{S_{2(N^*)}\Delta t} & : & a_{2N} e^{S_{2N(N^*)}\Delta t} \end{bmatrix}; \tag{2.36}$$

$$\mathbf{\Lambda} = \begin{bmatrix} e^{S_1 t_1} & e^{S_1 t_2} & : & e^{S_1 t_L} \\ e^{S_2 t_1} & e^{S_2 t_2} & : & e^{S_2 t_L} \\ : & : & : & : \\ e^{S_{2N} t_1} & e^{S_{2N} t_2} & : & e^{S_{2N} t_L} \end{bmatrix} \tag{2.37}$$

Where $t_k = k\Delta t$, N is the total number of modes considered to be identification and L is the number of correlation values per row. The model order N is usually not known a priori but can be increased until the identified parameters converge.

A similar equation can be written by shifting all the discrete response values by Δt as follows:

$$\hat{\mathbf{X}} = \hat{\mathbf{A}}\Lambda \tag{2.38}$$

Now let us define a system matrix $\mathbf{S}_{2N\times 2N}$ so that

$$\mathbf{S}\mathbf{A} = \hat{\mathbf{A}} \tag{2.39}$$

Pre-multiplying Eq. 2.35 by $\mathbf{S}$, gives

$$\mathbf{SX} = \mathbf{SA\Lambda} \tag{2.40}$$

And inserting definition Eq. 2.39, gives

$$\mathbf{SX} = \hat{\mathbf{A}}\mathbf{\Lambda} \tag{2.41}$$

Finally, taking account of Eq. 2.38 gives :

$$\mathbf{S}_{2N\times 2N}\mathbf{X}_{2N\times 2N} = \hat{\mathbf{X}}_{2N\times 2N} \tag{2.42}$$

Eq. 2.42 uses a single-output signal due to a single input (correlation between i and j). In order to find a SIMO variant of ITD, it can be noted that the system matrix $\mathbf{S}$ is independent of the location of measurements and thus that equation remains valid for any SISO combination. Hence, the value of $\mathbf{S}$ can be obtained by considering several responses due to an input and satisfying Eq. 2.42 in a least-square sense. Eq. 2.42 for n responses due to a single impulse (SIMO) can be written as:

$$\mathbf{S}_{2N\times 2N}\underbrace{\left[\begin{array}{cccc}\mathbf{X}^1 & \mathbf{X}^2 & \ldots & \mathbf{X}^n\end{array}\right]}_{(2N\times L_n)} = \underbrace{\left[\begin{array}{cccc}\hat{\mathbf{X}}^1 & \hat{\mathbf{X}}^2 & \ldots & \hat{\mathbf{X}}^n\end{array}\right]}_{(2N\times L_n)} \tag{2.43}$$

Where $\mathbf{X}^j$ is a matrix of correlation expressed between the reference i and an output j. In more compact form, it can be expressed as:

$$\mathbf{S}_{(2N\times 2N)}\,\mathbf{Y}_{(2N\times 1N)} = \hat{\mathbf{Y}}_{(2N\times 1N)} \tag{2.44}$$

A least-squares solution of $\mathbf{S}$ in Eq. 2.44 can be computed using a singular value decomposition of $\mathbf{S}$.

Observing that Eq. 2.39 can be decomposed as:

$$\mathbf{S}_{2N\times 2N}\begin{Bmatrix} a_r e^{S_{r0}\Delta t} \\ : \\ : \\ a_r e^{S_{r0}\Delta t} \end{Bmatrix} = \begin{Bmatrix} a_r e^{S_{r0}\Delta t} \\ : \\ : \\ a_r e^{S_{r(2N-1)}\Delta t} \end{Bmatrix} e^{S_r \Delta t} \ , \ r-1,2,.....2N \tag{2.45}$$

the eigenvalues of $\mathbf{S}$ can be subtracted from the matrix $\mathbf{S}$ itself, to arrive at the standard eigenvalue problem according to:

$$\left[\mathbf{S} - e^{S_r \Delta t}\mathbf{I}\right]\begin{bmatrix} a_r e^{S_{r0}\Delta t} \\ : \\ : \\ a_r e^{S_{r(2N-1)}\Delta t} \end{bmatrix} = 0 \tag{2.46}$$

S_r can be estimated using Eq. 2.46 from which modal frequencies and damping can be computed.

2.1.5 Frequency Domain Decomposition method

The underlying concept of the frequency domain decomposition technique is the observation that the singular value decomposition(SVD) of the spectral density matrix evaluated at each of the PSD peaks reduces the matrix into a set of auto-spectral density functions; each corresponding to a single degree of freedom system.

The starting point of this algorithm is the relationship between the unknown inputs $x(t)$ and the measured responses $y(t)$ in frequency domain, which can be expressed as [11]:

$$\mathbf{G}_{yy}(j\omega) = \bar{\mathbf{H}}(j\omega)\,\mathbf{G}_{xx}(j\omega)\,\mathbf{H}(j\omega)^T \tag{2.47}$$

where $\mathbf{G}_{xx}(j\omega)$ is the $r \times r$ power spectral density (PSD) matrix of the input, r is the number of inputs, $\mathbf{G}_{yy}(j\omega)$ is the $m \times m$ PSD matrix of the responses, m is the number of responses, $\mathbf{H}(j\omega)$ is the frequency response function of size $m \times r$ and $\bar{\mathbf{H}}(\mathbf{j}\omega)$ is the complex conjugate of the frequency response function.

Using partial expansion technique and by assuming that the structure is lightly damped Eq. 2.47 can be expressed as [13]:

$$\mathbf{G}_{yy}(j\omega) = \sum_{k \in \omega} \frac{d_k \phi_k \phi_k^T}{j\omega - \lambda_k} + \frac{\bar{d}_k \bar{\phi}_k \bar{\phi}_k^T}{j\omega - \bar{\lambda}_k} \tag{2.48}$$

where ϕ_k and λ_k represents the mode shape and the modal participation constants and d_k is another scalar constant.

In the frequency domain decomposition technique, the basic step is the estimation of the PSD $\mathbf{G}_{yy}(j\omega)$ observed at discrete frequencies $\omega = \omega_i$ and then decomposing the PSD matrix using singular value decomposition:

$$\mathbf{G}_{yy}(j\omega) = \mathbf{U}_i \mathbf{S}_i \mathbf{U}_i^H \tag{2.49}$$

where the matrix $\mathbf{U}_i$ is the unitary matrix of singular vectors and $\mathbf{S}_i$ is a diagonal matrix of singular values. The mode shapes are estimated from the singular vectors stored in the $\mathbf{U}_i$ matrix and the corresponding singular value is the auto power spectral density function of the corresponding single degree of freedom system.

This power spectral density function is identified around the peaks by comparing the mode shape estimate $\hat{\phi}$ with the singular vectors for the frequencies around the peak. If the singular vector found has a high MAC value then it corresponds to a mode. On other hand, if none of the singular vectors has a MAC larger than a threshold Ω, the search for matching parts of the auto spectral density is terminated. For the fully or partially identified SDOF auto spectral density function, the natural frequency and damping are

obtained by converting the spectral density function back in the time domain by inverse FFT.

2.2 Drawbacks of the Traditional methods

- All the time domain modal identification algorithms discussed earlier have a serious problem in model-order determination. The identification requires pre-selection of model order, and frequently over determination of model order becomes a problem in itself to deal with. Spurious modes are generated while extracting the structural or physical modes. For random response data, the problem becomes more acute. Use of stability charts and modal assurance criteria to distinguish pure modes from the noisy ones is an effective measure, but they have shown limited success over the years.

- The SSI method assumes a zero mean Gaussian white noise input. If the input contains dominant frequency components in addition to the white noise, then those frequency components cannot be separated from the eigen frequencies of the system.

- In many cases of identification, it has been observed that almost all of the time domain modal identification methods fail to identify structures with moderate to high damping [80]. Literature is replete with instances where most of the aforementioned methods have consistently failed to identify structures in moderate to high damping environments with sufficient degree of confidence.

- Most modal identification procedures can be reduced to a set of linear equations, which are solved using least-squares techniques. Therefore, bias error or variance error could occur due to noise effects, including measurement noise, leakage, residues, etc. Engineering practice has shown that very little improvement can be done to

reduce the error at the expense of heavy computational penalty. Accuracy issues would be significant where there are many measurements in noisy media, or where the structures are complex in nature, e.g., structures with supplemental damping devices like active and tuned mass dampers, and structures containing closely spaced modes in highly damped environments.

2.3 Newer Trends in System Identification

Recently, research in information theory and signal processing has witnessed tremendous efforts towards developing the theories of *blind source separation* (BSS) and time-frequency signal decomposition known as *empirical mode decomposition* (EMD). BSS involves extracting individual but physically different sources from output measurements where only a mixture of the sources is observed. Two main approaches have been explored here in detail, namely, the independent component analysis (ICA) and second order blind identification (SOBI).

EMD [43], on the other hand, is a powerful signal processing algorithm, that can decompose any given signal into mono-harmonic components even in the presence of non-stationary environments in an adaptive manner. It has shown significant promise in the area of output only system identification of structures.

2.3.1 Empirical Mode Decomposition

Empirical mode decomposition [43] is a recently developed signal processing algorithm that has shown significant promise in the area of output only system identification of structures in the time-frequency [88, 87] domain.

EMD reduces a signal into intrinsic mode functions (IMFs) that admit a well-behaved

Hilbert transform [43] (see APPENDIX G). The power of EMD lies in its ability to decompose any given signal into IMFs, even in non-stationary environments, in an adaptive manner, without the need of choosing a predetermined basis. For multi-degree-of-freedom structures, the IMFs extracted from the free-vibration responses can be regarded as the modes of vibration [88]. An IMF is defined as a function that satisfies the following conditions: (i) it is mono-component, and (ii) the mean values of the envelopes defined by the local maxima and the local minima are zero. The procedure of extracting an IMF is called sifting. Suppose $x(t)$ is the signal to be decomposed. The sifting process is implemented by identifying local extremum in the data between successive pairs of zero crossings and connecting all the local maxima by a cubic spline line to create the upper envelope. Local minima are connected in the same fashion to produce the lower envelope. If their mean is m_1, the difference $x(t) - m_1 = h_1$ is the first IMF. Ideally, h_1 should satisfy the conditions necessary to be called an IMF. If it does not satisfy the necessary conditions, then the sifting process is repeated by treating h_1 as the original data until the requirements for an IMF are fulfilled. The original signal is then subtracted from the IMF and the sifting process is repeated to decompose the data into n IMFs. Although one could extract the natural frequencies and the corresponding damping estimates directly using this sifting technique [88], measurements at all the degrees of freedom are required to extract the corresponding modes.

Mathematically, the procedure can be expressed as:

$$\ddot{r}_p(t) = \sum_{j=1}^{m} c_{pj}(t) + \epsilon_p(t) \tag{2.50}$$

in which $c_{pj}(t)$ for $j = 1, 2, ..., m$ are the m IMFs of the free acceleration response $\ddot{r}_p(t)$ of any $n-$DOF system and $\epsilon_p(t)$ is the residue.

The sifting process sometimes causes the IMFs to contain more than one frequency components leading to mode-mixing ([88]; [76]). Mode mixing is avoided by applying

suitable band pass filters to the signal in the approximate frequency range $\omega_{jL} < \omega_j < \omega_{jH}$ for each natural frequency, determined from the Fourier spectrum of the free acceleration response $\ddot{r}_p(t)$. The signal obtained from the jth band-pass filter is then processed through EMD, to obtain the jth modal response. Repeating the procedure for $j = 1, 2, 3....., n$, n modal responses are obtained according to,

$$\ddot{r}_p(t) \approx \sum_{j=1}^{n} r_{pj}(t) + \epsilon_p(t) \tag{2.51}$$

EMD, when used in combination with the HT method, also known as Hilbert-Huang Transform (HHT), can be used to identify linear Multi-degree-of-freedom (MDOF) structures under free vibration [88], as well as white noise forced excitation [88]. For free vibration case, the modal parameters of a structure can be identified by the application of Hilbert transform to the IMFs to obtain the instantaneous amplitude and phase angle time histories, followed by a linear least-square procedure to identify the natural frequency and damping ratio from the instantaneous amplitude and phase angle for each modal response. For white noise excitation case, the cross-correlation functions of the structural responses are calculated, which by virtue of NExT [46] resembles free responses. Once the cross-correlations are estimated, the natural frequencies and modes are identified by the application of Hilbert transform as mentioned earlier.

Although estimating natural frequencies and damping is relatively straightforward using the HHT method, estimating the natural modes is involved. The coordinates of the mode shapes ϕ_{pj} and ϕ_{qj} of the j^{th} mode, at the floor levels p and q are estimated according to:

$$\frac{|\phi_{pj}|}{|\phi_{qj}|} = \exp\left[A'_{pj}(t_0) - A'_{qj}(t_0)\right] \tag{2.52}$$

where $A'_{pj}(t_0)$ and $A'_{qj}(t_0)$ are, respectively, the magnitudes at the time $t = t_0$ of the average least-square straight lines for the decaying amplitudes $lnA_{pj}(t)$ and $lnA_{qj}(t)$ [88]. A key drawback of this approach is the requirement of measured responses at all floor

levels. Furthermore, the selection of intermittency criteria poses challenges in estimating higher modes of vibration.

2.4 Blind Source Separation

The separation of original source waveforms from the sensor signals, without the knowledge of the system characteristics and the sources, is known as blind source separation (BSS). BSS is formulated as an inverse problem, where, based on the observed records of sensor signals in discrete time, from an unknown MIMO (multiple-input/multiple-output) mixing system, an inverse system is identified in order to estimate the primary source signals. This estimation is performed based on the output signals only. Instead of estimating the source signals directly, it is sometimes more convenient to identify the mixing system first (e.g., especially when system is over complete with the number of observations is less than the number of source signals) and then estimate source signals implicitly by exploiting some apriori information about the mixing system and applying a suitable optimization procedure. The problem of source separation can be expressed briefly as a number of related BSS problems, which are known in the literature as independent component analysis (ICA) and its extensions, multidimensional ICA, subband decomposition-ICA, sparse component analysis, sparse PCA, smooth component analysis, and multichannel blind deconvolution. For the details of the aforesaid classifications and explanations, readers are referred elsewhere [49, 22, 19, 44].

For most applications, the sources are related to the outputs by simple linear mixing models. The principle is illustrated in Fig. 2.1. Depending on the specific applications [19], the mixing processes of the unknown input sources may have different mathematical or physical models. One of the main applications of the linear mixing models is the modal identification of structural systems from ambient vibration data.

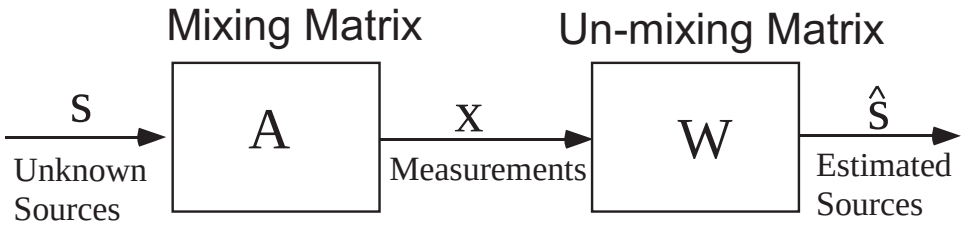

Figure 2.1: Illustration of blind source separation

There are two ways to represent the mixing of sources, expressed by two different mixing models: the instantaneous mixing model, and the convolved mixing model. The first one can be expressed by the simple matrix factorization problem in which given the observation (often called sensor data) matrix, one can write

$$\left.\begin{aligned} \mathbf{x}(k) &= \mathbf{A}\mathbf{s}(k) \\ \hat{\mathbf{s}}(k) &= \mathbf{y}(k) = \mathbf{W}\mathbf{x}(k) \end{aligned}\right\} \tag{2.53}$$

$\mathbf{A} = [a_{ij}]_{n\times n}$ is the instantaneous mixing matrix

$\mathbf{W}_{n\times n} = \mathbf{A}^{-1}_{\mathbf{n}\times\mathbf{n}}$ is the un-mixing matrix, which is the pseudo inverse of $\mathbf{A}$

$\mathbf{s}(k) = \{s_j(k)\}$ $j = 1, 2, ...N$ sources input to the system

$\mathbf{x}(k) = \{x_i(k)\}$ $i = 1, 2, ...N$ sensor signals system output

$\mathbf{y}(k) = \{y_j(k)\}$ $j = 1, 2, ...N$ estimated Sources

For convolutive mixtures, Eq. 2.53 becomes,

$$\left.\begin{aligned} \mathbf{x}(k) &= \sum_p \mathbf{H}_p(k)\mathbf{s}(k-p) \\ &= [\mathbf{H}(z)]\,\mathbf{s}(k) \end{aligned}\right\} \quad k = 1, 2....\mathbf{T} \tag{2.54}$$

Where $\mathbf{H}_p(k) = \lfloor h_{ijp}(k) \rfloor_{N\times M}$ is the mixing matrix at p^{th}delay

$h_{ijp}(k)$ is the impulse response at time instant k

Eq. 2.53 represents the static mixing problem, which does not explicitly use time properties. That is, it is not necessary for the sources and the outputs to be a function

of time. Eq. 2.54 explicitly represents a dynamic problem where the sources and the outputs have well defined time properties and the co-efficients of the un-mixing system are essentially the co-efficients of a deconvolution filter (e.g., FIR filter). Some important acronyms relevant to the subsequent discussions are provided in Table. 2.1.

Table 2.1: Important Acronyms

BSS	Blind Source Separation
MCC	Modified Cross-Correlation
WMCC	Wavelet based modified Cross-Correlation
SOBI	Second-Order Blind Identification
ICA	Independent Component Analysis
MDOF	Multi-Degrees-of-Freedom
MAC	Modal Assurance Criterion
PGA	Peak Ground Acceleration
ARMA	Auto-Regressive-Moving-Average

Modal Identification using Blind Source Separation

Although there is a lot of literature on the blind source separation algorithms, modal identification using BSS appears to be a relatively less explored area. The modal identification problem consists of extracting a set of natural frequencies, damping factors, and mode shapes of a structure based on only the information extracted from the output data. Among these parameters, mode shapes provide mathematical description of deflection patterns of vibration when the system vibrates at one of the natural frequencies. From another viewpoint, the mode shapes describe the participation of each independent, oscillation in the output response. The dynamic structural system defined by Eq. 2.11 can be approached

from both the static and the convolutive viewpoints. The static approach considers the output as product of the modal state vectors and the exponential decay expressed as under:

$$\mathbf{x}(t) = \sum_{i=1}^{n} \mathbf{\Psi}_i \exp\left(\left(-\xi_i + j\omega_i\right) t\right) \tag{2.55}$$

This, in matrix form, lends itself into the following statement:

$$\mathbf{X} = \mathbf{\Psi Q} \tag{2.56}$$

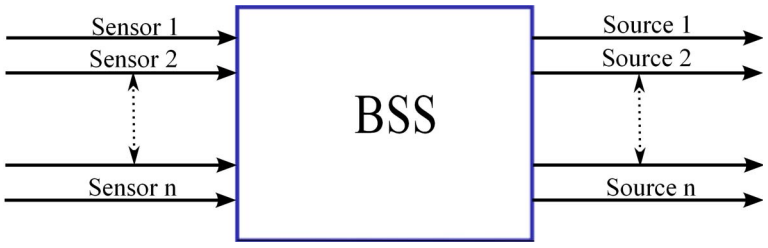

Figure 2.2: Modal Identification using BSS

Where $\mathbf{X} \in \Re^{m \times N}$ the trajectory matrix is composed of the sampled components of x, and $\mathbf{Q} \in \Re^{m \times N}$ is a matrix of the corresponding modal coordinates and $\mathbf{\Psi}$, the modal transformation matrix. From the convolutive viewpoint, the system can also be viewed as a dynamic mixture of the sources, since the output can be expressed as the convolution product of the external force vector and the impulse response according to Eq. 2.54. Whereas, there is explicit appearance of the sources in the convolutive approach, the same for the static counterpart seems conjectural.

Under certain special circumstances [54], the normal modes or the modal coordinates can be regarded as the most independent sources (termed as virtual sources), thus rendering the presence or the absence of the external force inconsequential. Thus the modal coordinates $\mathbf{Q}(\mathbf{t})$ are a special case of general sources $\mathbf{s}$ with time structure, and $\mathbf{\Psi}$ the mixing

matrix **H**. Furthermore, distinct modal coordinates automatically meet the requirement of independence as well as uncorrelation of sources in BSS. Most BSS algorithms focus on finding the demixing matrix **W**. These algorithms could also be implemented to extract mode shape information of a vibration system in noisy environments.

Fig. 2.2 shows the schematic illustration of mode extraction process based on BSS. The signals on the left-hand side are output vibration signals and the signals on the right-hand side are the separated modes. Thus, the key idea is to appreciate the normal coordinates of a dynamic system as virtual sources with different spectral contents. Under certain assumptions [54], BSS techniques provide a one-to-one mapping between the mixing matrix and the vibration modes of the structure, which forms the basis of the modal identification procedure. The system identification can be carried out by performing experimental measurements on the tested system to obtain time response data at different observable sensor positions, or by the use of the ambient data and subsequent application of the BSS techniques to the measured time series $\mathbf{x}(t)$ to estimate the mixing matrix **H** and the sources $\mathbf{s}(t)$. The mode shapes are contained in the mixing matrix **H**. It is then straightforward to identify the natural frequencies and damping ratios of the corresponding vibration modes [92]. The natural frequency can be identified either by observation of the cycles in the time series, or by observing the Fourier spectrum, and the damping can be estimated using the logarithmic decrement method, or the half-power bandwidth method.

2.4.1 Independent Component Analysis (ICA)

Independent Component Analysis is one of the most popular methods for performing BSS [49, 22]. ICA assumes that the observed data are linear combinations of statistically independent (or as independent as possible) sources. The sources are termed as independent components, and the ICA basis vectors (i.e., the columns of the mixing matrix **A**) are the ICA modes in the present study, which are linearly independent.

The ICA of a random vector $\mathbf{x}(k) \in \Re^m$ is obtained by finding a $n \times m$ full rank separating (transformation) matrix $\mathbf{W}$ with $m \geq n$ such that the output signal vector $\mathbf{y}(k) = [y_1(k), ..., ..., y_m(k)]^T$ (components) estimated by:

$$\mathbf{y}(k) = \mathbf{W}\mathbf{x}(k) \tag{2.57}$$

are as independent as possible. The independence is measured by an information-theoretic cost function such as maximization of cumulants [22].

Principles of ICA

ICA is based on the premise of three main principles: statistical independence, non-Gaussianity, and whitening

- Statistical Independence

  For ICA to be implemented, the sources should be physically independent. Physical independence implies several degrees of statistical independence. For example, if two sources $\mathbf{s}_1(t)$ and $\mathbf{s}_2(t)$ are considered then the first implication is that $\mathbf{s}_1(t)$ and $\mathbf{s}_2(t)$ are temporally uncorrelated, i.e. $\langle \mathbf{s}_1(t)\mathbf{s}_2(t) \rangle = \langle \mathbf{s}_1(t) \rangle \langle \mathbf{s}_2(t) \rangle$ where $\langle \bullet \rangle$ denotes the time averaging operator. Generally, this is not a strong enough requirement to yield a unique solution. For instance, it is easy to check that combinations $\{\mathbf{s}_1(t) + \mathbf{s}_2(t)\}$ and $\{\mathbf{s}_1(t) - \mathbf{s}_2(t)\}$ are also uncorrelated while obviously not being the expected solution. A popular criterion is to additionally force the nullity of the fourth-order statistics $\left\langle |\mathbf{s}_1(t)|^2 |\mathbf{s}_2(t)|^2 \right\rangle - \left\langle |\mathbf{s}_1(t)|^2 \right\rangle \left\langle |\mathbf{s}_2(t)|^2 \right\rangle$, an operation which may be physically understood as searching for sources with uncorrelated variations of energy. The most important representation of statistical independence of 2 random variables $\mathbf{s}_1(t)$ and $\mathbf{s}_2(t)$ is given by the relationship

$$p(\mathbf{s}_1(t), \mathbf{s}_2(t)) = p(\mathbf{s}_1(t)) p(\mathbf{s}_2(t)) \tag{2.58}$$

where $p(\mathbf{s}_1(t))$ denotes the probability density function of the random variable $\mathbf{s}_1(t)$. In other words, signals are independent if their joint density function can be factorized.

- Non-Gaussianity

  Independent component analysis prohibits the sources to be Gaussian. This is attributed to the fact that the higher order cumulants are zero for Gaussian distributions, and this seriously hinders the possibility of using higher order statistics, which are deemed very essential for the estimation of the independent components. The central limit theorem is exploited in creating contrast functions e.g., kurtosis and negentropy. The basic idea of central limit theorem is illustrated in Fig. 2.3. In this figure it can be observed that if different random variables mutually independent of each other characterized by different magnitudes of kurtosis are linearly combined, the outcome is a random variable that tends to be more gaussian than the individual components. As seen in Fig. 2.3, the random variable produced out of the components s_1, s_2 and s_3 has a kurtosis value of 2.83 which is close to the kurtosis of a Gaussian random variable of value 3. The outcome of using central limit theorem is that the distribution of a sum of independent random variables tends toward Gaussian. Thus, to extract a source, the key step is to maximize the non-gaussianity of a linear combination of sensor signals which ensures that an individual source is further away from a Gaussian distribution compared to the mixture of sources.

- Whitening

  As a preprocessing step, it is necessary to whiten the data. Whitening de-correlates the sensor signals. It is essentially a transformation that renders the covariance matrix of the signals an identity matrix. Whitening plays an important role in fulfilling the statistical independence condition. Since uncorrelated Gaussian signals are also independent, satisfying non-Gaussianity and whitening automatically satisfies

statistical independence.

Ambiguities of ICA

Solving the ICA problem uniquely is possible within two fundamental indeterminacies relating to the scaling factor, and the labelling of the sources:

- Can't determine the variances (energies) of the IC's

  Since both $\mathbf{s}$ and $\mathbf{A}$ are unknowns, any scalar factor of $\mathbf{s}$ in the equation $\mathbf{x}(k) = \mathbf{A}\mathbf{s}(k)$ can always be canceled by multiplying the corresponding column of $\mathbf{A}$ by it. Hence,

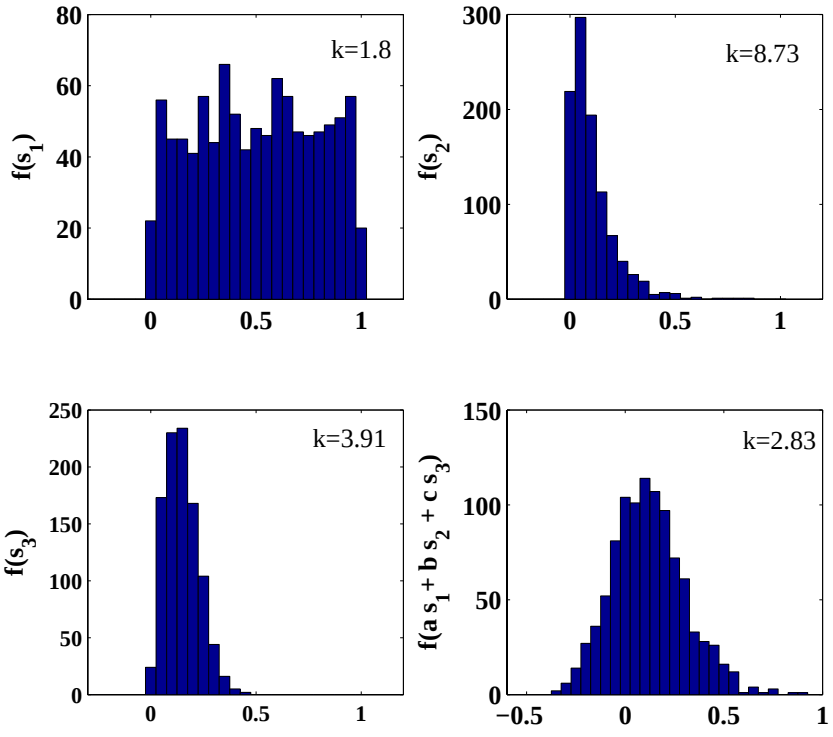

Figure 2.3: Illustration of Central Limit theorem and Gaussianity

the only possibility of taking care of this ambiguity is by fixing the magnitudes of IC's assuming unit variance: $E\{s_i^2\} = 1$.The ambiguity of sign however still remains.

- Can't determine the order of the IC's

  The order of the ICs can be freely changed, because both $\mathbf{s}$ and $\mathbf{A}$ are unknown. So any independent component can be labeled as the first one.

The ICs of the vector of sensor signals $\mathbf{x}(k) \in \Re^m$ is obtained by estimating the demixing matrix $\mathbf{W}$ and estimated sources $\mathbf{y}(k) \in \Re^m$.

A wide class of algorithms for ICA can be expressed in general form [19]:

$$\mathbf{W}(l+1) - \mathbf{W}(l) = \eta \mathbf{F}(\mathbf{y}) \mathbf{W}(l) \tag{2.59}$$

where $\mathbf{y}(k) = \mathbf{W}(l)\mathbf{x}(k)$ and the matrix $\mathbf{F}(\mathbf{y})$ take different forms, for example $\mathbf{F}(\mathbf{y}) = \Lambda_n - \mathbf{f}(\mathbf{y})\mathbf{g}^T(\mathbf{y})$ with suitably chosen nonlinearities $\mathbf{f}(\mathbf{y}) = [f(y_1), .., .., f(y_n)]$ and $\mathbf{g}(\mathbf{y}) = [g(y_1), .., .., g(y_n)]$ [24, 25, 21, 20]. Assuming a prior knowledge of the source distributions $p_i(y_i)$, $\mathbf{W}$ can be estimated by using the principle of maximum likelihood, where the likelihood function is given by :

$$J(\mathbf{y}, \mathbf{W}) = -\frac{1}{2}\log\left(\left|\det\left(\mathbf{W}\mathbf{W}^T\right)\right|\right) - \sum_{i=1}^{n} E\{\log(p_i(y_i))\} \tag{2.60}$$

The traditional maximum likelihood ICA method [44] uses stochastic gradient methods of optimization in which the term $E\{\log(p_i(y_i))\}$ is replaced by $E\left\{\mathbf{f}(\mathbf{y})\mathbf{y}^T\right\}$.

Using natural gradient descent to increase likelihood, one obtains:

$$\mathbf{W}(l+1) = \eta\left[\mathbf{I} - E\left\{\mathbf{f}(\mathbf{y})\mathbf{y}^T\right\}\right]\mathbf{W}(l) \tag{2.61}$$

Where $\mathbf{f}(y) = [f(y_1), \ ..., \ ....., f(y_n)]$ is an entry-wise non-linear score function [24, 20, 44, 16]defined by:

$$\mathbf{F}_i(y_i) = \frac{p_i'(y_i)}{p_i(y_i)} = -\frac{d\log(p_i(y_i))}{d(y_i)} \tag{2.62}$$

For signals corrupted by additive Gaussian noise, higher order matrix cumulants can be used [24]. Cichocki and Amari [4] suggested the use of the following cost function in which the term $E\{\log(p_i(y_i))\}$ is replaced by the term $\frac{1}{1+q}\sum_{i=1}^{N}|C_{1+q}(y_i)|$

$$J(y, \mathbf{W}) = -\frac{1}{2}\log\left(\left|\det\left(\mathbf{W}\mathbf{W}^T\right)\right|\right) - \frac{1}{1+q}\sum_{i=1}^{N}|C_{1+q}(y_i)| \tag{2.63}$$

Where $C_q(y_i)$ denotes the q-order cumulants of the signal y_i. The readers are referred to [24, 16] and [4] for the details. The first term in Eq. 2.63 ensures that the determinant of the global matrix will not approach zero. The second term forces the output signals to be as far as possible from Gaussianity, since the higher order cumulants are a natural measure of Non-Gaussianity. It can be shown that for such a cost function, one can derive the following equivariant and robust with respect to Gaussian noise [19, 20, 21]:

$$\mathbf{W}(l+1) - \mathbf{W}(l) = \eta\left\lfloor \mathbf{I} - \mathbf{C}_{1,q}(\mathbf{y},\mathbf{y})\,\mathbf{S}_{1+q}(\mathbf{y})\right\rfloor \mathbf{W}(l) \tag{2.64}$$

Where $\mathbf{S}_{1+q}(y) = sign\left(diag\left(\mathbf{C}_{1,q}(\mathbf{y},\mathbf{y})\right)\right)$ and $F(y) = \mathbf{I} - \mathbf{C}_{1,q}(\mathbf{y},\mathbf{y})\,\mathbf{S}_{1+q}(y)$.

2.4.2 Second Order Blind Identification (SOBI)

SOBI [10] family of methods use the time information contained in the signals as opposed to treating them as mere random variables as ICA does. If the ICs are time signals, they usually contain much better defined structure than ordinary random variables. For example, the auto-covariances for several time lags have well-defined statistics. The SOBI family of methods do not make any prior assumptions of statistical independence or non-gaussianity of sources. They rely purely on second-order temporal statistics. The basic

assumptions include full rank of the matrix $\mathbf{A}$, existence of autocorrelation function of the sources, spatial non-correlation of the sources, stationarity of the sources, and the presence of independent noises. SOBI is based on the premise of simultaneous diagonalization of two covariance matrices $\hat{\mathbf{R}}_{\mathbf{x}}(0)$ and $\hat{\mathbf{R}}_{\mathbf{x}}(p)$, defined by the relations as under:

$$\left.\begin{aligned} \mathbf{R}_{\mathbf{s}}(p) &= E\left\{\mathbf{s}(k)\,\mathbf{s}^{\mathbf{T}}(k-p)\right\} \\ \mathbf{R}_{\mathbf{x}}(0) &= E\left\{\mathbf{x}(k)\,\mathbf{x}^{\mathbf{T}}(k)\right\} = \mathbf{A}\mathbf{R}_{\mathbf{s}}(0)\,\mathbf{A}^{T} \\ \mathbf{R}_{\mathbf{x}}(p) &= E\left\{\mathbf{x}(k)\,\mathbf{x}^{\mathbf{T}}(k-p)\right\} \end{aligned}\right\} \tag{2.65}$$

for some non-zero time-lag p. The simultaneous diagonalization is performed in three basic steps: whitening, orthogonalization, unitary transformation. Whitening is a linear transformation in which $\hat{\mathbf{R}}_{\mathbf{x}}(0) = \left(1/N\right)\left(\sum_{K=1}^{N}\mathbf{x}(k)\,\mathbf{x}^{T}(k)\right)$ is first diagonalized using singular value decomposition that is accomplished as $\hat{\mathbf{R}}_{\mathbf{x}}(0) = \mathbf{V}_{\mathbf{x}}\mathbf{\Lambda}_{\mathbf{x}}\mathbf{V}_{\mathbf{x}}^{\mathbf{T}}$. Then, the standard whitening is realized by a linear transformation expressed as under:

$$\bar{\mathbf{x}}(k) = \mathbf{Q}\mathbf{x}(k) = \mathbf{\Lambda}_{\mathbf{x}}^{-\frac{1}{2}}\mathbf{V}_{\mathbf{x}}^{\mathbf{T}}\mathbf{x}(k) \tag{2.66}$$

Because of whitening, $\mathbf{R}_{\mathbf{x}}(p)$ becomes $\mathbf{R}_{\bar{\mathbf{x}}}(p)$ which is given by the equation underneath:

$$\mathbf{R}_{\bar{\mathbf{x}}}(p) = \frac{1}{N}\left(\sum_{k=1}^{N}\bar{\mathbf{x}}(k)\bar{\mathbf{x}}^{T}(k)\right) = \mathbf{Q}\mathbf{R}_{x}(p)\,\mathbf{Q}^{T} \tag{2.67}$$

The second step, called orthogonal transformation, is applied to diagonalize the matrix $\hat{\mathbf{R}}_{\mathbf{x}}(p)$. The eigen value decomposition of $\hat{\mathbf{R}}_{\bar{\mathbf{x}}}(p)$ has the form $\hat{\mathbf{R}}_{\bar{\mathbf{x}}}(p) = \mathbf{V}_{\bar{\mathbf{x}}}\mathbf{\Lambda}_{\bar{\mathbf{x}}}\mathbf{V}_{\bar{\mathbf{x}}}^{T}$. Using Eqs. 2.65 and 2.67, one obtains:

$$\hat{\mathbf{R}}_{\bar{\mathbf{x}}}(p) = \mathbf{Q}\mathbf{H}\hat{\mathbf{R}}_{\mathbf{s}}(p)\,\mathbf{H}^{T}\mathbf{Q}^{T} \tag{2.68}$$

If the diagonal matrix $\mathbf{\Lambda}_{\bar{\mathbf{x}}}$ has distinct eigen values then the mixing matrix can be estimated uniquely by the following equation:

$$\hat{\mathbf{H}} = \mathbf{Q}^{-1}\mathbf{V}_{\bar{\mathbf{x}}} = \mathbf{V}_{\bar{\mathbf{x}}}\boldsymbol{\Lambda}_{\bar{\mathbf{x}}}^{1/2}\mathbf{V}_{\bar{\mathbf{x}}} \tag{2.69}$$

Simultaneous diagonalization of two symmetric matrices can be carried out without going through the last two steps of the procedure, by converting the problem to the generalized eigenvalue decomposition.

Problems with Modal Identification using Blind Source Separation

It has been observed that ICA, one of the potential methods to perform BSS, fails to perform adequately in the presence of even relatively small amounts of damping [54]. In the present context, a value of structural damping in the range of $0.5\% - 2\%$ is considered low damping. Damping in the range $2.0\% - 5.0\%$ is considered moderate and values greater than 5% is considered high. SOBI holds lot of promise in modal identification in presence of moderate to high damping. The performance of SOBI to identify small systems has been clearly demonstrated [54, 92]. However, even the traditional SOBI method has performance issues related to ambient system identification of structures. The aim of the present research is to address these shortcomings of SOBI in a systematic manner, and expand the range of applicability of the second order blind source separation methods. The key shortcomings of SOBI addressed in this dissertation can be summarized as under:

1. The state of the art ambient system identification methods involving the use of SOBI utilize the response measurements directly. Hence, damping cannot be estimated using the SOBI method as it is. This is due to the fact that the responses under random excitation grow and decay in the same manner as the input and thus free decay cannot be observed unlike impulse responses. This issue is addressed through MCC method in chapter 3, by considering the correlation of response measurements using the concept of NExT [46], and utilizing the correlation of responses to perform blind source separation in the subsequent step.

2. A key shortcoming of SOBI appears when the response measurements contain spatially un-correlated noise which is usually modeled as gaussian and white . The measurement noise needs to be treated separately using prior knowledge of noise covariances. If response covariances are used instead of the noisy measurements directly, this problem is solved automatically. This issue is addressed within the framework of the MCC method discussed in detail in chapter 3.

3. The current form of the SOBI method works well in simulation studies where all the modes have sufficient energy content. This condition is hardly satisfied in large scale real life structures, in which the higher modes of vibration may not have sufficiently high energy contents. The issue is addressed in chapter 4 by extending the basic principles of SOBI for the static mixtures using the stationary wavelet transform (SWT) in order to enhance the separability of sources with low energy, thereby improving the quality of identification by making them more sparse [56].

4. Presently, SOBI is not equipped to handle ambient system identification of structures when the number of sensors is less than the number of identifiable modes. Physically, such situations arise in flexible structures that are instrumented with a relatively small number of sensors due to cost or other reasons. This problem is addressed in chapter 5 by developing a hybrid time and time-frequency approach, where the output is first decomposed into IMFs by utilizing EMD, and using the IMFs as initial estimates of sources to form an iterative approach within the framework of the MCC method.

5. Due to the response of closely spaced modes and relatively high damping, SOBI methods are not able to handle ambient system identification of structures equipped with tuned mass damper (TMDs). Chapter 6 presents the development of a novel hybrid time and time-frequency domain blind source separation algorithm, utilizing EMD, to identify structures equipped with tuned mass dampers(TMDs). The ob-

jective here is to extend the identification method to re-tune TMDs under ambient excitations, a problem that has important practical significance.

2.5 Summary

This chapter presents a survey of key methods of system identification, the traditional ones followed by the more recent ones. The literature on traditional modal identification described the detailed development of the subject and many limitations associated with it. The main problems are: i) Distinguishing pure modes from spurious modes arising due to arbitrary choice of model orders ii) lack of robustness in the presence of noise iii) difficulty in estimating modes accurately in high damping environments. SOBI methods addresses these basic drawbacks and appears to address the problem of modal identification in noisy and highly damped environments in a robust manner. However, SOBI suffers from shortcomings that don't allow accurate ambient system identification of structures under a wide spectrum of practical situations like presence of measurement noise, insufficiency in energy content of higher vibrating modes of large flexible structures, unavailability of complete measurements, presence of supplemental damping devices, etc. With this, the focus of the present work is firmly established. The present work concentrates on the reformulation of BSS methods in the time and time-frequency domains in order to identify realistic full-scale structures under ambient excitations using full and partial response measurements.

Chapter 3

Modified Cross Correlation Method

This chapter presents the theoretical development of a new method called the modified cross-correlation method (MCC). MCC method extends the concept of SOBI to identify full-scale structures subjected to ambient excitations. The chapter is organized as follows. The problem statement is presented first wherein the general problem of structural system identification is cast in a BSS framework. The formulation of SOBI and MCC methods is presented next, followed by the results of the numerical simulation of a simple three degree-of-freedom mass, spring, and dashpot system. Experimental results for a two-storey building model are presented next. Finally, the results of identification using the MCC method are presented for the case of a full-scale tower structure excited by both wind and earthquake forces, followed by a summary.

3.1 Motivation

The performance of SOBI to identify small systems in the presence of moderate to high damping has been clearly demonstrated [54, 92]. But, SOBI suffers from performance issues related to ambient system identification of full-scale structures.

Modal identification with the aid of SOBI requires the use of response measurements directly. Hence, damping cannot be estimated from the recovered sources directly. Once the sources are recovered, damping is estimated *aposteriori*, utilizing the concepts of NExT [46] to obtain the free responses, and fitting single degree of freedom systems using least squares procedures. Estimation of damping in the aforementioned manner, is prone to errors for noisy measured responses. Furthermore, the measurement noise is not accounted within the framework of the method. Noisy responses are prone to source separability issues, and the recovered sources do not represent structural modes when the signal to noise ratio is low. Even an extension of SOBI method to accommodate noise requires the prior knowledge of noise covariances, a condition difficult to fulfill for practical structures. Moreover, the problem of structural system identification under general wind or seismic loadings has not been examined in the literature so that it can be solved within the framework of SOBI.

The aforementioned practical problems motivates the need for a method which extends the concepts of SOBI to identify damping directly from the recovered sources, and also to address the problem of noisy measurements. This is accomplished by treating the auto and cross-correlation of the measurements as the outputs of the system, rather than the actual measurements, using the concepts of the NExT algorithm presented in the literature [46]. This method is termed as the modified cross-correlation method (MCC).

3.2 Problem Formulation

In order to perform modal identification for structural systems under general excitation cases, the dynamic equations of motion first needs to be cast in the form of Eq. 2.53. In this context, it is necessary to relate the term *source* to the characteristic modes of the system. Consider again, the equation of motion for a multi-degrees-of-freedom structure under the action of an excitation force vector $\mathbf{F}(t)$ given by Eq. 2.11, where $\mathbf{x}(t)$ is a vector

of displacement coordinates at the degrees of freedom. Under special cases of the excitation vector $\mathbf{F}(t)$, such as when $\mathbf{F}(t) = 0$, which corresponds to the case of free vibration, the solution to Eq. 2.11 can be written in terms of an expansion of vibration modes. In matrix form,

$$\mathbf{x} = \mathbf{\Psi q} \tag{3.1}$$

where $\mathbf{x} \in \Re^{n \times N}$ is the trajectory matrix composed of the sampled components of $\mathbf{x}$, $\mathbf{q} \in \Re^{n \times N}$ is a matrix of the corresponding modal coordinates, and $\mathbf{\Psi}$ the modal transformation matrix. Note the similarity between Eq. 3.1 and Eq. 2.53. Under special circumstances [54], the normal modes or the modal coordinates can be regarded as the most independent sources (termed as virtual sources), thus rendering the presence or the absence of the external force inconsequential. Thus, the modal coordinates $\mathbf{q}$ are a special case of general sources $\mathbf{s}$ with time structure. Furthermore, distinct modal coordinates automatically meet the requirement of independence as well as non-correlation of sources in BSS, and form the basis of the modal identification procedure.

For the case of excitations, when $\mathbf{F}(t)$ corresponds to uncorrelated white noise, it is possible to write the correlation of responses in Eq. 2.11 in the form of Eq. 3.1 [46]. This is accomplished as follows. The cross-correlation between the locations denoted by i and j due to an input at k is given by

$$R_{ijk}(T) = E[x_{ik}(t+T)x_{jk}(t)] \tag{3.2}$$

Assuming that the disturbance is a white noise process,

$$E[\ f_k(\tau_1)f_k(\tau_2)] = \alpha_k \delta(\tau_1 - \tau_2) \tag{3.3}$$

where α_k is a constant and δ is the Dirac delta function. Under these conditions,

$$R_{ijk}(T) = \sum_{r=1}^{s} A_r e^{-\zeta_r \omega_{nr} T} \left[\alpha_r \cos \omega_{dr} T + \beta_r \sin \omega_{dr} T\right] \tag{3.4}$$

where

$$\begin{aligned} A_r &= \frac{\alpha^k \phi_{ri} \phi_{kr}}{m^r \omega_{dr}} \\ \alpha_r &= \sum_{s=1}^{n} \frac{\phi_{sj} \phi_{ks}}{m^s \omega_{ds}} \int_0^{\infty} e^{-(\zeta_r \omega_{nr} + \zeta_s \omega_{ns})\lambda} \sin \omega_{dr} \lambda \sin \omega_{ds} \lambda \; d\lambda \\ \beta_r &= \sum_{s=1}^{n} \frac{\phi_{sj} \phi_{ks}}{m^s \omega_{ds}} \int_0^{\infty} e^{-(\zeta_r \omega_{nr} + \zeta_s \omega_{ns})\lambda} \cos \omega_{dr} \lambda \sin \omega_{ds} \lambda \; d\lambda \end{aligned} \tag{3.5}$$

The quantity $\lambda = t - \tau$ and ω_d represents the damped natural frequency. For the r^{th} mode, $\omega_{dr} = \omega_{nr}\sqrt{1-\zeta_r^2}$ where $\omega_{nr},\ \zeta_r$ are the undamped natural frequency and the critical damping of the r^{th} mode, respectively. Making the substitution

$$s_r = e^{-\zeta_r \omega_{nr} T} \left[\alpha_r \cos \omega_{dr} T + \beta_r \sin \omega_{dr} T\right] \tag{3.6}$$

In matrix form, Eq. 3.4 becomes

$$\mathbf{r}(t) = \mathbf{R}(T) = \mathbf{A}_r \mathbf{s}_r(t) \tag{3.7}$$

In the above form, it is easy to recognize the similarity between Eq. 3.1 and Eq. 3.7, provided the correlation of the responses contained in $\mathbf{R}$ is used *in lieu* of $\mathbf{x}$. Therefore, under the cases of free vibration and broadband white excitations, the problem of modal identification can be cast into the framework of BSS, wherein the modes represent the independent sources and the modal coordinates are contained in the mixing matrix. An example of the auto and cross correlations of the floor accelerations for $3-DOF$ numerical model (see section 3.4 for relevant details) is shown in Fig. 3.1.

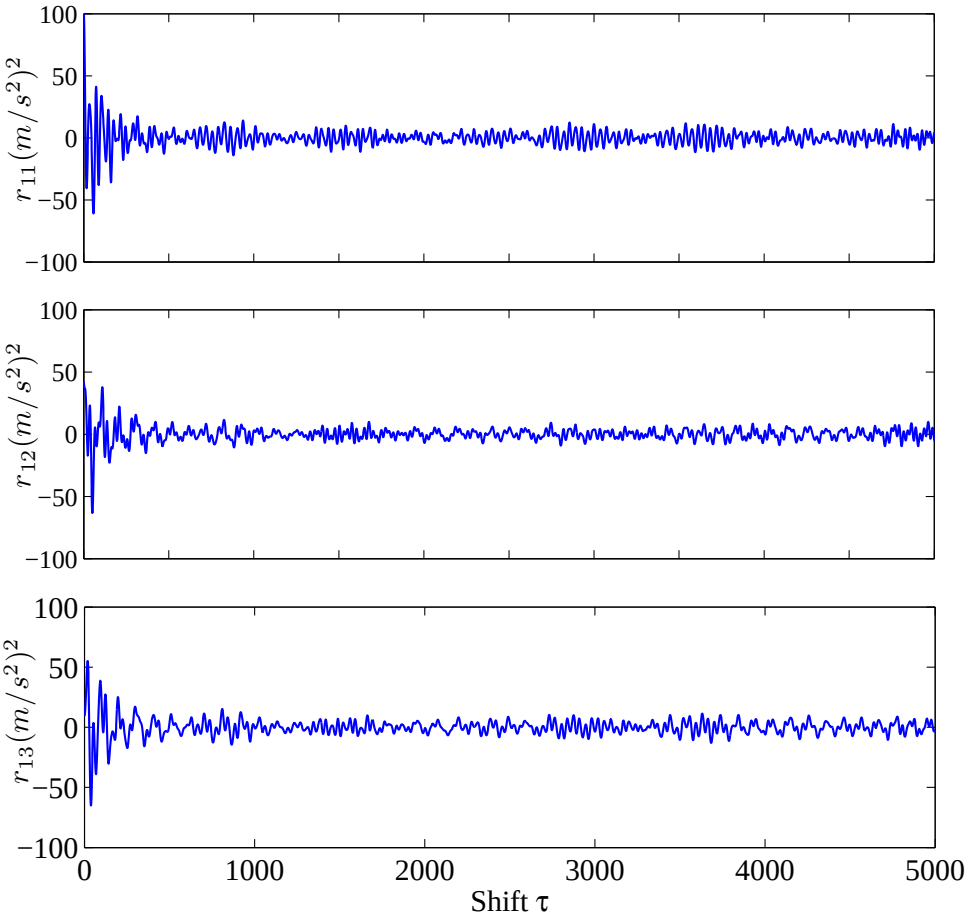

Figure 3.1: Auto and cross-correlation of the floor accelerations

3.3 Solution using Modified Cross-Correlation Method

Most popular BSS tools (perhaps, the only available class of methods for performing BSS), are ICA and SOBI. The details of ICA are discussed in chapter 2 and hence not repeated here. Since the MCC method is based on SOBI class of methods, the formulation is developed only for the MCC method, and key differences between SOBI and MCC methods are discussed within.

3.3.1 General Principles of MCC Method

SOBI methods utilize the time structure of the signals as opposed to treating them as mere random variables. For example, the auto-covariances for several time lags have well defined statistics. The SOBI family of methods do not make any prior assumptions of statistical independence or non-Gaussianity of sources; they rely purely on second order temporal statistics. The basic assumptions include full rank of the matrix $\mathbf{A}$, existence and spatial non-correlation of the stationary sources, and the presence of independent random noise.

The proposed MCC method deviates from SOBI in two key respects: (i) whereas SOBI method operates directly on the responses (measurements) $\mathbf{x}(t)$, the proposed MCC method operates on the correlation of the responses (vector, $\mathbf{r}(t)$) calculated at all time lags; (ii) whereas the diagonalization procedure in SOBI involves several time-lagged covariance matrices of the responses, covariance matrices obtained from multiple non-overlapping windows are used in the MCC method. This process is further illustrated in the numerical example following the formulation section.

In the presence of noise, the correlation of the measurements in Eq. 2.11 can be written as:

$$R_{ijk}(T) = E[(x_{ik}(t+T) + n_i)\,(x_{jk}(t) + n_j)] \tag{3.8}$$

where, $n_i,\ n_j$ represent noise at the i^{th} and j^{th} locations. Assuming that the noise is white, and the noise and responses are uncorrelated, then Eq. 3.8 is mathematically the same as Eq. 3.2. Hence, the problem of BSS can be treated as one of linear mixtures in Eq. 2.53 without the presence of additive noise. This means that the noise variance need not be known *a priori*, which is an advantage in using the MCC method. In contrast, the noise statistics are required in the traditional SOBI method (For details refer to APPENDIX C).

The next step is the simultaneous diagonalization of two covariance matrices $\hat{\mathbf{R}}_{\mathbf{r}}(0)$ and $\hat{\mathbf{R}}_{\mathbf{r}}(p)$ evaluated at the time-lag zero and p, defined as,

$$\begin{aligned} \hat{\mathbf{R}}_{\mathbf{r}}(0) &= E\left\{\mathbf{r}(k)\mathbf{r}^T(k)\right\} = \mathbf{A}_r\mathbf{R}_{\mathbf{s}}(0)\mathbf{A}_r^T \\ \hat{\mathbf{R}}_{\mathbf{r}}(p) &= E\left\{\mathbf{r}(k)\mathbf{r}^T(k-p)\right\} = \mathbf{A}_r\mathbf{R}_{\mathbf{s}}(p)\mathbf{A}_r^T \end{aligned} \tag{3.9}$$

where,

$$\mathbf{R}_{\mathbf{s}}(p) = E\left\{\mathbf{s}_r(k)\mathbf{s}_r^T(k-p)\right\} \tag{3.10}$$

The simultaneous diagonalization is performed using the following three basic steps: whitening, orthogonalization and unitary transformation. Whitening is a linear transformation in which, $\hat{\mathbf{R}}_{\mathbf{r}}(0) = (1/N)(\sum_{K=1}^{N}\mathbf{r}(k)\mathbf{r}^T(k))$ is first diagonalized using singular value decomposition, $\hat{\mathbf{R}}_{\mathbf{r}}(0) = \mathbf{V}_{\mathbf{r}}\mathbf{\Lambda}_{\mathbf{r}}\mathbf{V}_{\mathbf{r}}^T$ where $\mathbf{V}_{\mathbf{r}}$ are the eigenvectors of the co-variance matrix of $\mathbf{r}$. Then, the standard whitening is realized by a linear transformation expressed as,

$$\bar{\mathbf{r}}(k) = \mathbf{Q}\mathbf{r}(k) = \mathbf{\Lambda}_{\mathbf{r}}^{-\frac{1}{2}}\mathbf{V}_{\mathbf{r}}^T\mathbf{r}(k) \tag{3.11}$$

Because of whitening, $\hat{\mathbf{R}}_{\mathbf{r}}(p)$ becomes $\mathbf{R}_{\bar{\mathbf{r}}}(p)$, which is given by the equation,

$$\mathbf{R}_{\bar{\mathbf{r}}}(p) = (1/N)(\sum_{K=1}^{N}\bar{\mathbf{r}}(k)\bar{\mathbf{r}}^T(k-p)) = \mathbf{Q}\mathbf{R}_{\mathrm{r}}(p)\mathbf{Q}^T \tag{3.12}$$

The second step, called orthogonalization, is applied to diagonalize the matrix $\hat{\mathbf{R}}_{\bar{\mathbf{r}}}(p)$ whose eigen-value decomposition is of the form, $\hat{\mathbf{R}}_{\bar{\mathbf{r}}}(p) = \mathbf{V}_{\bar{\mathbf{r}}}\mathbf{\Lambda}_{\bar{\mathbf{r}}}\mathbf{V}_{\bar{\mathbf{r}}}^T$. Using the Eq. 3.12 and Eq. 3.9,

$$\hat{\mathbf{R}}_{\bar{\mathbf{r}}}(p) = \mathbf{Q}\mathbf{A}_r\mathbf{R}_{\mathbf{s}}(p)\mathbf{A}_r^T\mathbf{Q}^T \tag{3.13}$$

If the diagonal matrix $\mathbf{\Lambda}_{\bar{\mathbf{r}}}$ has distinct eigen-values, then the mixing matrix can be estimated uniquely by the equation,

$$\hat{\mathbf{H}} = \mathbf{Q}^{-1}\mathbf{V}_{\bar{\mathbf{r}}} = \mathbf{V}_{\mathbf{r}}\boldsymbol{\Lambda}_{\mathbf{r}}^{1/2}\mathbf{V}_{\bar{\mathbf{r}}} \tag{3.14}$$

where, $\hat{\mathbf{H}}$ is the estimated mixing matrix, $\mathbf{A}_r$. It is easy to see that the product $\mathbf{QA}_r$ is a unitary matrix since the sources are assumed to be uncorrelated and scaled to have a unit variance. The problem now becomes one of unitary diagonalization of the correlation matrix $\hat{\mathbf{R}}_{\bar{\mathbf{r}}}(p)$ at one or several non-zero time lags.

Eq. 3.13 is a key result, which states that the whitened matrix $\hat{\mathbf{R}}_{\bar{\mathbf{r}}}(p)$ at any non-zero time lag p is diagonalized by the unitary matrix $\mathbf{QA}_r$. Since $\mathbf{R}_s(p)$ is a diagonal matrix (the sources are assumed to be mutually uncorrelated), the problem now becomes one of diagonalizing the matrix $\hat{\mathbf{R}}_{\bar{\mathbf{r}}}(p)$ resulting in the unitary matrix, $\mathbf{QA}_r$. The existence of the unitary matrix for any time lag p is guaranteed by Eq. 3.13, and the determination of the unitary matrix is carried out using a numerical procedure.

3.3.2 Joint Diagonalization for p Lags and L Time Windows

As seen in Eq. 3.13, the problem of finding $\mathbf{A}_r$ is solved by unitarily diagonalizing $\hat{\mathbf{R}}_{\bar{\mathbf{r}}}(p)$. Due to estimation errors, finding an exact diagonalizing unitary matrix may not be possible and estimating $\mathbf{QA}_r$ is possible only in an approximate sense. Another issue is that the information of the proper choice of the lag parameter p is not available *a priori*. Hence, in this study, several values of time lags, $p = 1, 2, \cdots, l$ are chosen, and the matrices $\hat{\mathbf{R}}_{\bar{\mathbf{r}}}(p)$ are diagonalized for L non-overlapping windows such that after h iterations the sum of the off-diagonal terms for all the time lags are minimum in a norm sense. In other words, the set of L co-variance matrices to be jointly diagonalized (APPENDIX E) appear as:

$$\left\langle \hat{\mathbf{R}}_{\bar{\mathbf{r}}}(p) \right\rangle = \left\{ \underset{1}{\begin{bmatrix} . & \cdots & \\ \vdots & \ddots & \\ & & \ddots \end{bmatrix}} \underset{2}{\begin{bmatrix} . & \cdots & \\ \vdots & \ddots & \\ & & \ddots \end{bmatrix}} \cdots \cdots \underset{L}{\begin{bmatrix} . & \cdots & \\ \vdots & \ddots & \\ & & \ddots \end{bmatrix}} \right\}$$

Denoting $\mathbf{V} = \mathbf{Q}\mathbf{A}_r$, $\mathbf{D}^p = \mathbf{V}^T \hat{\mathbf{R}}_{\bar{\mathbf{r}}}(p)\mathbf{V}$, we can write the problem statement mathematically as finding the minimum of the performance index J given by,

$$J(\mathbf{V}, p) = \sum_{L} \sum_{1 \le i \ne j \le m} \left| D_{ij}^{p} \right|^2 \tag{3.15}$$

Then, the unitary matrix $\mathbf{V}$ corresponding to minimum J over fixed h iterations is said to be an approximate joint diagonalizer. The joint-approximate diagonalization technique [10] is utilized to approximately diagonalize the L windowed non-overlapping matrices. Prior to the diagonalization process, the covariance matrices are symmetrized according to $\hat{\mathbf{R}}_{\bar{\mathbf{r}}}(p) = \frac{1}{2}\left(\hat{\mathbf{R}}_{\bar{r}}(p) + \hat{\mathbf{R}}_{\bar{r}}^{T}(p)\right)$ [7].

The diagonalization is performed for several time lags p, and the non-stationary aspect of the sources is addressed by partitioning the pre-whitened data into L non-overlapping blocks. The partitioning procedure is illustrated in Fig. 3.2 by considering the responses of the $3-DOF$ system (see Section 3.4 for details). The shifted covariance matrices are then estimated in each window and the covariance matrices are stacked column-wise for each lag and jointly diagonalized for $i = 1, 2, ..., p$ lags. The selection of p and L is problem dependent, the details of which are discussed in the next section, and the computations are performed in MATLAB (The MathWorks®).

A summary of the key steps involved in the MCC method are summarized below.

1. Calculate the correlations of the responses to obtain the vector $\mathbf{r}$

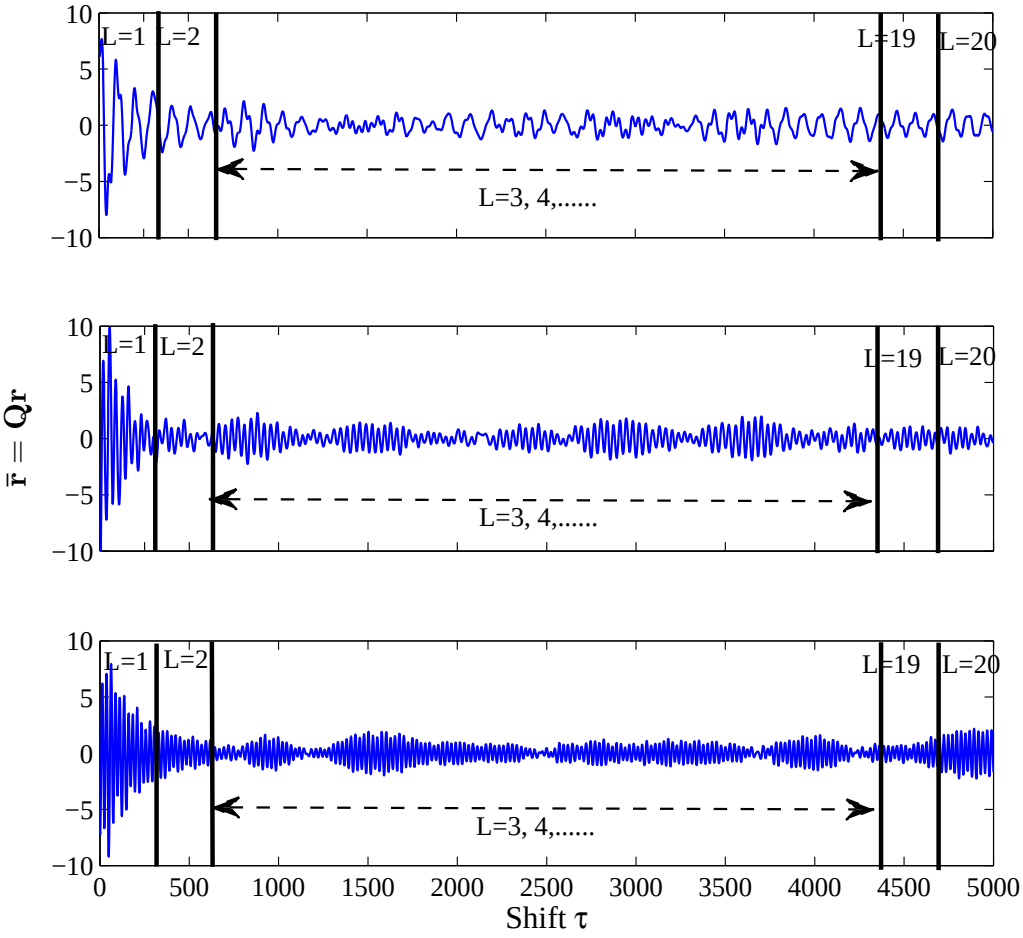

Figure 3.2: Windowing procedure for the whitened responses

2. Obtain the whitened vector $\bar{\mathbf{r}}(k) = \mathbf{Q}\mathbf{r}(k)$

3. Divide $\bar{\mathbf{r}}(k)$ into L non-overlapping blocks (Fig. 3.2) and estimate the set of covariance matrices $\hat{\mathbf{R}}_{\bar{\mathbf{r}}}(T_i, p)$ for $i = 1, \cdots, L \forall p$

4. Find an unitary matrix that approximately diagonalizes the set of L matrices at each lag, p, $\mathbf{V} \forall \left\langle \hat{\mathbf{R}}_{\bar{\mathbf{r}}}(p) \right\rangle$ using the criterion shown in Eq. 3.15

5. The mixing matrix is computed as $\hat{\mathbf{H}} = \mathbf{Q}^{-1}\mathbf{V}$

The above procedure can be extended to take multiple lags into account by first calculating the average co-variance matrix $\hat{\mathbf{R}}_{\bar{\mathbf{r}}}$ for several non-zero lags p, and then utilize this averaged covariance matrix for L non-overlapping windows to perform the approximate diagonalization. The resulting matrix can be viewed as an *averaged covariance matrix* and the process of diagonalization then proceeds exactly as outlined earlier. A summary of the results is explained next.

3.4 Numerical Study

3.4.1 Structural model and simulation parameters

Numerical simulations are carried out on a simple three degree-of-freedom (3DOF) mass, spring, and dashpot system, shown in Fig. 3.3. For convenience in studying the effect of damping, the damping is assumed to be mass proportional. The state equations (see APPENDIX **A** for details) for this system subjected to an external excitation vector $\mathbf{w}$ can be written as:

$$\begin{aligned} \dot{\mathbf{x}} &= \mathbf{A}\mathbf{x} + \mathbf{E}\,\mathbf{w} \\ \mathbf{y} &= \widetilde{\mathbf{C}}\mathbf{x} \end{aligned} \tag{3.16}$$

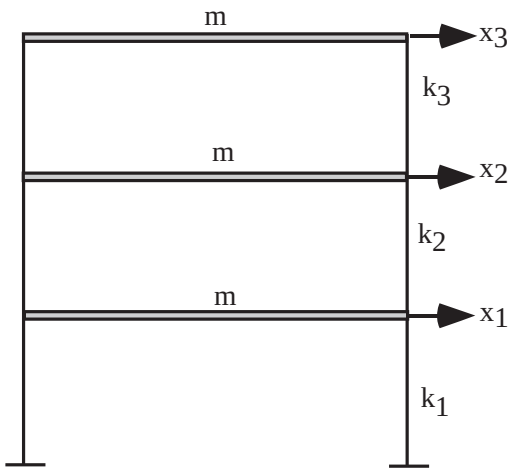

Figure 3.3: 3−DOF model

Here, the vector **x** is a vector of states, and the vector **y** represents the output vector, which is governed by the $\widetilde{\mathbf{C}}$ matrix. The system matrix **A**, and the excitation matrix **E** are given by :

$$\begin{aligned} \mathbf{A} &= \begin{bmatrix} [\mathbf{0}]_{3\times3} & [\mathbf{I}]_{3\times3} \\ -\mathbf{M^{-1}K} & -\mathbf{M^{-1}C} \end{bmatrix} \\ \mathbf{E} &= \begin{bmatrix} 0 & 0 & 0 & -\frac{1}{m} & -\frac{1}{m} & -\frac{1}{m} \end{bmatrix}^T \end{aligned} \tag{3.17}$$

The system matrices **M, C, K,** are written as under :

$$\mathbf{M} = \begin{bmatrix} m & 0 & 0 \\ 0 & m & 0 \\ 0 & 0 & m \end{bmatrix};\ \mathbf{C} = \begin{bmatrix} c & 0 & 0 \\ 0 & c & 0 \\ 0 & 0 & c \end{bmatrix};\ \mathbf{K} = \begin{bmatrix} k_1+k_2 & -k_2 & 0 \\ -k_2 & k_2+k_3 & -k_3 \\ 0 & -k_3 & k_3 \end{bmatrix} \tag{3.18}$$

where, m represents the mass at each floor level which is 10 kg, c is the damping coefficient, and $k_1,\ k_2$, and k_3 correspond to the linear stiffness at each degree of freedom.

Constant stiffness of 2 kN/m is used for the springs, and the mass-proportional form for damping coefficient, $c = \alpha m$ is used, where, $\alpha = 0.01\eta$. The system is simulated using stationary and non-stationary gaussian white noise excitation of zero mean and unit variance sampled at 100 Hz. The responses are obtained by solving the Eq. 3.16 in time domain by numerical integration at each time step using runge-kutta 4^{th} order solver ODE-45 in MATLAB. The natural frequencies of the system are 1, 2.8 and 4.05 Hz respectively. The variable η is used to vary the level of damping to study the performance of the BSS methods. The correlation between the vibration modes and BSS modes is performed using the modal assurance criterion (MAC) [65]. MAC values range between 0 and 1, a value of 1 meaning a perfect correlation. MAC is defined as:

$$MAC_i = \frac{(\psi_i^T \bar{\psi}_i)^2}{(\psi_i^T \psi_i)(\bar{\psi}_i^T \bar{\psi}_i)} \tag{3.19}$$

Here, ψ_i and $\bar{\psi}_i$ represent the i^{th} theoretical and the estimated mode shape vectors respectively. The effect of increasing the damping parameter η is studied first, and the results are presented in Table 3.1. The results of ICA, SOBI and MCC methods are presented along with the Stochastic Sub-space Iteration [83] method. SSI is included in this study as a point of reference for other BSS methods, as SSI has been used extensively in the structural system identification literature. The details of SSI have been documented in the previous chapter, and not repeated here for the sake of brevity.

3.4.2 Results

The effect of damping is achieved by gradually increasing the value of η from 10 to 165 which corresponds to a range of 0.8 %-13% critical damping in the first mode. From the results in Table 3.1, it is clear that ICA can identify structures only for small levels of damping. MAC values begin to deteriorate beyond $\eta = 18$, which corresponds to 1.4 %

critical damping in the first mode. SOBI identifies the structural model relatively well compared to ICA and outperforms both ICA and SSI in terms of MAC values. The effect of damping on the deterioration of the performance of ICA has also been observed by other researchers [54]. The MCC method performs relatively better, especially at higher values of damping. These results are clearly evident in Fig. 3.4, where the lowest MAC value (MAC3, which is the least amongst the three MACs) is shown for all the methods as a function of η.

The results in Table 3.2 correspond to the case when an amplitude modulating function of the type $e^{-\lambda t}(\lambda = 0.5$ is used in this study) is applied to a Gaussian white noise. The effect of non-stationarity is clearly evident in the results of the SOBI method, which performs poorly at higher values of η compared to MCC. The results of SSI and SOBI methods are comparable. From these results, it is clear that considering several time-lagged windows has a significant effect on the identification results, especially for the case of non-stationary sources.

3.4.3 Effect of p and L

In order to study the effect of the time lag p and the number of time-windows L, simulations are carried out for p ranging from 1-100 for the 3DOF system described in the previous section. The effect of non-stationarity of the sources is analyzed by dividing $\bar{\mathbf{r}}(k)$ into several time blocks, ranging from a single window ($L = 1$) to $L = 50$. The correlations of the floor acceleration responses are shown in Fig. 3.1. The corresponding whitened quantities are partitioned into L non-overlapping windows for an arbitrary value of lag p (whitened responses are shown in Fig. 3.2) and the covariance matrices are calculated.

Table 3.1: Comparison of ICA, SOBI and SSI methods for various η

η	Mac1	Mac2	Mac3	Mac1	Mac2	Mac3	Mac1	Mac2	Mac3	Mac1	Mac2	Mac3
–	–	ICA	–	–	SOBI	–	–	SSI	–	–	MCC	–
10	1	1	1	1	1	1	1	1	1	1	1	1
15	1	1	0.99	1	1	1	1	1	1	1	1	1
18	0.99	0.77	0.64	1	1	1	1	1	0.99	1	1	1
20				0.99	0.99	0.99	0.99	0.98	0.98	1	1	1
30				0.99	0.99	0.99	0.99	0.97	0.97	1	1	1
50				0.99	0.99	0.99	0.94	0.92	0.91	1	1	1
100				0.99	0.99	0.99	0.9	0.82	0.8	1	1	1
150				0.98	0.98	0.97	0.86	0.74	0.72	1	0.99	0.99
165				0.97	0.96	0.95	0.81	0.7	0.67	0.99	0.99	0.98

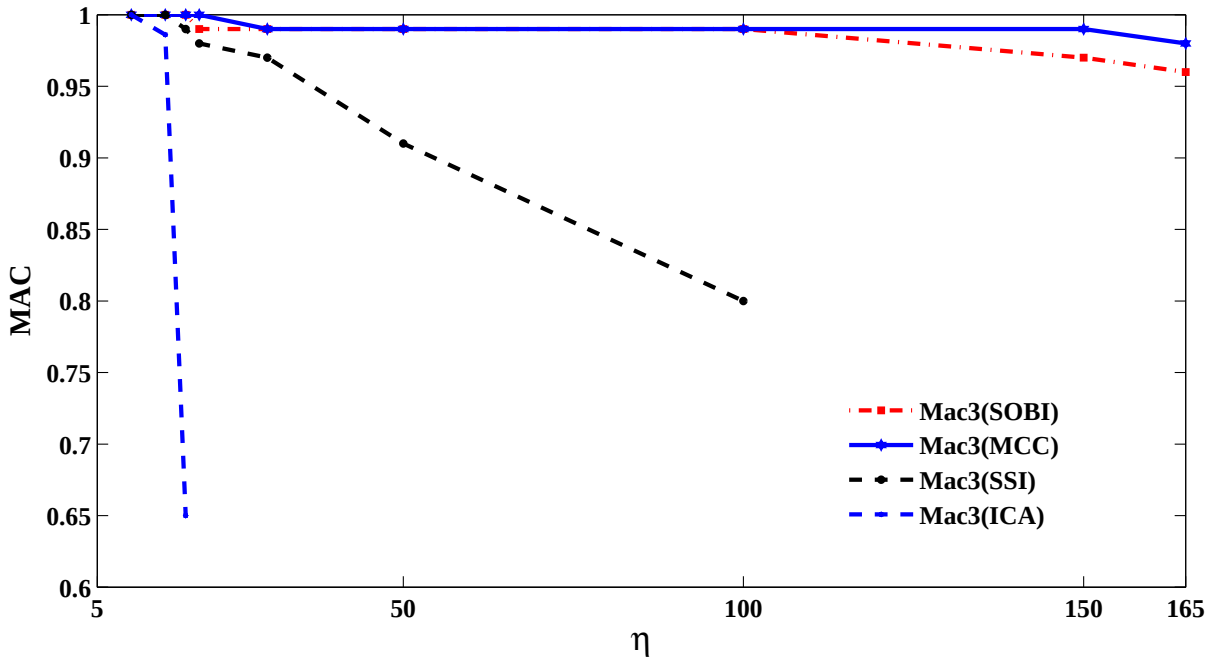

Figure 3.4: Effect of damping on identification

Table 3.2: Comparison of MCC, SOBI and SSI methods for the case of non-stationary white noise

η	Mac1	Mac2	Mac3	Mac1	Mac2	Mac3	Mac1	Mac2	Mac3
–	–	SOBI	–	–	SSI	–	–	MCC	–
10	1	1	1	1	1	1	1	1	1
15	1	1	1	1	1	1	1	1	1
18	1	1	0.98	0.99	0.98	0.99	1	1	1
20	0.99	0.96	0.94	0.96	0.94	0.97	1	1	1
30	0.98	0.92	0.89	0.91	0.89	0.90	1	1	1
50	0.98	0.89	0.81	0.87	0.82	0.83	0.99	0.99	1
100	0.91	0.86	0.76	0.83	0.78	0.72	0.99	0.99	1
150	0.89	0.81	0.71	0.8	0.7	0.62	0.99	0.99	1
165	0.86	0.75	0.65	0.7	0.57	0.6	0.99	0.99	1

The results of the effect of the time lag p and the number of time-windows L are displayed in Fig. 3.5. From the results in Fig. 3.5 it is clear that accounting for the non-stationary characteristics of the sources by using multiple windows achieves better performance, as indicated by the square root of the sum of squares of the off-diagonal terms, than the case when a single window is used to calculate the covariance matrix for several time lags. However, from the results presented here, it is safe to conclude that the optimal values of p and L are problem dependent. Specifically, since the total length of the signal was fixed, the performance of the algorithm is dependent not only on the number of windows, but also on the sample length in each window. For the ensuing experimental study, and for the numerical simulations on a full-scale tower structure (discussed after the experimental results), $p = 50$ and $L = 20$ are used. It is worth noting that the *averaged co-variance*

matrices within each window yielded similar results to the case when a single lag was used.

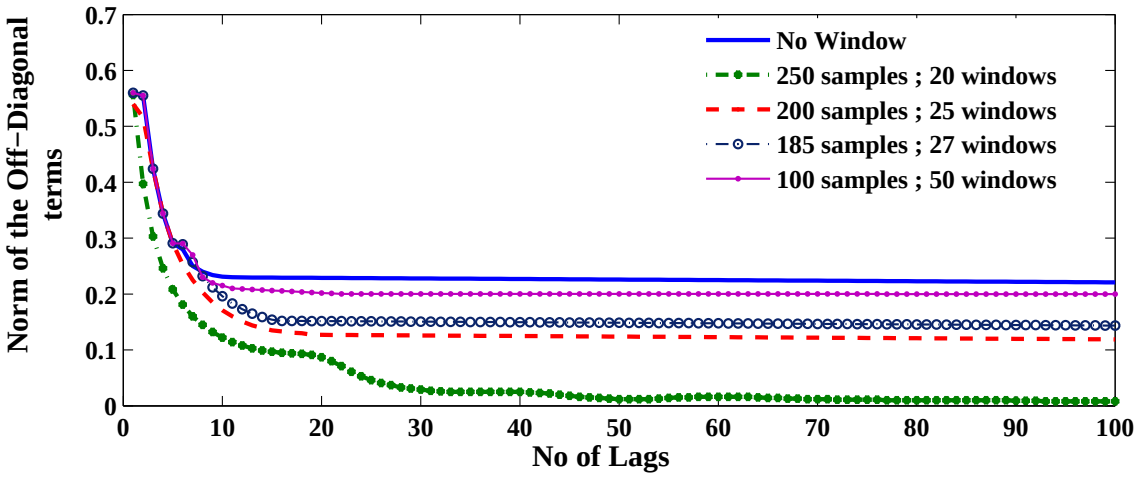

Figure 3.5: Effect of window and number of lags on the joint diagonalization for non-stationary responses

3.5 Experimental Study

3.5.1 Experimental Model

In order to demonstrate the practical application of this method, an experiment is conducted to identify the translational frequencies and modes of a two-story model shown in Fig. 3.6. The model consists of two steel plates of dimensions $30 \times 30 \times 1.9$ cm to serve as floor masses, four 1.25 cm aluminum equal angles to serve as columns with a total height 140 cm and 0.16 cm thick and continuous between both the floors. The top story is braced in one direction using aluminum bars of dimensions $0.3 \times 0.95 \times 1.25$ cm. The model is instrumented at both the floor levels, in both the directions, using four accelerometers.

The structure is subjected to impact excitation using a rubber mallet, and the acceleration data is collected using DSPACE1104 DAQ and control board. The sampling frequency is set at 100 Hz.

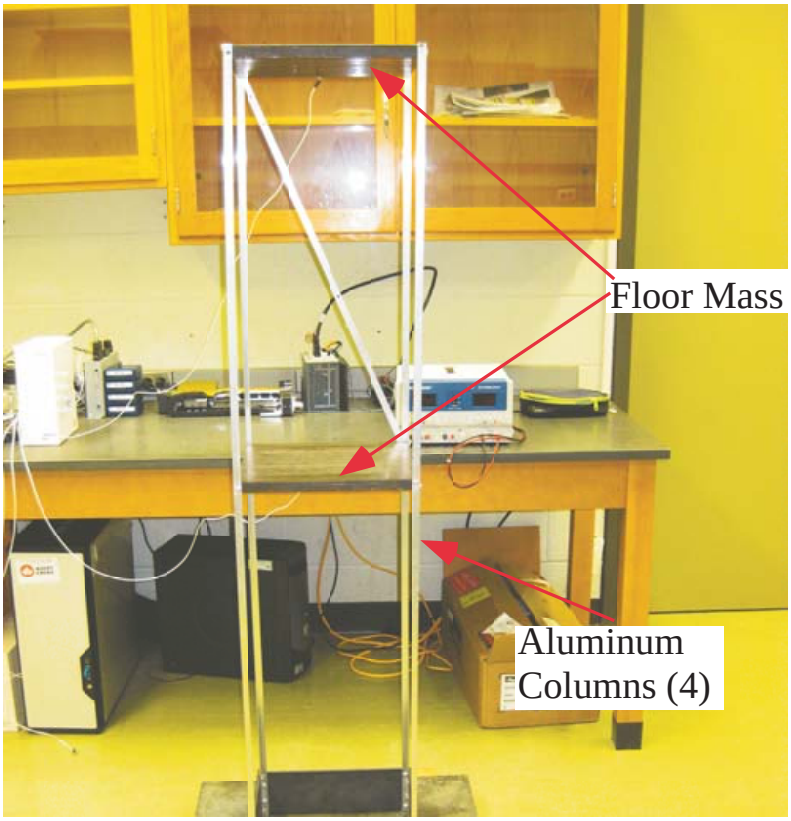

Figure 3.6: Experimental model

3.5.2 Results

The power spectral density plot of the recorded response of the second floor is shown in Fig. 3.7. The recorded acceleration responses are processed using both MCC method and SSI method without performing any post-processing on the data (such as de-noising, etc.). The results of the identification are presented in Table 3.3. The MAC numbers comparing SSI and MCC methods show that the quality of identification is comparable in both these

methods, and the identified frequencies correspond well with the peaks in the PSD estimate shown in Fig. 3.7. This shows that the MCC method is well equipped to handle practical measurement data as well, at least for the case of impact excitation considered in this paper. A detailed simulation study is performed next using a realistic structural model excited by synthetic wind and earthquake time histories.

Table 3.3: System-identification of the experimental model

Mode #	Identified Frequency(Hz) MCC	Identified Frequency(Hz) SSI	Modal Amplitude Coherence (SSI)	MAC (SSI-MCC)
1	1.37	1.41	0.96	0.96
2	1.46	1.41	0.98	0.97
3	4.74	4.75	0.99	0.99
4	32.16	32.17	1	0.99

3.6 Full-Scale Simulation Study

3.6.1 The Tower model

A full-scale tower structure is considered next. The model of this structure is based on an actual structure (name withheld) located in Toronto, Canada, and consists of 13 floors plus the roof, with a total height of 40 m. The structural system comprises of steel frames, composite steel decks, concrete floor and roof system. The model was produced using the commercially available finite-element program, SAP2000 (CSI, Berkeley 2008). The geometry, materials, and sections are determined from the structural and architectural design drawings. The model (Fig. 3.8) comprises of 1208 joints and 2386 stiffness degrees

of freedom (DOF). 1% critical damping is assumed for the first two modes, and the form of the damping matrix is assumed to be of Rayleigh type.

In order to conduct the identification study, the number of DOF is limited to the DOF corresponding to the center of mass of all the floor levels, using the rigid diaphragm assumption, resulting in a total of 42 DOF. This model was further reduced to 18 DOF using the system equivalent reduction expansion process [73]. In order to satisfy the full rank condition for the mixing matrix, the number of sensors need to be equal to, or greater than the number of sources. For this study, all the 18 DOF are assumed to be measured, resulting in a square mixing matrix. It is observed that utilizing either the displacements or the accelerations result in nearly identical identification results.

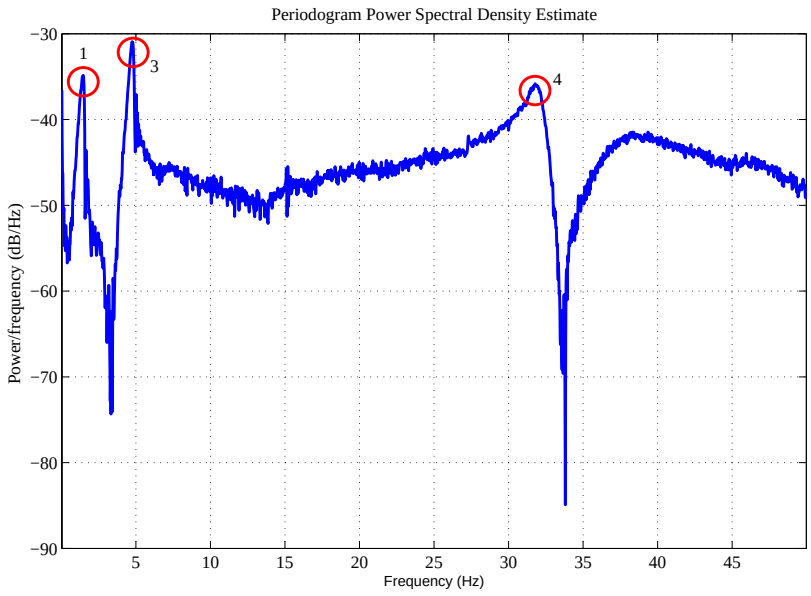

Figure 3.7: PSD estimate of the top floor response

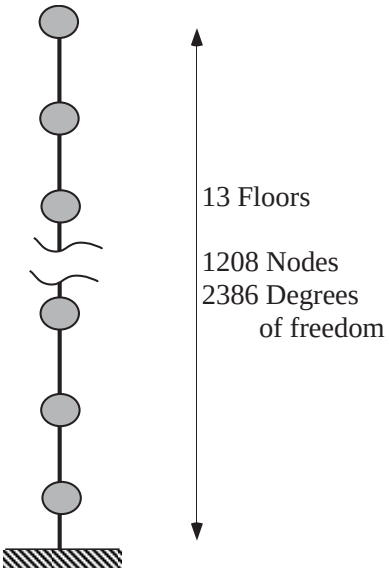

Figure 3.8: Schematic of the full-scale tower structure

Two types of excitations are considered, stationary wind and non-stationary earthquake. Before the results for both these cases are discussed, the method used to generate the wind time histories is briefly reviewed. Synthetic time-histories for the turbulent fluctuations in the longitudinal and transverse directions, and vortex shedding in the transverse direction are simulated. For this purpose, an auto-regressive moving average (ARMA) model [77, 17] to simulate a stationary correlated Gaussian source with zero mean and unit variance is utilized. Scaled time histories corresponding to various heights of the tower are generated using this procedure and used to excite the state-space model in two directions, simultaneously. Brief details of this procedure are given in the APPENDIX D, and the readers are referred to other references on this topic [77, 17] for details. In order to simulate earthquake response of the structure, scaled El Centro ground motion (scaled to peak $0.1g$) is used. A short note on the types of excitations considered in this study: Synthetic wind excitations generated from stationary gaussian white noise process are quasi-stationary with respect to the structure in the sense that the excitation depends

on the height of the structure. Earthquake excitations on other hand are non-stationary in nature since the variance changes with time. Unlike wind and white noise, they are not necessarily broad band. Impact loads on other hand are of transient type whose responses don't sustain but decay with time.

3.6.2 Results

From the results presented in Tables 3.4 and Table 3.5, it is clear that the MCC method is capable of identifying the eigen properties of the structure with a good degree of confidence as reflected in the MAC values nearly equal to 1. Sample identification results for the sources in the time-domain are shown in Fig. 3.9. The results show that the MCC method is capable of handling non-stationary sources equally well, which is promising from a structural modal identification standpoint.

3.7 Summary

In this chapter, BSS methods have been studied in the context of structural system identification. Clearly, ICA, one of the potential candidates to perform BSS, fails to perform adequately in the presence of even relatively small amounts of damping. In this regard, SOBI performs much better. The MCC method, which is an extension of the traditional SOBI technique, was developed and shown to perform well under both stationary and non-stationary excitations. The ability to identify modal information even at higher levels of damping demonstrates that the MCC method holds significant promise in the area of structural system identification. Preliminary experimental results show that the MCC method is capable of performing satisfactorily under practical situations.

Table 3.4: Results for the case of the tower subjected to wind excitation

Mode #	Model f(Hz)	Identified f(Hz)	MAC	Error f(%)	Error ζ(%)
1	0.66	0.66	1.00	0.00	0.1
2	0.92	0.91	0.99	1.10	0.1
3	1.40	1.39	0.99	0.72	0.2
4	2.73	2.70	0.98	1.25	0.85
5	3.01	2.97	0.97	1.43	0.95
6	3.36	3.35	0.99	0.30	0.35
7	4.59	4.59	0.99	0.00	0.45
8	6.08	5.97	0.96	1.89	1.3
9	6.71	6.52	0.94	2.91	1.85
10	9.01	9.00	0.99	0.11	0.45
11	9.43	9.29	0.98	1.51	0.93
12	10.09	10.06	0.99	0.30	0.40
13	11.20	11.09	0.98	0.99	0.40
14	12.02	11.96	0.98	0.50	0.90
15	13.83	13.82	0.99	0.10	0.51
16	14.41	14.29	0.98	0.84	0.92
17	15.72	15.71	0.99	0.06	0.75
18	16.84	16.69	0.98	0.89	1.2

Even though MCC performs well for the cases studied, it requires complete response measurements to perform satisfactorily. As well, the method does not account for situations where the separability of sources is not adequate due to their insufficient energy content. This issue is addressed in detail in the forthcoming chapter.

Table 3.5: Results for the tower subjected to El-centro(0.1g) ground motion

Mode #	Model f(Hz)	Identified f(Hz)	MAC	Error f(%)	Error ζ(%)
1	0.66	0.66	1.00	0.00	0.25
2	0.92	0.92	1.00	0.55	0.35
3	1.40	1.39	1.00	0.57	0.47
4	2.73	2.71	1.00	0.88	1.00
5	3.01	2.98	0.97	1.09	0.65
6	3.36	3.35	1.00	0.30	0.55
7	4.59	4.59	1.00	0.00	0.45
8	6.08	5.98	0.96	1.66	1.86
9	6.71	6.62	0.94	1.36	1.94
10	9.01	9.00	1.00	0.11	0.52
11	9.43	9.30	0.99	1.40	1.45
12	10.09	10.04	1.00	0.50	0.71
13	11.20	11.01	0.98	1.73	1.52
14	12.02	11.97	1.00	0.42	0.52
15	13.83	13.81	1.00	0.17	0.62
16	14.41	14.39	1.00	0.14	0.73
17	15.72	15.70	1.00	0.13	0.83
18	16.84	16.80	1.00	0.23	0.81

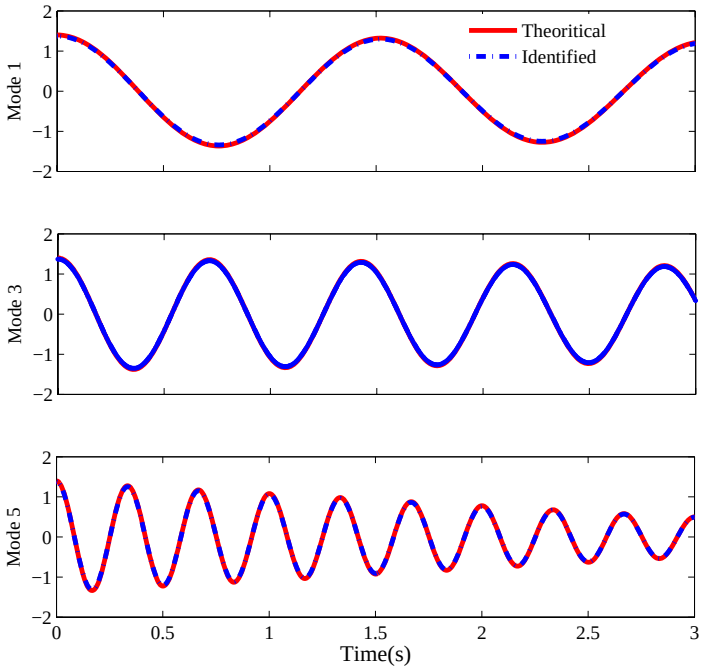

Figure 3.9: Comparison of the modal responses and the identified sources for the tower structure subjected to wind excitation

Chapter 4

Wavelet-Based Modified Cross Correlation Method

This chapter presents the theoretical development of a new hybrid time and time-frequency source separation method called the wavelet based modified cross correlation method(WMCC). The WMCC method extends the concept of MCC to improve the separability of sources with low energy content, and to identify full-scale structures subjected to ambient excitations. The chapter is organized as follows. The fundamental concepts of discrete wavelet transform (DWT) and stationary wavelet transform (SWT), central to the development of the proposed methodology, are reviewed first. The formulation of WMCC method is presented next, followed by the results of the numerical simulation of a simple three degree-of-freedom mass, spring, and dashpot system. Finally, the results of identification are presented for the *UCLA Factor Building*, using recorded ambient vibration data, and also for recorded responses from the Parkfield earthquake, followed by the main summary of this study.

4.1 Motivation

In the previous chapter, the concepts of SOBI were extended to develop MCC method which clearly showed improved results for the case of nonstationary input using all the available response measurements. In the previous case, the energy content in all the modes was sufficient to facilitate successful extraction. These conditions, however, are difficult to be fulfilled in large real life structures, whose higher modes are likely to have lower energy contents. Achieving accurate identification of such structures with many vibrating modes, operating on time-domain alone, is a not an easy task. Moreover, when the number of instrumented sensors are constrained to be fewer than the possible degrees of freedom (due to cost or other considerations), the separability of sources becomes even more challenging. Motivated by these practical performance issues the basic principles of SOBI for the static mixtures case are extended using the stationary wavelet transform (SWT) in order to improve the quality of identification. The wavelet basis provides a sparse representation of the sensors and sources. The basic idea of sparsity is that owing to the smoothness, compactness, rapid decaying characteristics and vanishing higher order moments of the wavelet basis, the wavelet coefficients of sensors and sources retain all the useful information content of the signal and throw away the unnecessary contributions from noise. This improves the spectral characteristics of the signals: make them more localized, compact, smooth and noise free. This is the first hybrid time and time-frequency method explored in this thesis.

4.2 Background on Wavelet Transforms

Wavelet transforms have gained significant attention in the literature for the purposes of structural identification and health monitoring [32, 59, 55, 41, 8]. The wavelet transforms provide a useful way of representing signals by the use of basis functions that satisfy certain

properties of linear vector spaces in $\Re^3$. The use of sinusoidal basis in fourier transforms hinders the non-stationary properties of system response to be captured, which seriously limits its application in ambient system identification. As the fourier basis functions are localized in frequency but not in time, an alternative to accommodate the time information by the use of short time fourier transform (STFT)was introduced [66]. However, due to fixed nature of the window function used in STFT, the obtainable time and frequency resolutions are considerably constrained by virtue of the Hiesenberg's uncertainty principle, according to which it is impossible to achieve good time and frequency resolutions simultaneously. This motivated the development of another alternative approach to time-frequency representation of signals, featuring basis functions that have compact support both in frequency and time to yield a multiresolution analysis of signals termed as wavelet transform [66].

The wavelet transform of a signal $x(t)$ is a linear transform, defined as :

$$w_k^j(x) = \frac{1}{\sqrt{j}} \int_{-\infty}^{\infty} x(t)\, \psi_k^{j*}(t)\, dt \tag{4.1}$$

where the function ψ is commonly known as the mother wavelet and $*$ stands for complex conjugation. j and k denotes scale and translation parameters respectively. Thus, wavelet transform decomposes a signal $x(t)$ via basis functions, that are simply scaled and translated versions of the mother wavelet. Wavelet transforms can be broadly classified under two categories: (i) Non redundant wavelet transforms (ii) Redundant wavelet transforms. Discrete wavelet transform (DWT) belongs to the former category, and continuous wavelet transforms (CWT) and stationary wavelet transforms (SWT) belong to the later. Due to numerical integration procedures, estimation of CWT requires lot of computational effort and is not pursued here. On other hand, implementation of DWT and SWT with the aid of filter banks make them more robust and amenable for BSS applications. In this section, a brief background on DWT and SWT are presented with special emphasis on

their time-invariant properties.

4.2.1 Discrete Wavelet Transform (DWT)

In the context of multi-resolution analysis [66], an orthogonal wavelet decomposition of a signal, $x(t) \in L^2(\Re)$ leads to wavelet co-efficients given by the inner product

$$w_k^j(x) =< x(t), \frac{1}{2^{j/2}}\psi(\frac{t}{2^j} - k) >= \frac{1}{2^{j/2}} \int_{-\infty}^{\infty} x(t)\psi^*(\frac{t}{2^j} - k)\ dt = \frac{1}{2^{j/2}} \int_{-\infty}^{\infty} x(t)\psi_k^{j*}(t)\ dt \quad (4.2)$$

where the function ψ is commonly known as the mother wavelet and $*$ stands for complex conjugation. The transform is computed at discrete values on a grid corresponding to dyadic values of scales (2^j) and translations (k), where $k,\ j \in Z^2$ i.e., integers. This is commonly known as the discrete wavelet transform (DWT). A signal *x(t)* can be expressed in terms of wavelet coefficients w_j^k as

$$x(t) = \sum_j \sum_k w_k^j \psi_k^j \quad (4.3)$$

The basis function ψ and its integer translates $\psi(t-k)$ satisfy the condition of orthogonality [66]. For fast implementation, the integration procedures are replaced by successive application of filter banks [66].

Implementation of DWT to a signal x involves low-pass filtering followed by high pass filtering using appropriate filters, known as quadrature mirror filters. The co-efficients resulting from these filtering operations are known as approximation and detail coefficients. However, since half of the frequencies of the signal have now been removed, half of the samples can be discarded according to Nyquists rule. Thus, the filter outputs are then sub-sampled by a factor 2 [66] as shown in the Fig. 4.1. Details of DWT implementation

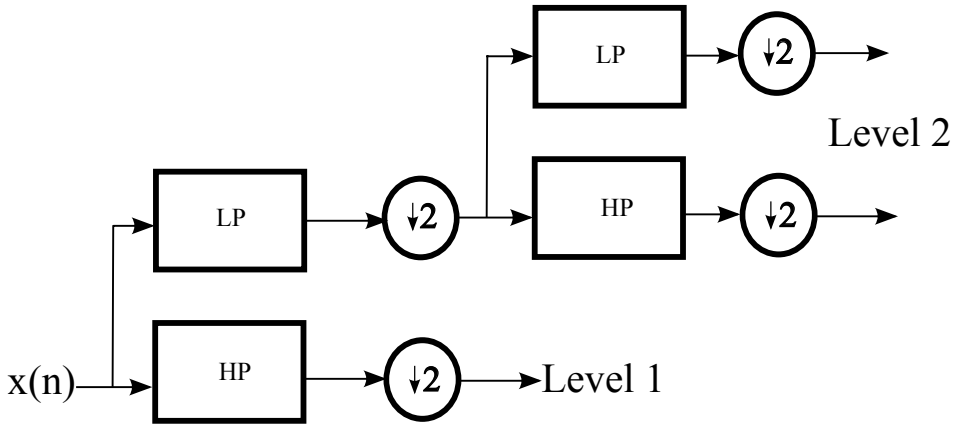

Figure 4.1: Filter bank implementation of DWT

are beyond the scope of this work and the readers are referred to seminal works [66] on the topic for details.

Of interest here is the issue of time non-invariance that arises due to the DWT procedure. This means that the wavelet coefficients of a time shifted signal, say $x(t-\tau)$, are not delayed versions of the transform of the original signal. That is:

$$w_k^j(x(t-\tau)) \neq w_{k-\tau}^j(x(t)) \tag{4.4}$$

The invariance issue shown above can be addressed through a redundant version of the DWT, which is called SWT as explained in the following.

4.2.2 Stationary Wavelet Transform (SWT)

Consider the following transform, known as the stationary wavelet transform (SWT), of $x(t)$ [70, 28].

$$d_k^j \triangleq \left\langle x(t) \;\middle|\; 2^{-j/2}\psi\left(\frac{t-k}{2^j}\right)\right\rangle = \frac{1}{2^{j/2}}\int_{-\infty}^{\infty} x(t)\psi^*\left(\frac{t-k}{2^j}\right)dt \tag{4.5}$$

The basic idea of SWT is similar to DWT, where the time sequence whose transform is to be carried out is applied through appropriate high and low pass quadrature mirror filters to produce two sequences at the next level. But unlike DWT, the coefficients are not decimated, but up-sampled, and hence the filtered sequences have the same length as the original sequence. The implementation of SWT is illustrated in Fig. 4.2.

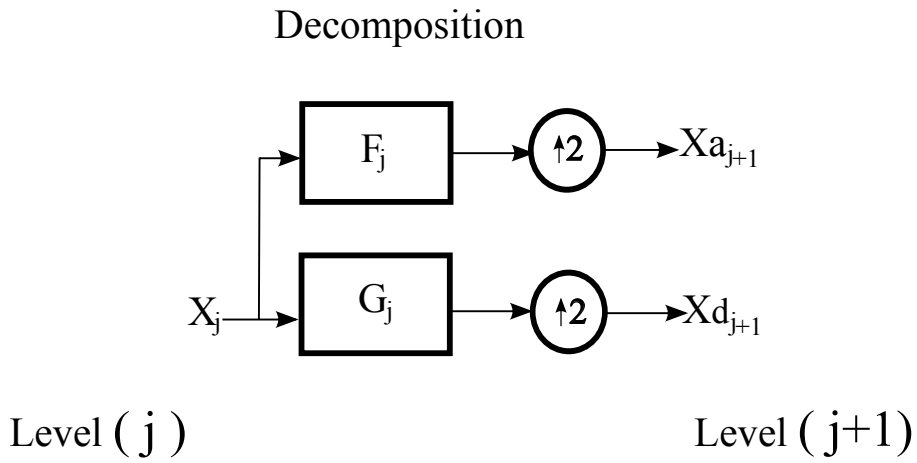

Figure 4.2: Filter bank implementation of SWT

If the original time signal is shifted by an amount τ, then the wavelet coefficients at any scale are also shifted by the same amount, τ. This an important property of the SWT (see APPENDIX F for proof) and this can observed if we consider the shifted version of the signal $x(t-\tau)$ and substituting $d_j^k\{x(t-\tau)\}$ in Eq. 4.5. That is,

$$d_k^j(x(t-\tau)) = d_{k-\tau}^j(x(t)) \tag{4.6}$$

which means that the coefficients of a delayed signal are a time shifted version of those of the original signal as illustrated in Fig. 4.3. This invariance property of SWT is crucial to constructing the covariance matrices in WMCC method.

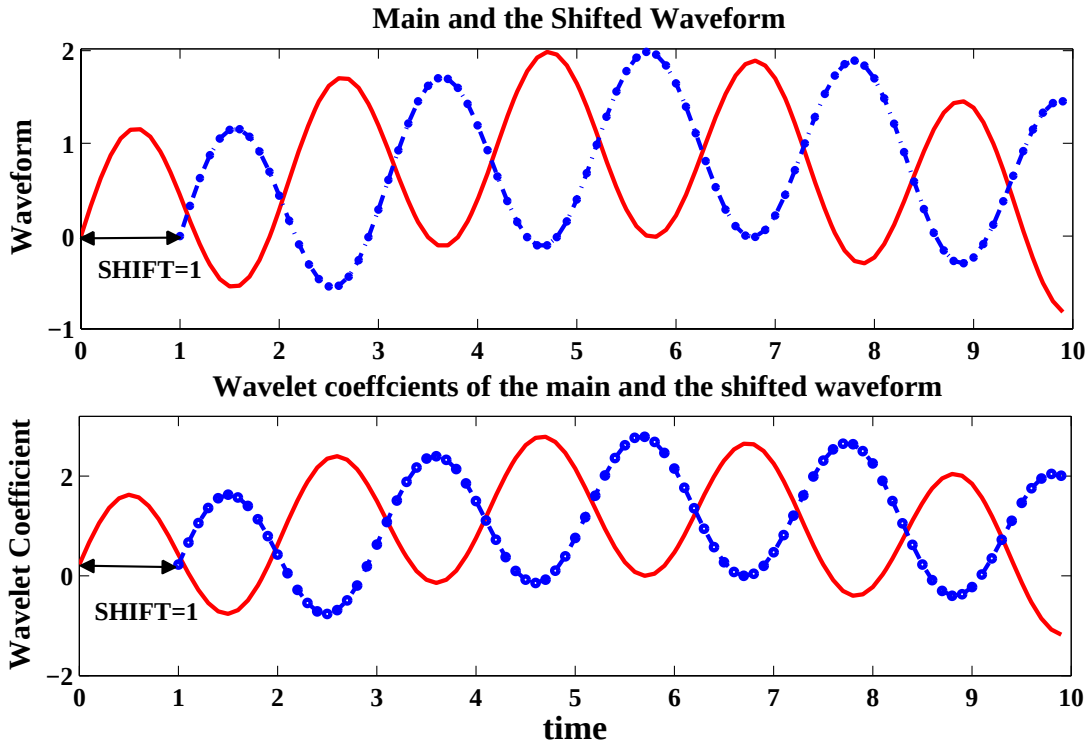

Figure 4.3: Illustration of time-invariance of Stationary Wavelet Transform

4.3 Modal Identification using WMCC method

The traditional MCC method works in three steps: (i)The correlation of output measurements ($\mathbf{r}$) is first substituted for the physical responses as described in Eq. 3.7 by virtue of NExT/ERA [46, 47], (ii) A whitening transformation of the correlation of measurements($\mathbf{r}$), obtained from the co-variance the physical responses ($\mathbf{r}$) that converts the problem of determining the mixture matrix $\mathbf{A}$ to one of a unitary matrix, and (iii) determination of the unitary matrix by jointly diagonalizing the covariance matrices of the whitened measurements for several non-zero time lags.

The current study extends the concepts MCC in two ways. First, the wavelet coefficients obtained through the stationary wavelet transform (SWT) of the correlation of

measurements are used instead of the measurements directly. Estimating the mixing matrix and sources then proceeds similar to the traditional MCC method. Secondly, the non-stationary nature of the sources is handled through the use of several time-lagged non-overlapping windows. This method is known as the wavelet-based modified cross-correlation method (WMCC) and the details are presented in the following. Symlet is used as the basis function due to its orthogonality property, compact support, and the ability to perform DWT.

4.3.1 Details of the Algorithm

Considering the orthogonal wavelet decomposition of the sources, we can express each source signal in terms of its decomposition coefficients:

$$s_m^j(t) = \sum_k c_{km}^j {\psi_k}^j(t) \qquad m = 1, 2, ..., N \tag{4.7}$$

Where, j represents the scale, m represents source index, and k represents the shift index. $\psi(t)$ is the chosen wavelet and c_{km}^j are the decomposition coefficients. Along the same lines, each component of the measurements $\mathbf{x}$ can be expressed as:

$$x_m^j(t) = \sum_k f_{km}^j {\psi_k}^j(t) \qquad m = 1, 2, ..., N \tag{4.8}$$

Where, m represents sensor index, and and f_{km}^j are the decomposition coefficients. Considering the wavelet coefficients at the l^{th} shift of sensor responses and sources, inserting Eq. 4.7 and Eq. 4.8 in Eq. 2.53 and finally applying the orthogonality conditions for wavelets, we get [56]:

$$\mathbf{f}_l = \mathbf{A}\mathbf{c}_l \tag{4.9}$$

where $\mathbf{A} = [A_{ij}]_{N\times N}$ is the instantaneous mixing matrix for the case N sensor responses and N sources, and the vectors constructed from the l^{th} coefficients of the mixtures and sources are given by $\mathbf{f}_l$ and $\mathbf{c}_l$, respectively.

The next step of the formulation is to derive the autocorrelation matrices of the wavelet coefficients of the sources c_{kl}^j, and the responses f_{kl}^j, respectively, which requires the use of SWT. Define the covariances of the signals and sources $\hat{R}_s(p)$ and $\hat{R}_x(p)$ respectively, for some non-zero time lag p, as : $R_s(p) = E\left\{s(k)s^T(k-p)\right\}$ and $R_x(p) = E\left\{x(k)x^T(k-p)\right\}$. Inserting Eq.4.7 and Eq.4.8 into the expression for the two covariance matrices and making use of Eq. 4.6, we get:

$$\begin{aligned} R_s(\tau) &= E\left[\sum_l c_l^j \psi_l^j(t) \sum_m c_{m+\tau}^j \psi_m^j(t+\tau)\right] \qquad \tau \neq 0 \\ R_x(\tau) &= E\left[\sum_l f_l^j \psi_l^j(t) \sum_m f_{m+\tau}^j \psi_m^j(t+\tau)\right] \qquad \tau \neq 0 \end{aligned} \tag{4.10}$$

Using orthogonal properties of the wavelet basis,

$$\begin{aligned} R_s(\tau) = R_{ws}(\tau) &= E\left[c_l^j c_{l+\tau}^j\right] \\ R_x(\tau) = R_{wx}(\tau) &= E\left[f_l^j f_{l+\tau}^j\right] \end{aligned} \tag{4.11}$$

Now consider Eq. 4.9 (for N sources and measurements). Multiplying both sides by $\mathbf{f}_{l+p}$ (where, p is an index that has the same meaning as τ) and taking the mathematical expectation on both the sides, we obtain:

$$E\{\mathbf{f}_l \mathbf{f}_{l+p}^T\} = \mathbf{A} E\{\mathbf{c}_l \mathbf{c}_{l+p}^T\} \mathbf{A}^T \tag{4.12}$$

Using Eq. 4.11 and Eq. 4.12, we have :

$$\mathbf{R}_{w\mathbf{x}}(p) = \mathbf{A}\mathbf{R}_{w\mathbf{s}}(p)\mathbf{A}^T \tag{4.13}$$

From here on, the procedure follows similar to SOBI. The key step is the simultaneous diagonalization of the two covariance matrices $\hat{\mathbf{R}}_{\mathbf{x}}(0)$ and $\hat{\mathbf{R}}_{w\mathbf{x}}(p)$ evaluated at 0 time-lag and non-zero time lag p. The procedure is accomplished in three basic steps: whitening, orthogonalization and unitary transformation. Whitening is a linear transformation in

which $\hat{\mathbf{R}}_{\mathbf{x}}(0) = (1/N)(\sum_{K=1}^{N} \mathbf{x}(k)\mathbf{x}^T(k))$ is first diagonalized using singular value decomposition, $\hat{\mathbf{R}}_{\mathbf{x}}(0) = \mathbf{V}_{\mathbf{x}}\mathbf{\Lambda}_{\mathbf{x}}\mathbf{V}_{\mathbf{x}}^T$, where $\mathbf{V}_{\mathbf{x}}$ are the eigenvectors of the co-variance matrix of $\mathbf{x}$. Then, the standard whitening is realized by a linear transformation expressed as under:

$$\bar{\mathbf{x}}(k) = \mathbf{Q}\mathbf{x}(k) = \mathbf{\Lambda}_{\mathbf{x}}^{-\frac{1}{2}}\mathbf{V}_{\mathbf{x}}^T\mathbf{x}(k) \tag{4.14}$$

The second step, called orthogonalization, is applied to diagonalize the matrix $\hat{\mathbf{R}}_{w\bar{\mathbf{x}}}(p)$ whose eigen-value decomposition is of the form $\hat{\mathbf{R}}_{w\bar{\mathbf{x}}}(p) = \mathbf{V}_{\mathbf{f}_l^j(\bar{\mathbf{x}})}\mathbf{\Lambda}_{\mathbf{f}_l^j(\bar{\mathbf{x}})}\mathbf{V}_{\mathbf{f}_l^j(\bar{\mathbf{x}})}^T$. Substituting $\bar{\mathbf{x}}(k) = \mathbf{Q}\mathbf{x}(k)$ from Eq. 4.14 into $\hat{\mathbf{R}}_{\mathbf{x}}(p) = (1/N)(\sum_{K=1}^{N} \mathbf{x}(k)\mathbf{x}^T(k-p))$ and making use of the relationship that $\mathbf{R}_{\mathbf{x}}(p) = \mathbf{R}_{w\mathbf{x}}(p)$, we get :

$$\hat{\mathbf{R}}_{w\bar{\mathbf{x}}}(p) = \mathbf{Q}\mathbf{A}\mathbf{R}_{w\mathbf{s}}(p)\mathbf{A}^T\mathbf{Q}^T \tag{4.15}$$

If the diagonal matrix $\mathbf{\Lambda}_{\mathbf{f}_l^j(\bar{\mathbf{x}})}$ has distinct eigen-values, then the mixing matrix can be estimated by the equation,

$$\hat{\mathbf{A}} = \mathbf{Q}^{-1}\mathbf{V}_{\mathbf{f}_l^j(\bar{\mathbf{x}})} = \mathbf{V}_{\mathbf{x}}\mathbf{\Lambda}_{\mathbf{x}}^{1/2}\mathbf{V}_{\mathbf{f}_l^j(\bar{\mathbf{x}})} \tag{4.16}$$

If the sources are assumed to be uncorrelated and scaled to have a unit variance, the product $\mathbf{QA}$ is a unitary matrix , say,$\mathbf{V}_{\mathbf{f}_l^j(\bar{\mathbf{x}})}$, and the problem now becomes one of unitary diagonalization of the correlation matrix $\hat{\mathbf{R}}_{w\bar{\mathbf{x}}}(p)$ at one or several non-zero time lags.

Eq. 4.15 is a key result, which states that the whitened matrix $\hat{\mathbf{R}}_{w\bar{\mathbf{x}}}(p)$ at any non-zero time lag p and scale level j is diagonalized by the unitary matrix, $\mathbf{QA}$. Since $\mathbf{R}_{w\mathbf{s}}(p)$ is a diagonal matrix (since the sources are assumed to be mutually uncorrelated), the problem now becomes one of diagonalizing the matrix $\hat{\mathbf{R}}_{w\bar{\mathbf{x}}}(p)$ resulting in the unitary matrix, $\mathbf{QA}$. Though the existence of the unitary matrices for any time lag p is implied by Eq. 4.15, the determination of such unitary matrices is a numerical procedure.

4.3.2 Joint Diagonalization for s^{th} Scale, p Lags and L Time Windows

As seen from Eq. 4.15, the problem of finding $\mathbf{A}$ is solved by unitarily diagonalizing $\hat{\mathbf{R}}_{\mathbf{w}\bar{\mathbf{x}}}(p)$. Due to estimation errors, finding an exact diagonalizing unitary matrix may not be possible, and estimating $\mathbf{QA}$ may be possible only in an approximate sense. There are two major issues that influence the diagonalization. First issue is the proper choice of the lag parameter p, which is not available *a priori*. Secondly, the scale level of the stationary wavelet decomposition that will diagonalize $\hat{\mathbf{R}}_{w\bar{\mathbf{x}}}(p)$ is not known. However, selecting the scale level is not an issue provided there is information regarding the dominant modes of interest of the system. In this study, the scale level of wavelet decomposition s is fixed, and then several values of time lags, $p = 1, 2, \cdots, l$ is chosen, and the matrices $\hat{\mathbf{R}}_{w\bar{\mathbf{x}}}(p)$ are diagonalized such that after h iterations, the sum of the off-diagonal terms for all the time lags is minimum in a norm sense. Denoting $\mathbf{V} = \mathbf{QA}$, $\mathbf{D}^p = \mathbf{V}^T\hat{\mathbf{R}}_{w\bar{\mathbf{x}}}(p)\mathbf{V}$, we can write this statement mathematically as finding the minimum of the performance index J given by,

$$J(V, s) = \sum_{p=1,l} \sum_{i \neq j, m} \left| D_{ij}^p \right|_s^2 \tag{4.17}$$

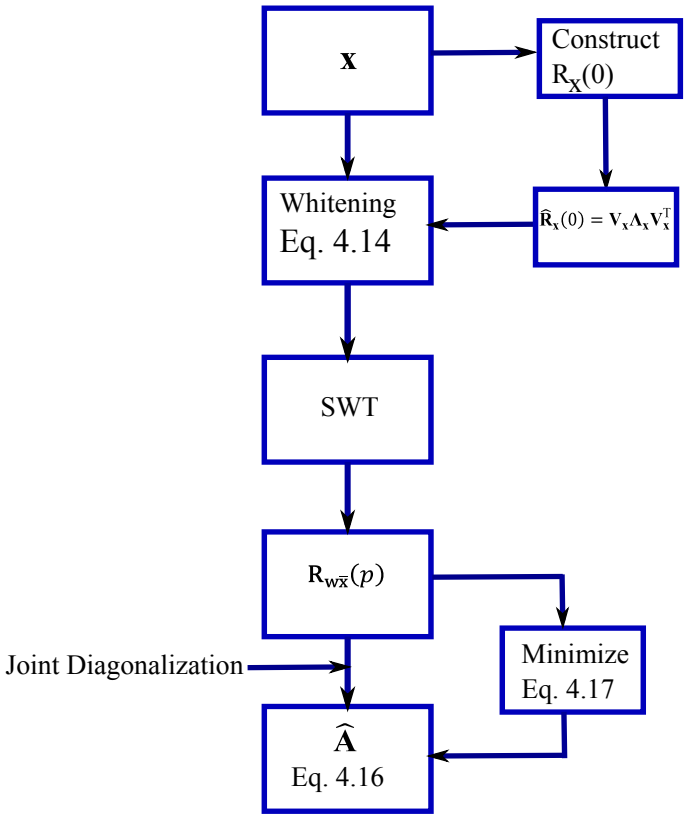

Figure 4.4: Flowchart for WMCC method

Then, the unitary matrix $\mathbf{V}$ corresponding to minimum J over fixed h iterations is said to be an approximate joint diagonalizer. The Jacobi technique[33] for diagonalizing a real, symmetric matrix is utilized for this purpose. In addition to considering several time lags p for the diagonalization purposes, the non-stationary aspect of the sources is addressed by partitioning the pre-whitened data into L non-overlapping blocks (time windows T_i) and the time-delayed covariance matrices are estimated in each window. The key steps in the WMCC method are summarized in the form of a flow-chart in Fig. 4.4.

In order to demonstrate the effect of the simultaneous diagonalization, a mass-spring-dashpot system with three degrees-of-freedom is considered, with a lumped mass m =10kg and a constant stiffness of 2 kN/m at each degree of freedom. The damping is considered

to be of Rayleigh type with 2% critical in the first mode. The effect of the non-stationarity of the sources is analyzed by dividing $\bar{\mathbf{x}}(k)$ into several time blocks, ranging from $L = 1$ to $L = 50$. The results are displayed in Fig. 4.5. Though there appears to be no direct relationship between the efficiency of diagonalization and the parameters, it is safe to conclude that accounting for the non-stationary characteristics of the sources by using multiple windows achieves better performance, as indicated by the square root of the sum of squares of the off-diagonal terms, than the case when a single window (or, no window) is used to calculate the covariance matrix for several time lags. For the simple system considered for the parametric study $L = 20$ yields the best result and is used for all the ensuing simulations. The time required for such computations is less due to reduced numerical complexity of the algorithm. A detailed analysis of the running times when compared to all of the existing methods, is beyond the purview of the present study.

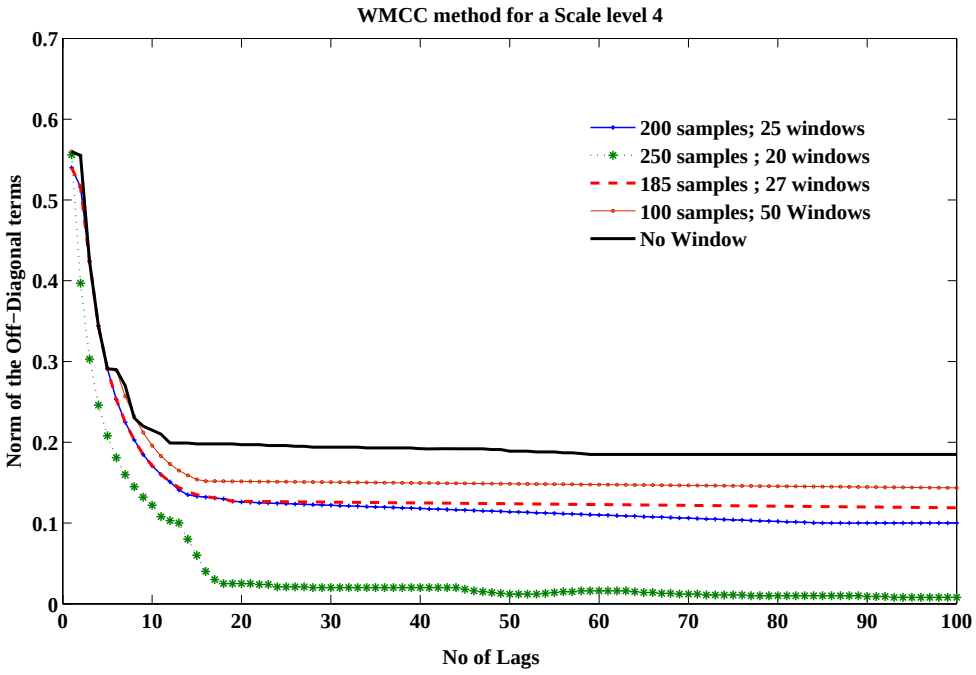

Figure 4.5: Effect of window size and the number of lags on the joint diagonalization

4.4 Case Study: Identification Results for the UCLA Factor Building

4.4.1 Description of the UCLA Factor Building

In order to demonstrate the application of the WMCC method developed in the previous sections, the earthquake and ambient responses from the UCLA Doris and Louis Factor building, called UCLA Factor Building (UCLAFB), are utilized. A general layout of this building is shown in Fig. 4.6, which houses several centers for the health sciences and other biomedical facilities of UCLA. This building is one of the most heavily, permanently instrumented buildings in North America, whose vibration data in real-time is made available for researchers world-wide through a remote data-base server. Designed and constructed in the late 1970s, the 17-story, 216.5 ft high building consists of a Special Moment resisting (steel) frames (SMFs) supported by concrete bell caissons and spread footings. Following the 1994 Northridge earthquake, the building was instrumented with an array of 72 Kinemetrics FB-11 uniaxial-accelerometers at the floor levels including the basement and the sub-basement levels. Each level has two pairs of orthogonal sensors parallel to the NS and EW directions as shown in the figure 4.6. The building's sensor network was upgraded in 2003 to a 24-bit network that continuously records data that includes numerous small earthquakes to date. Details of this building along with significant seismic events recorded by this network has been extensively documented elsewhere [57, 71, 80].

For the current identification study, floor accelerations recorded during the event that occurred on September 28, 2004, 10:15 AM PDT, due to ground shaking originating (with Mw = 6.0 on the moment magnitude scale) from Parkfield, CA, epicentered 163 miles from the UCLAFB are selected. The peak acceleration recorded at the roof of UCLAFB was 0.0025g. In addition to the earthquake vibration data, 3 sets of wind excited acceleration responses were used. The first data set (DS1) consists of the acceleration records collected

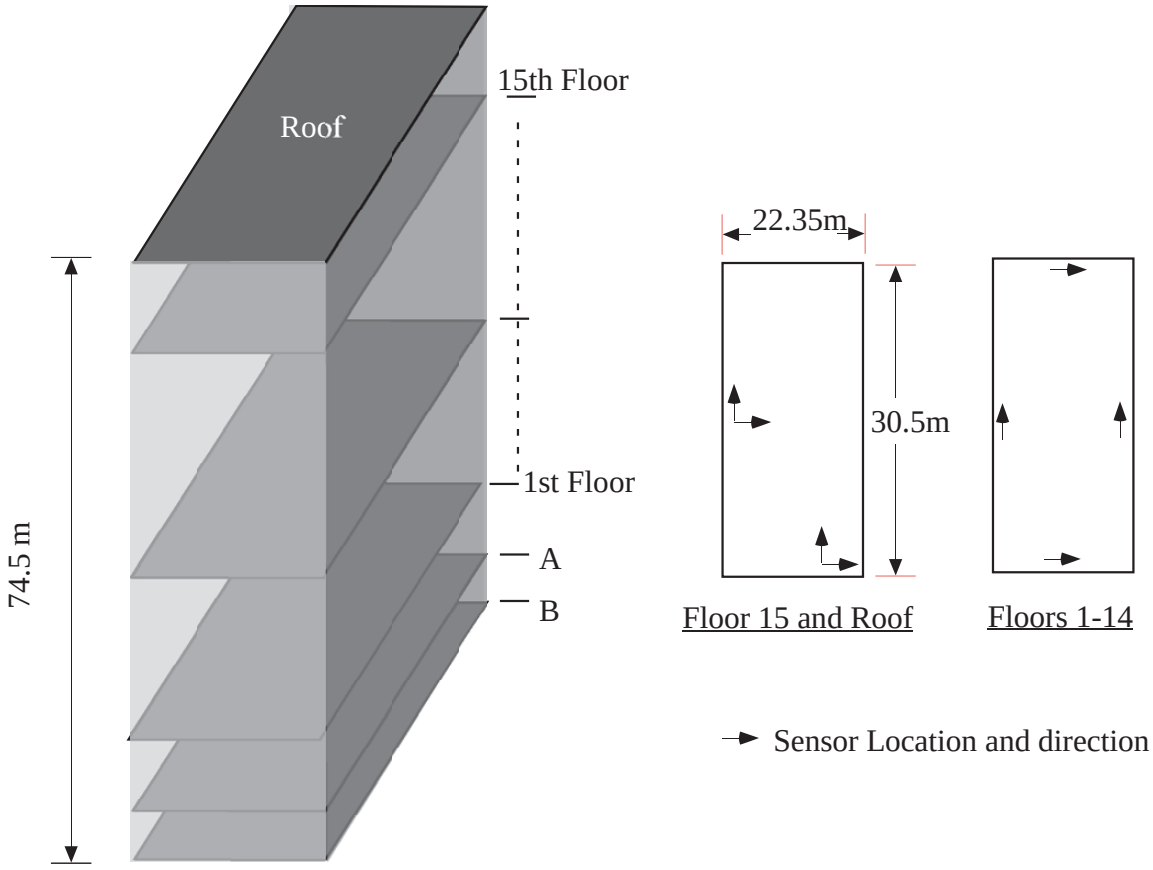

Figure 4.6: Sketch of the UCLA Factor building with the sensor Locations

on September 28, Thursday, 2004. The second data set (DS2) consists of acceleration responses collected on September 29, Thursday, 2004 and the third data set (DS3) consists of acceleration responses collected on January 2, 2008. A total of 80 sets of ambient vibration data resulted from the recordings were used for further analysis. The sensor responses at each floor level Fig. 4.6 are converted to a triad of 3 responses at the center of mass using co-ordinate transformations [71, 80]. Thus, using a total of 48 transformed channels of measurements, blind identification was carried out and the results are reported in the following discussion.

Table 4.1: Identified natural frequencies and damping statistics of the UCLA Factor building using ambient data

Mode	Shapes	Natural Frequencies (Hz) Mean (COV(%))			Damping % Critical Mean (COV(%))		
No	Dir	SOBI	MCC	WMCC	SOBI	MCC	WMCC
1	EW	0.54(1.50)	0.54(1.30)	0.55(1.00)	3.8(35.0)	3.5(33.0)	3.5(27.0)
2	NS	0.56(1.30)	0.57(1.20)	0.58(1.20)	4.8(42.0)	4.1(39.0)	4.1(37.5)
3	Tor	0.76(3.90)	0.77(2.90)	0.79(2.20)	5.0(27.5)	4.5(26.0)	4.2(25.4)
4	EW	1.60(2.15)	1.61(2.10)	1.65(1.50)	2.7(15.2)	2.6(15.0)	2.3(14.8)
5	NS	1.74(2.25)	1.77(2.20	1.80(1.15)	1.8(16.3)	1.7(15.0)	1.7(14.4)
6	Tor	2.37(1.85)	2.42(1.75)	2.47(1.70)	3.4(25.4)	3.2(23.6)	3.0(22.0)
7	EW	2.74(1.00)	2.76(0.97)	2.80(0.95)	2.7(16.0)	2.6(15.2)	2.5(13.4)
8	NS	2.97(1.25)	2.99(1.25)	3.09(1.25)	2.2(23.0)	2.0(21.2)	1.9(18.3)
9	Tor	3.94(2.35)	3.98(2.25)	4.01(2.20)	3.6(26.5)	3.4(24.1)	3.2(19.3)
10	EW	4.31(1.50)	4.28(1.41)	4.27(1.35)	2.5(27.0)	2.4(23.3)	2.2(21.0)
11	NS	4.77(1.93)	4.73(1.89)	4.75(1.83)	3.0(28.0)	2.8(22.1)	2.9(21.2)
12	Tor	5.06(2.56)	5.04(2.49)	5.09(2.43)	3.9(29.2)	3.5(24.2)	3.3(21.2)
13	EW	5.31(2.63)	5.36(2.46)	5.39(2.41)	4.0(30.0)	3.6(26.5)	3.4(24.7)
14	NS	5.69(3.13)	5.72(3.09)	5.81(3.03)	3.3(27.0)	3.1(21.2)	2.9(17.5)
15	Tor	6.21(3.67)	6.25(3.53)	6.28(3.47)	3.7(28.2)	3.4(22.3)	3.1(17.6)

4.4.2 Results

The identification results for the 15 dominant modes for the ambient vibration cases are reported in terms of their first and second-order statistics, namely mean and coefficient of variation (CV), in Table 4.1. It is worth mentioning that although only 15 modes are

reported with the full-sensor data, over 20 modes were identified. Results of identification using three methods, SOBI, MCC and WMCC are presented alongside each other in columns. It can be seen that the estimated natural frequencies and damping ratios are quite close to each other for the three methods presented. The normalized mode-shapes for the first six modes are shown in Fig. 4.7. The results from a statistical analysis of the natural frequencies is reported in Fig. 4.8. The results of identification are obtained by conducting approximately 100 trials of identification using the WMCC method described earlier using the three ambient data sets.

It is clear from Fig. 4.8 that the statistics follow nearly a normal distribution and the variability in the results in the natural frequency estimates is relatively small. Additionally, the natural frequencies are consistent with the reported values (12 modes have been reported) for this building [57, 80, 71]. A comforting feature of the results is that the estimation statistics reported here follow closely to the results presented recently [71] using a much larger data-set of ambient records. For example, the mean value for the first two lateral modes and the torsional mode obtained using WMCC method are 0.55, 0.58 and 0.79 Hz compared to 0.55, 0.60 and 0.81 reported in in the aforementioned study [71]. The CV's are also very close to those that have been reported in the same study [71]. The results of identification estimated from the data during the ground shaking that occurred due to the Parkfield earthquake is reported in Table 4.2. As before, the results of identification using the three methods, SOBI, MCC and WMCC, are presented alongside each other in columns. As reported in an earlier studies [57, 80], the natural frequencies for the earthquake case are generally lower than those that have been estimated using ambient responses.

Upon examination of the results from ambient case in Table 4.1 and for the earthquake case in Table 4.2, the frequencies for the ambient vibrations are consistently higher for all modes. This result has also been reported in earlier studies [57], which can be attributed

Table 4.2: Identified natural frequencies of the UCLA Factor building using earthquake data

Mode	Shapes	Natural Frequencies (Hz)			Damping % Critical		
No	Dir	SOBI	MCC	WMCC	SOBI	MCC	WMCC
1	EW	0.50	0.48	0.47	4.3	3.8	3.4
2	NS	0.53	0.52	0.51	4.1	3.6	3.2
3	Torsion	0.69	0.69	0.68	4.5	3.9	3.4
4	EW	1.55	1.52	1.48	4.3	3.8	3.3
5	NS	1.52	1.57	1.64	4.0	3.6	3.4
6	Torsion	2.47	2.46	2.37	5.4	5.0	4.3
7	EW	2.73	2.69	2.67	3.4	3.1	2.8
8	NS	3.00	2.94	2.88	3.9	3.7	3.3
9	Torsion	3.99	3.92	3.83	3.7	3.4	3.0
10	EW	4.74	4.36	4.20	3.0	2.8	2.3
11	NS	4.79	4.67	4.55	3.5	3.3	2.9
12	Torsion	5.27	5.19	5.00	3.7	3.4	3.1
13	EW	5.65	5.56	5.31	2.7	2.3	2.1
14	NS	6.39	6.03	5.69	2.6	2.4	2.2
15	Torsion	6.56	6.44	6.19	3.0	2.7	2.5

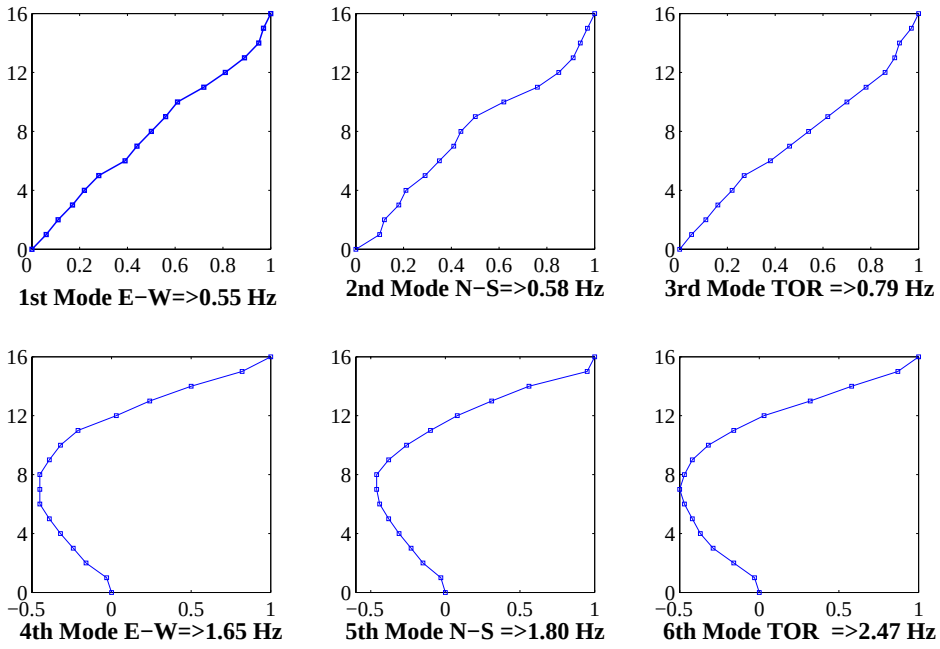

Figure 4.7: Identified mode shapes

to the effects of soil-structure interaction and nonlinearity. The mean value of the damping for the first few dominant modes is generally in the range of reasonable values for structures of this construction type, around 3-5% for the first few modes, and is similar to the results reported in independent studies [71]. However, given the rather large variation reported here and in other studies (as high as 69% in some studies) drawing definite conclusions regarding damping is difficult. Similarly, making definitive statements regarding the magnitude of damping for the earthquake case based on point estimates is likely to be misleading. Nonetheless, it is safe to say that the damping estimates for the earthquake case appear to be what one would expect for structures of this type, of the order of $2\%-4\%$ critical, and the variation is expected to be large.

In order to study the effects of reducing the number of sensors on identification, the number of sensors used to estimate the modal information are gradually reduced from the

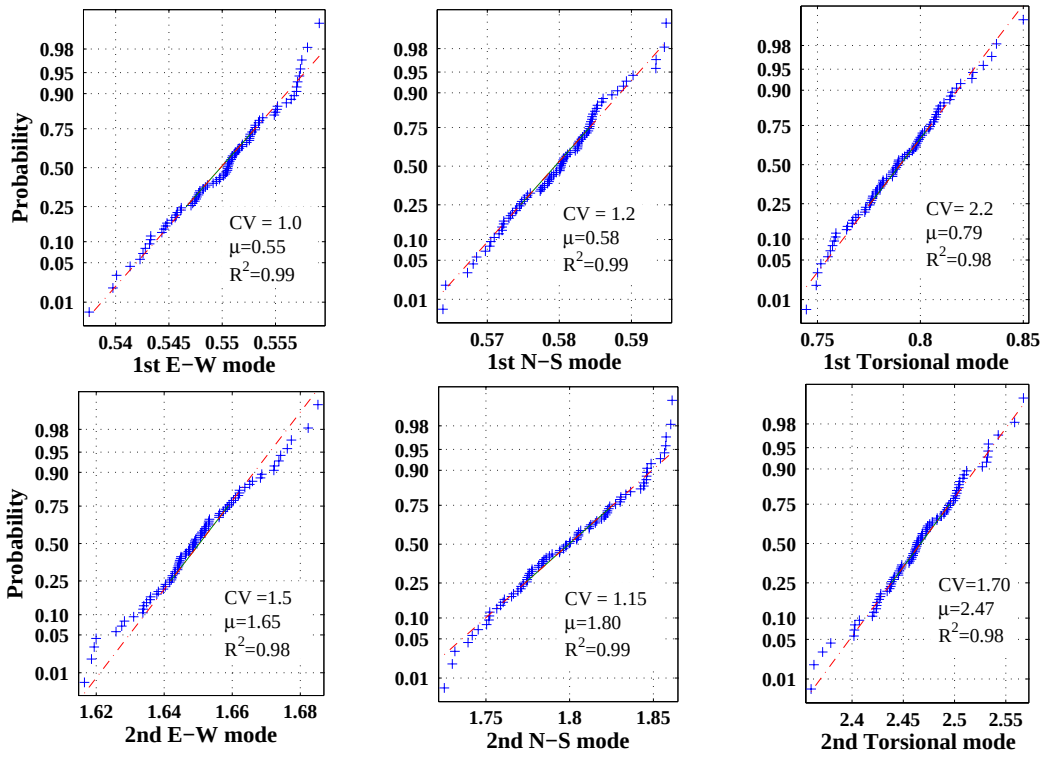

Figure 4.8: Normal probability paper plot for ambient data

complete set of 48 channels. The channels at the basement and subbasement levels are not considered as their RMS response levels are very low. The transformed data from the sensors are used for description purposes noting the fact that four sensors at each floor level are used to produce 3 channels of measurements. Starting with the roof and proceeding towards the first floor (basement channels excluded), the channels corresponding to the center-of-mass in the E-W, N-S and rotation are named $R_1,\ R_2,\ R_3, \cdots$ respectively.

Table 4.3: Performance of WMCC method with reduced sensor density

	MAC values for Ambient Data				MAC values for Earthquake Data			
		Number of Sensors			Number of Channels			
No	Dir	26	24	18	17	26	24	18	17
1	EW	0.99	0.99	0.99	0.94	0.98	0.98	0.98	0.94
2	NS	0.99	0.99	0.98	0.94	0.98	0.98	0.98	0.95
3	Tor	0.99	0.99	0.98	0.98	0.98	0.98	0.97	0.97
4	EW	0.98	0.98	0.98	0.98	0.98	0.98	0.98	0.97
5	NS	0.98	0.98	0.97	0.97	0.98	0.98	0.97	0.97
6	Tor	0.98	0.98	0.97	0.97	0.98	0.98	0.97	0.96
7	EW	0.98	0.98	0.98	0.98	0.98	0.98	0.97	0.98
8	NS	0.98	0.98	0.98	0.98	0.98	0.98	0.97	0.98
9	Tor	0.98	0.98	0.98	0.98	0.98	0.98	0.97	0.98
10	EW	0.98	0.98	0.98	0.97	0.98	0.97	0.97	0.97
11	NS	0.98	0.98	0.98	0.97	0.98	0.97	0.97	0.97
12	Tor	0.98	0.98	0.97	0.97	0.97	0.97	0.96	0.97
13	EW	0.99	0.98	0.96	0.97	0.99	0.95	0.92	0.96
14	NS	0.99	0.95	0.95	0.93	0.99	0.94	0.93	0.92
15	Tor	0.99	0.98	0.97	0.94	0.98	0.98	0.95	0.93

With this naming convention, four cases cases are considered with 26, 24, 18 and 17 channels. These cases are as shown below:

26 channels: $[R_1, \cdots, R_{17}, R_{19}, R_{22}, R_{25}, R_{28}, R_{31}, R_{34}, R_{37}, R_{40}, R_{43}]$

24 channels: $[R_1, \cdots, R_{17}, R_{19}, R_{22}, R_{25}, R_{28}, R_{31}, R_{37}, R_{43}]$

18 channels: $[R_1, \cdots, R_{11}, R_{13}, R_{17}, R_{21}, R_{22}, R_{28}, R_{35}, R_{39}]$

17 channels: $[R_1, \cdots, R_{11}, R_{13}, R_{17}, R_{19}, R_{23}, R_{25}, R_{29}]$

The correlation between the vibration modes obtained using full-sensor density and reduced density is performed using the modal assurance criterion (MAC). MAC values range between 0 and 1, a value of 1 meaning a perfect correlation. MAC is defined as:

$$MAC_i = \frac{(\psi_i^T \bar{\psi}_i)^2}{(\psi_i^T \psi_i)(\bar{\psi}_i^T \bar{\psi}_i)} \tag{4.18}$$

Here, ψ_i and $\bar{\psi}_i$ represent the i^{th} mode shape vectors for the full sensor and reduced sensor densities, respectively. The results are presented in Table 4.3 and also in Fig. 4.9 for the cases of 26 and 17 channels only due to space limitations. Table 4.3 and Fig. 4.9 contains the MAC values obtained by comparing the results obtained using the complete sensor data (48 transformed channels) with the reduced cases. It can be seen that by reducing the number of channels to 26, the quality of identification is as good as those obtained by using the full set. If the number of sensors are further reduced, to yield 17 channels, there is a significant reduction in the accuracy. This is reflected by the decreasing MAC values. WMCC still provides reasonable estimates for 17 sensor case, where as SOBI and MCC fail to do so. Whereas SOBI fails to identify the first 2 modes, MCC is unable to identify the 1^{st} mode.

To assess the variability in the results of identification with respect to ambient data, approximately 80 subsets of data are considered and the mean and standard-deviation results for the first few modes are reported in Table 4.4 for the reduced channel cases. It can be seen from the results that although the dispersion increases with the reduction in the number of sensors, its magnitude still remains relatively small indicating a good degree of confidence in the estimation.

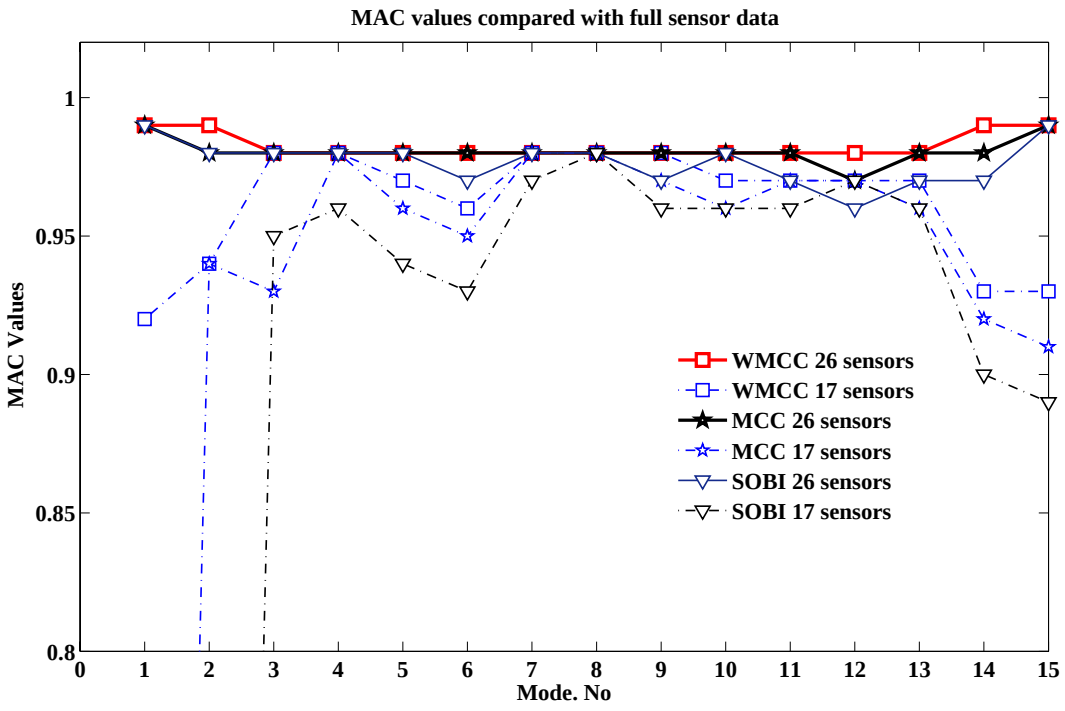

Figure 4.9: Comparative performance of BSS methods with respect to the reduction in the sensor density

Table 4.4: Identification results for reduced sensor cases

Mean of Frequencies (Hz)					Co-efficient of Variation(%)			
Mode No	Number of Channels				Number of Channels			
	26	24	18	17	26	24	18	17
1(E-W)	0.55	0.54	0.54	0.53	1.7	1.7	1.7	1.8
1(N-S)	0.57	0.55	0.55	0.54	1.5	1.5	1.5	1.6
1(TOR)	0.79	0.78	0.76	0.75	2.2	2.5	2.6	2.7
2(E-W)	1.64	1.60	1.59	1.56	1.5	1.6	1.7	1.8
2(N-S)	1.80	1.78	1.76	1.74	1.2	1.6	2.0	2.3
2(TOR)	2.48	2.43	2.40	2.39	1.7	2.1	2.3	3.0

4.5 Summary

A second-order blind identification method based on SWT, called WMCC, has been presented in this chapter. An important property of SWT is its time invariance, which has been exploited to construct the covariance matrices of the transformed data. Modal identification results for the UCLA Factor building show good correlation with published results for both the ambient and earthquake excitation cases. There is no need to pre-select the model order and multiple reference sensor locations, which is the main advantage of the proposed method over the ambient modal identification discussed earlier. Identification results show that the dispersion of the results for the natural frequencies is relatively small, indicating a good degree of confidence in the estimation procedure. The method is also shown to perform well under reduced number of sensors, which is clearly advantageous in dealing with practical economics of health monitoring and modal identification.

Even though WMCC method addresses many practical shortcomings of available methods, it does not address the case when the mixing matrix is rank deficient. This issue is dealt in detail in the next chapter where it is shown how the rank deficiency can be addressed in a hybrid approach, combining time and time-frequency domain representations of the responses and the sources.

Chapter 5

Under-Determined Blind Identification of Structures

In this chapter, a new hybrid time and time frequency domain blind identification method is developed to extend the MCC method to the under-determined blind identification of building structures. The under-determined case is encountered when the number of sensors is less than the number of identifiable modes. Such situations commonly arise in flexible structures containing several dominant modes, but instrumented with a relatively fewer number of sensors. This chapter begins with the description of the key steps of the hybrid method, followed by a full-scale demonstration of this method on the Apron Tower, located at the Pearson International Airport in Missisauga, Ontario. The key results and discussions are presented next, followed by some important conclusions.

5.1 Motivation

The problem of modal identification of a structure when the number of available measurements is less than the number of identifiable modes, is called under-determined blind

identification. In all of the previous studies involving SOBI, MCC and WMCC, the number of measurements is considered equal to the number of identifiable sources. In other words, the mixing matrix is square and of full rank.

The underdetermined BSS, for the static mixtures case, can be restated as:

$$\begin{aligned} \mathbf{x}(k) &= \mathbf{A}\mathbf{s}(k) \\ \hat{\mathbf{s}}(k) = \mathbf{y}(k) &= \mathbf{W}\mathbf{x}(k) \end{aligned} \tag{5.1}$$

where,

$\mathbf{A} = [a_{ij}]_{m\times n} \Rightarrow$ Instantaneous mixing matrix

$\mathbf{W}_{n\times m} = \mathbf{A}^{-1}_{m\times n} \Rightarrow$ Un-mixing matrix, which is the pseudo inverse of $\mathbf{A}$

$\mathbf{s}(k) = \{s_j(k)\}\ \ j = 1, 2, ...m$ sources input to the system

$\mathbf{x}(k) = \{x_i(k)\}\ \ i = 1, 2, ...n$ sensor signals system output

$\mathbf{y}(k) = \{y_j(k)\}\ \ j = 1, 2, ...m$ estimated Sources

The key point to note here is that whereas earlier the mixing matrix $\mathbf{A}$ is constrained to have full rank, the mixing matrix in Eq. 5.1 does not have such a constraint.

Identifying n sources or less when the matrix $\mathbf{A}$ is of rank n, is well-known [54, 6, 92]. However, for the under-determined case, i.e., when the number of sources of interest is larger than the size of outputs, the blind identification methods referred to earlier fail to identify all the sources (modes) of interest. Physically, such situations arise in flexible structures that are instrumented with a relatively small number of sensors due to cost or other reasons. In signal processing literature, the problem of underdetermined mixtures have been addressed through sparse time-frequency representations and by invoking external optimization or clustering [56, 93].

Approaching the under-determined source separation problem from time domain alone is difficult, since the mixing matrix is non-square and doesn't have a full column rank. To alleviate the rank deficiency problem, the available measurements are first decomposed into mono-harmonic components, referred to as intrinsic mode functions (IMFs), by utilizing a time-frequency decomposition called empirical mode decomposition (EMD) [43, 88, 87]. Once the IMFs are obtained, they are subsequently used as initial estimates for the sources and are operated upon by the standard time domain source separation technique, MCC, in an iterative framework. Initial estimates for the mixing matrix necessary to start the iterative process is selected using assumed shape functions that satisfy the essential boundary conditions. The need for sensor measurements at all the relevant degrees of freedom in order to identify the mode shapes is alleviated in this approach. This is the main advantage of the proposed method. Pre-processing of the measurements using EMD and the need for an initial estimate of the mixing matrix are the primary difficulties in the proposed method. These difficulties are easily overcome for the case of structure mode identification as explained in detail in this chapter.

The proposed method is applied to extract the vibration modes from measurement data collected from the Apron Control Tower in Mississauga, Canada. This data was a part of a larger experimental program to assess the condition of the TMD on the Apron Tower. During the fall of 2009, the structural dynamics and control group of the department of Civil and Environmental Engineering, University of Waterloo, conducted an extensive measurement program, where-in the structure was instrumented with a total of 12 seismic accelerometers along the height of the structure. The structure vibration measurements were obtained under wind and ambient excitations over a period of 3 months. The data utilized here was obtained by arresting the motion of the TMD. Furthermore, two significant wind events occurred during the measurement period, which resulted in high-fidelity measurements containing energies in several dominant modes. Key results using the newly proposed method are summarized and compared with the MCC method.

5.2 Modal Identification using EMD-MCC method

The key assumption in the MCC method is that the matrix, **A** in Eq. 5.1 is square, i.e., the number of outputs (or, measurements) is equal to the number of identifiable modes. The presence of noise in the measurements introduces difficulty in the estimation process due to the introduction of spurious modes. Specifically, the practically obtainable modes is only a sub-set of the rank of **A**. The MCC method described earlier is extended to the case when the number of sensors is less than the modes to be identified in two stages : (i) by extracting the intrinsic mode functions (IMFs) using EMD and, (ii) by treating the IMFs as pseudo-sources in an iterative procedure within the framework of the MCC method. EMD enables the size of the matrix of sources to be augmented as required, while the basic framework of the MCC method remains intact. Initial estimates for the mixing matrix are assumed using shape functions that satisfy the prescribed boundary conditions for the problem, and adjusted iteratively based on an energy criterion. For easy comprehension of the subsequent discussions, some useful acronyms are provided in Table. 5.1.

Table 5.1: Important Acronyms

EMD	Empirical Mode Decomposition
IMF	Intrinsic Mode Function
MCC	Modified Cross-Correlation
MAC	Modal Assurance Criterion

The EMD method reduces a signal into intrinsic IMFs that admit a well-behaved Hilbert transform [43]. For multi-degree-of-freedom structures, the IMFs extracted from the free-vibration responses can be regarded as the modes of vibration [88]. An IMF is defined

as a function that satisfies the following conditions: (i) it is mono-component and (ii) the mean values of the envelopes defined by the local maxima and the local minima are zero. The procedure of extracting an IMF is called sifting. Suppose $x(t)$ is the signal to be decomposed. The sifting process is implemented by identifying local extremum in the data between successive pairs of zero crossings and connecting all the local maxima by a cubic spline line to create the upper envelope. Local minima are connected in the same fashion to produce the lower envelope. If their mean is m_1, the difference $x(t) - m_1 = h_1$ is the first IMF. Ideally, h_1 should satisfy the conditions necessary to be called an IMF. If it does not satisfy the necessary conditions, then the sifting process is repeated by treating h_1 as the original data until the requirements for an IMF are fulfilled. The original signal is then subtracted from the IMF and the sifting process is repeated to decompose the data into n IMFs. Although one could extract the natural frequencies and the corresponding damping estimates directly using this sifting technique [88], measurements at all the degrees of freedom are required to extract the corresponding modes. This restriction is removed by using EMD in conjunction with the MCC method as described next.

Suitable band-pass filters are applied to the data to extract n IMFs, where n represents the number of desired modes [88]. In many cases, the availability of a FE model alleviates the difficulty in selecting appropriate filters. Alternatively, in the absence of such prior knowledge regarding the appropriate frequency bands, the uncertainty associated with the estimated values in contiguous frequency bands provides a measure to delineate real from spurious modes. This issue is discussed in detail in the next section. Once the IMFs are extracted, the pseudo-responses are then estimated using the relation $\tilde{\mathbf{x}}_e \approx \mathbf{A}_a \mathbf{\Gamma}$, where $\mathbf{\Gamma}$ and $\mathbf{A}_a$ represents the matrix of pseudo-sources (IMFs) and the mixing matrix, respectively.

To begin the iterative process, a mixing matrix of shape functions [68] that satisfy the prescribed boundary conditions is assumed. The pseudo responses $\tilde{\mathbf{x}}_e$ thus obtained are then scaled by the absolute maximum value of each response vector, followed by an update

of the assumed mode shape matrix $\mathbf{A}_a$ and an estimate for the pseudo-source $\tilde{\mathbf{s}}_e$ according to:

$$\begin{aligned} \hat{\mathbf{A}}_u &= \mathbf{Q}^{-1}\mathbf{V}_{\bar{\tilde{\mathbf{r}}}_e} \\ \tilde{\mathbf{s}}_e &= \hat{\mathbf{A}}_u^{-1}\tilde{\mathbf{x}}_e \end{aligned} \tag{5.2}$$

where, $\tilde{\mathbf{r}}_e(T) = E[\tilde{\mathbf{x}}_e(t+T)\tilde{\mathbf{x}}_e(t)]$ and $\hat{\mathbf{A}}_u$ is the updated mixing matrix.

The whitening factor, $\mathbf{Q}$, is obtained by diagonalizing:

$$\hat{\mathbf{R}}_{\tilde{\mathbf{r}}_e}(0) = \frac{1}{N}\left(\sum_{k=1}^{N}\tilde{\mathbf{r}}_e(k)\tilde{\mathbf{r}}_e^T(k)\right) = \mathbf{V}_{\tilde{\mathbf{r}}_e}\mathbf{\Lambda}_{\tilde{\mathbf{r}}_e}\mathbf{V}_{\tilde{\mathbf{r}}_e}^T \tag{5.3}$$

where, $\mathbf{V}_{\tilde{\mathbf{r}}_e}$ are the eigenvectors of the co-variance matrix of $\tilde{\mathbf{r}}_e$, which yields:

$$\mathbf{Q} = \mathbf{\Lambda}_{\tilde{\mathbf{r}}_e}^{-\frac{1}{2}}\mathbf{V}_{\tilde{\mathbf{r}}_e}^T \tag{5.4}$$

The unitary factor $\mathbf{V}_{\bar{\tilde{\mathbf{r}}}_e}$ (where, $\bar{\tilde{\mathbf{r}}}_e = \mathbf{Q}\tilde{\mathbf{r}}_e$) is obtained by diagonalizing the matrix,

$$\mathbf{R}_{\bar{\tilde{\mathbf{r}}}_e}(p) = \frac{1}{N}\left(\sum_{k=1}^{N}\bar{\tilde{\mathbf{r}}}_e(k)\bar{\tilde{\mathbf{r}}}_e^T(k-p)\right) = \mathbf{V}_{\bar{\tilde{\mathbf{r}}}_e}\mathbf{\Lambda}_{\bar{\tilde{\mathbf{r}}}_e}\mathbf{V}_{\bar{\tilde{\mathbf{r}}}_e}^T. \tag{5.5}$$

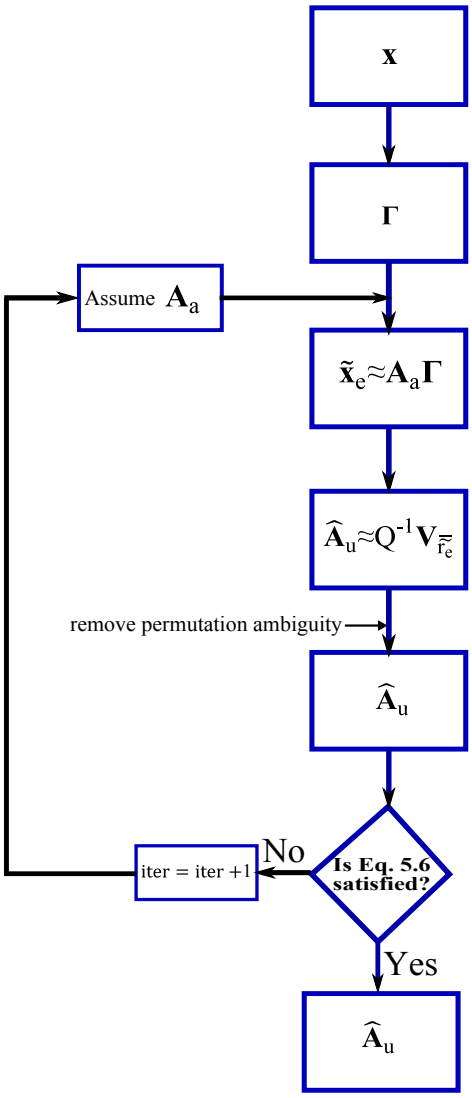

Figure 5.1: Flowchart for EMD-MCC method

From the estimated pseudo-sources $\tilde{\mathbf{s}}_e$, the natural frequency estimates are obtained using Hilbert transform. The permutation ambiguity in the estimates of $\hat{\mathbf{A}}_u$ and the pseudo-source matrices are corrected in each iteration. The mixing matrix is then updated in each step using the pseudo-sources obtained from the previous step. The update is terminated when the magnitude of the energy content in sources reaches a pre-defined

tolerance, ε, expressed by the following equation:

$$\left\| \frac{\tilde{s}_e^j(\omega) - \tilde{s}_e^{j-1}(\omega)}{\tilde{s}_e^{j-1}(\omega)} \right\| = \|\boldsymbol{\gamma}\| \leq \varepsilon \tag{5.6}$$

where $\tilde{s}_e(\omega)$ is the magnitude of the Fourier transform of $\tilde{\mathbf{s}}_e(t)$ vector, j represents the iteration step and $\|\cdot\|$ represents the 2-norm of the vector. For $j = 1$, $\tilde{s}_e(\omega) = \Gamma(\omega)$, where $\Gamma(\omega)$ is the Fourier transform of individual IMFs, $\boldsymbol{\Gamma}(t)$. The keys steps of the EMD-MCC algorithm are summarized in the flowchart shown in Fig. 5.1.

5.3 Identification Results

5.3.1 Structure Description and Measurement Program

Wind-induced vibration measurements from the Apron Control Tower located at the Toronto Pearson Airport, Missisauga, Canada, are used to demonstrate the application of the proposed EMD-MCC method. The Apron Tower at Toronto Pearson International Airport (Fig. 5.2) is a 49 m tall structure rising above the fourth level of Terminal 1. The total height of the structure above grade is 68.5 m. Constructed in 2000, the tower is a steel structure with composite steel deck and concrete floors providing a rigid diaphragm at each level. The tower has 10 core levels, consisting mainly of a scissor stairwell, elevator and service shafts. The structure is supported by six main steel columns resting on large transfer girders at the terminal roof level. Lateral loads is resisted by a combination of braced and moment frames.

Figure 5.2: Apron Control Tower at the Pearson International Airport, Toronto

During the fall of 2009, the structure was instrumented with PCB Piezotronics high sensitivity seismic ceramic flexural ICP accelerometers. The accelerometers have a frequency range of 0.07 to 300 Hz, sensitivity of 10.0 V/g, and a measurement range of 0.5 g ($g \approx 9.8 m/s^2$). The sensor's signal output was continuously recorded at a sampling rate of 500 Hz. Vibration data was recorded using a 12 channel simultaneous data acquisition system with 16-bit resolution. A total of twelve sensors were installed horizontally on three of the upper floors of the apron tower, including Level 2, 3, and 4, as well as in the upper chord of the roof truss structure, as shown in Fig. 5.3. Two sensors were installed in the north-south direction on each floor. A third sensor was installed in the east-west direction. The responses for three degrees of freedom (DOF) were considered at each level. In the east-west direction (x-DOF), one sensor was sufficient to provide this information at it was installed along the selected reference line corresponding to the center of mass in

north-south direction. In order to capture both the north-south direction (y-DOF) and torsion (θ -DOF), two sensors were mounted on each floor along the selected reference line away from the center of mass in the east-west direction. The tuned mass damper located on the roof of the tower was restrained during the measurement study.

An finite-element model (Fig. 5.4) of the Apron Tower was developed in the commercially available FE program, SAP2000. The model was made available to the author to validate the estimated frequencies and mode shapes. Brief description of the model is presented here; however, the details of the model are not considered author's work and hence excluded from the thesis. Only the liner roof of the terminal structure below the apron tower was modeled. Transfer girders are used to transfer the loads from the tower into the lower terminal structure. The liner roof was modeled and the joints translations and rotations were restrained (fixed support condition). The geometry, materials, and sections were determined using as-recorded drawings. The model contains 1208 joints, 2387 frame elements, and 2387 stiffness DOF. A rigid diaphragm assumption was made for the floor levels, and all the 3 degrees of freedom were retained at each level resulting in 42 DOF finite-element representation. A modal analysis was performed in order to estimate the frequencies and mode shapes of the structure.

Data collected on September 28 and October 7, 2009 are utilized for this study. These dates correspond to strong wind events with reported gusts in excess of 90 km/hr. The sensor responses at each floor level are converted to a triad of 3 responses at the center of mass using co-ordinate transformation. The correlation between the FE modes and identified modes is performed using the modal assurance criterion (MAC) defined by,

$$MAC_i = \frac{(\psi_i^T \bar{\psi}_i)^2}{(\psi_i^T \psi_i)(\bar{\psi}_i^T \bar{\psi}_i)}. \tag{5.7}$$

In Eq. 5.7, ψ_i and $\bar{\psi}_i$ represent the i^{th} mode shape vectors for the FE model and those obtained from the field data, respectively. MAC values range between 0 and 1, a value of

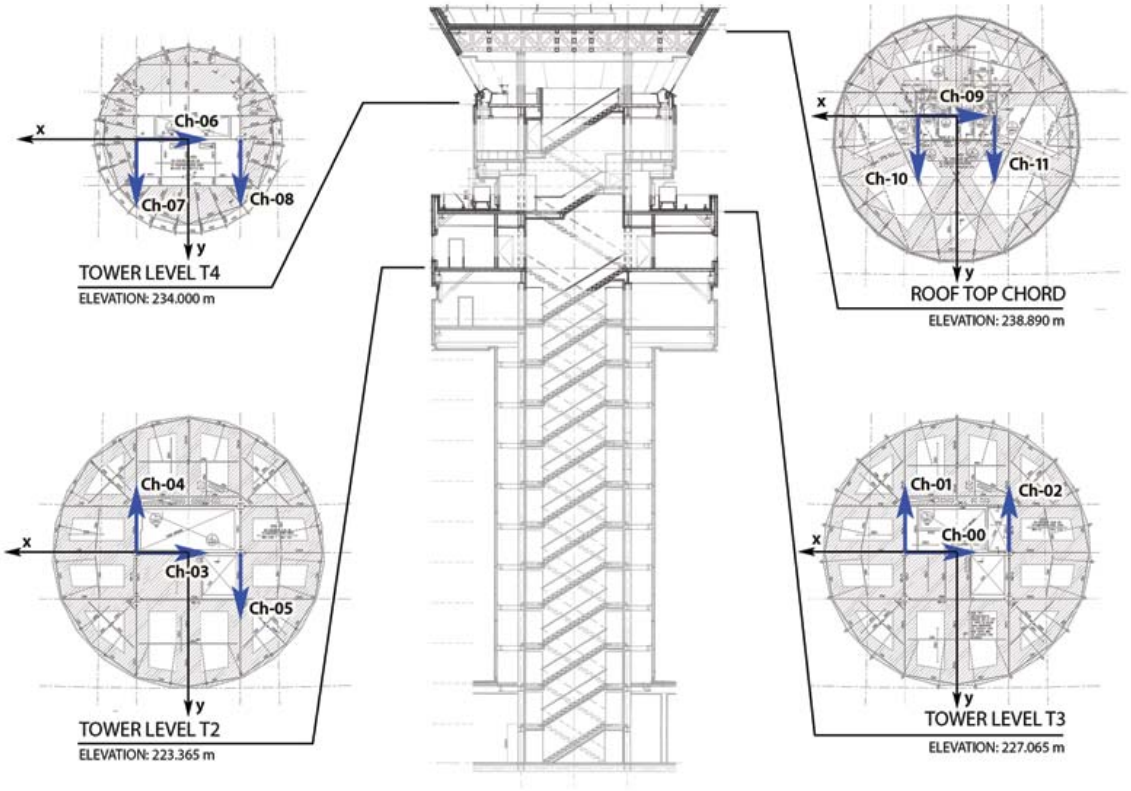

Figure 5.3: Sensor locations

1 meaning a perfect correlation.

5.3.2 Results and Discussion

Typical recorded accelerations at the roof of the structure are shown in Fig. 5.5. The presence of the dominant lateral modes in both the directions is clearly evident in the responses. The mean and the coefficient of variation (cov(%)) of the natural frequency and damping estimates for 100 trials using the MCC method are reported in Table 5.2. Nine dominant modes from a total of twelve sensor measurements were successfully identified using the MCC method. The MAC values between the FE estimates and the MCC

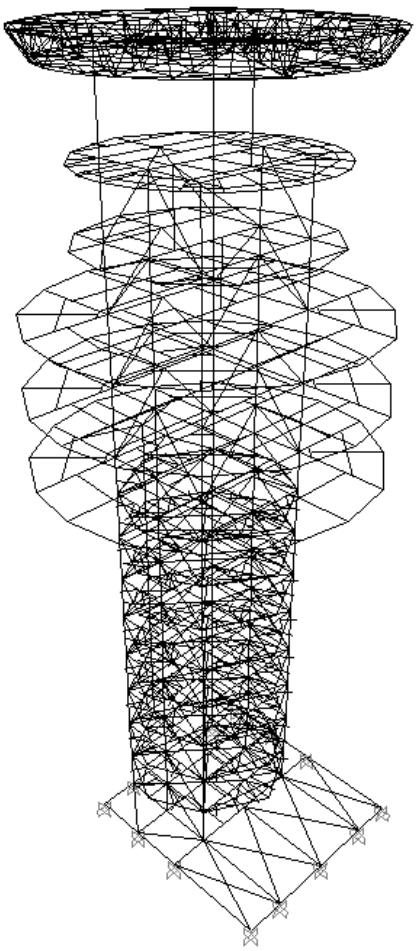

Figure 5.4: Finite-element Model of the Apron Control Tower

estimates for the nine modes are greater than 0.95. Furthermore, the covs for the natural frequency estimates are relatively small. These indicate good confidence in the estimation results, and the fidelity of the FE model. The mean values of modal damping are generally in the range of reasonable values for structures of this construction type, between 1-3% for the translational modes, and slightly higher for the torsional modes. A greater variation, characterized by larger cov, in the estimates of damping is also expected and consistent with the results from other studies [72]. The normalized mode-shapes for the first six modes is shown in Fig. 5.6. Statistical analysis of the natural frequencies obtained by

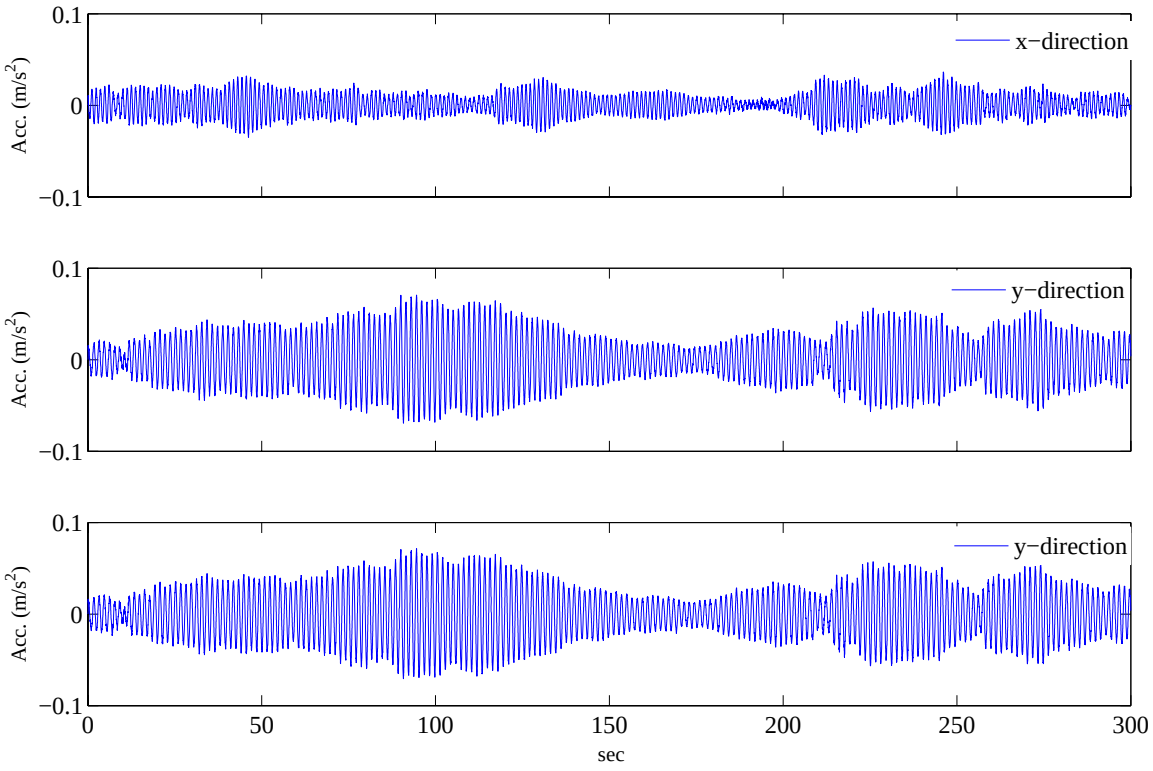

Figure 5.5: Roof acceleration responses for three sensors

conducting approximately 100 trials of identification is reported in the form of a normal probability plot in Fig. 5.7. It is clear from Fig. 5.7 that the identified frequencies follow a normal distribution and the statistical variability of the natural frequency estimates is relatively small.

Table 5.2: Identified frequencies and MAC values using the MCC method

Mode(#)	ω (Hz)	ω (Hz)		ζ(%)		MAC
	FEA	Mean	cov (%)	Mean	cov(%)	
1	0.66	0.68	1.30	0.84	23.0	0.98
2	0.92	0.86	3.50	1.98	19.0	0.96
3	1.40	1.50	1.90	2.91	21.0	0.97
4	2.70	2.66	1.80	1.20	15.0	0.99
5	3.01	2.92	1.80	2.81	15.0	0.98
6	3.36	3.47	2.00	4.30	22.6	0.97
7	4.59	4.65	2.10	2.65	15.2	0.98
8	6.08	6.11	1.80	2.96	21.2	0.99
9	6.71	6.62	2.20	4.56	24.1	0.98

Proceeding to the underdetermined case, only a sub-set of the sensor measurements, ranging from two sensors to six sensors, are assumed to be available for identification. Trigonometric shape functions are assumed for the initial estimate for the mixing matrix to start the iterative process. The n modes are discretely sampled from shape functions given by,

$$f^i\left(\frac{x}{l}\right) = \sin\left(\beta^i \frac{\pi}{2}\frac{x}{l}\right); \quad i = 1, 2, \cdots, n \tag{5.8}$$

where, x represents the location along the height of the structure and l the overall height.

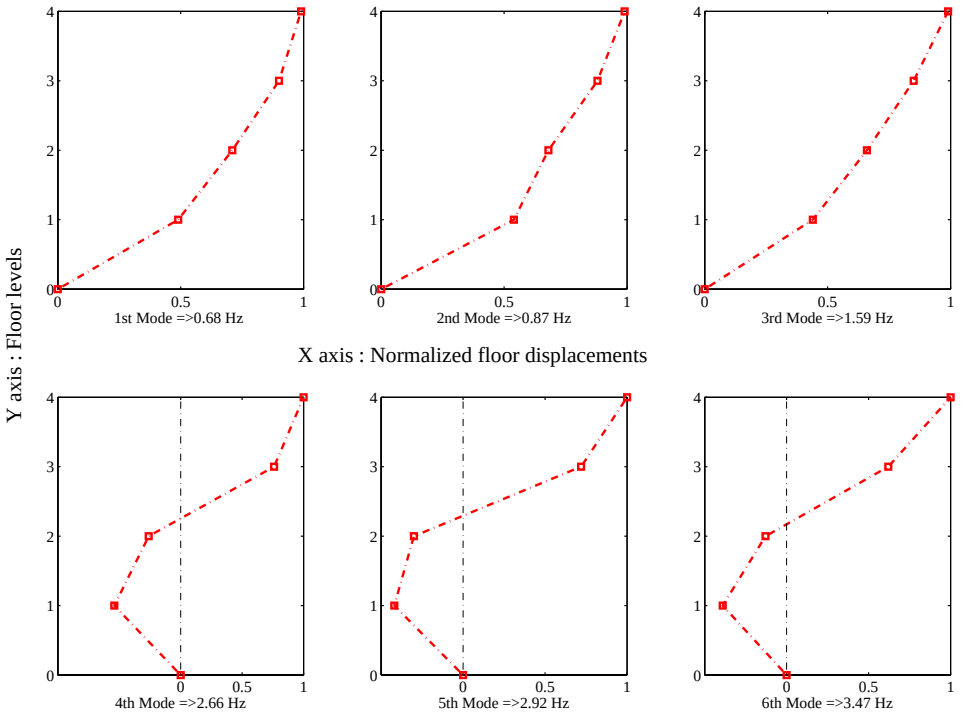

Figure 5.6: Mode shapes identified using MCC

The coefficients, β are normally distributed with mean values (μ) of 1, 3, 5 and 7 and standard deviations (σ) of 0.1, 0.25, 0.3 and 0.3 respectively. The reduced confidence in estimating higher modes is reflected in the larger values of standard deviations. Sensitivity study demonstrating the effect of β on the estimates, or lack thereof, is conducted by assuming distributions for β rather than point values. Initial estimates for n modes are generated by sampling n values from the distribution for each identification trial.

The results for the modes assuming mean values for β, $\mu + \sigma$ and an average for 50 trials by assuming samples from their respective distributions for β are shown in Fig. 5.8. The results are shown after the modes converge to the final estimate for the corresponding cases. The key conclusion is that the converged modes are relatively insensitive to the

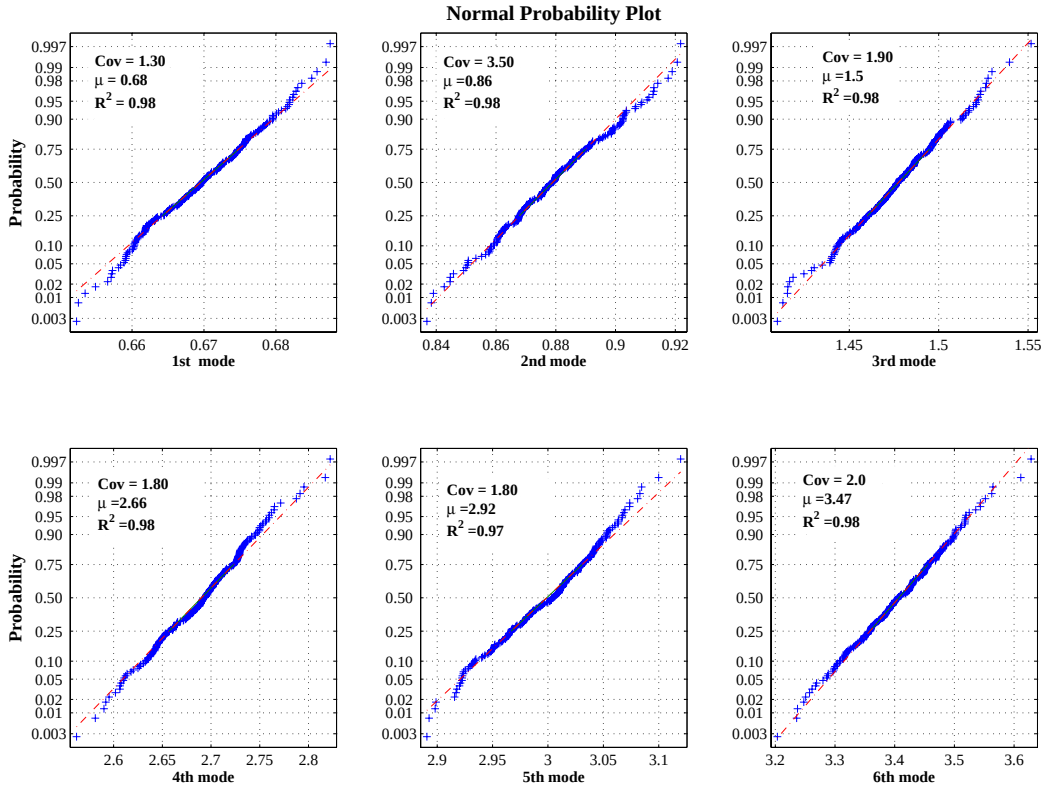

Figure 5.7: Normal probability paper plot of the identified natural frequencies

initial value for β, within the range considered, and all the initial estimates converge to their mean values. In order to study the effect of the number of sensors considered for identification, mean values are assumed for β and the identification is carried out on 100 data-sets. The average MAC values (with respect to FEA-modes) for the resulting modes are reported in Table 5.3 as a function of the number of sensors considered in each case. It is clear that the experiment results in identifying twelve modes for cases of 3 sensors or more. For the case where only 2 sensors are considered, the EMD-MCC method fails to identify the highest three modes. Typical IMFs for a sample case are shown in Fig. 5.9.

To assess the variability in the results amongst non-overlapping data-sets, 100 sub-sets

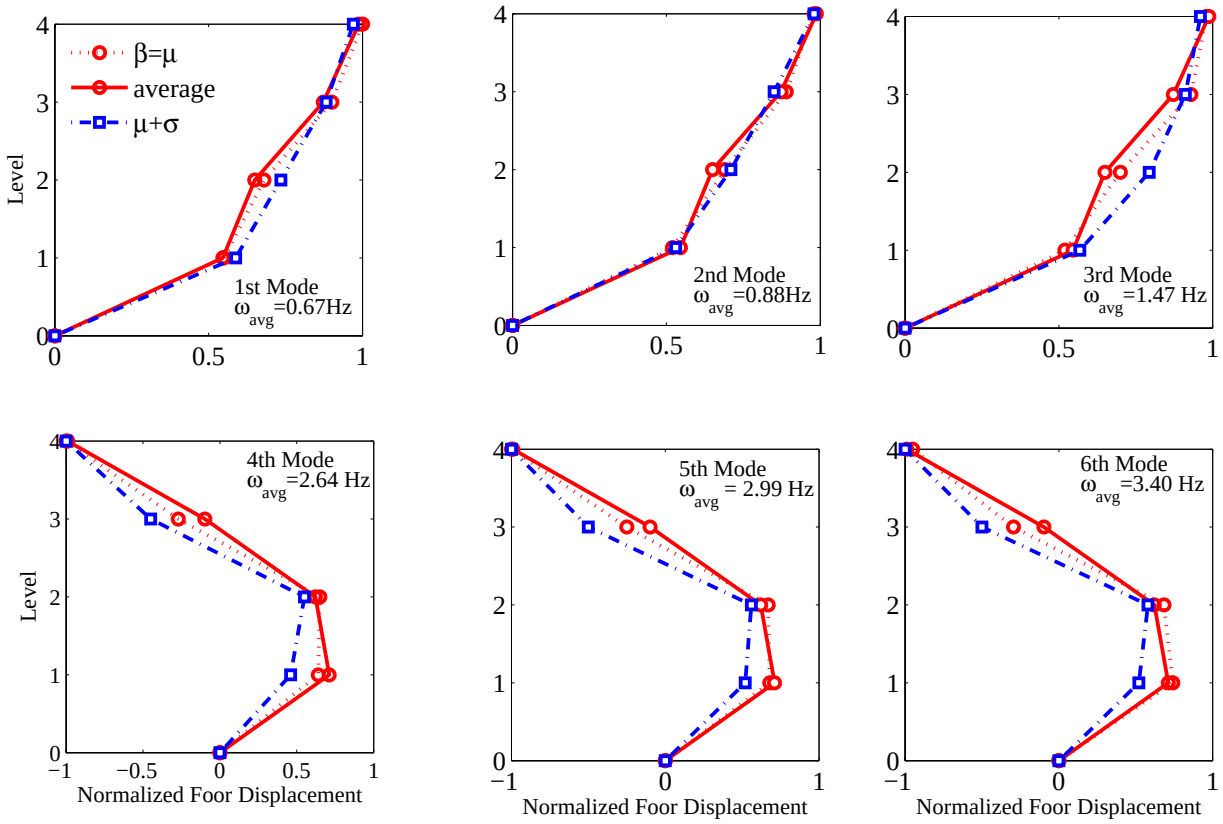

Figure 5.8: Sensitivity of identification to β

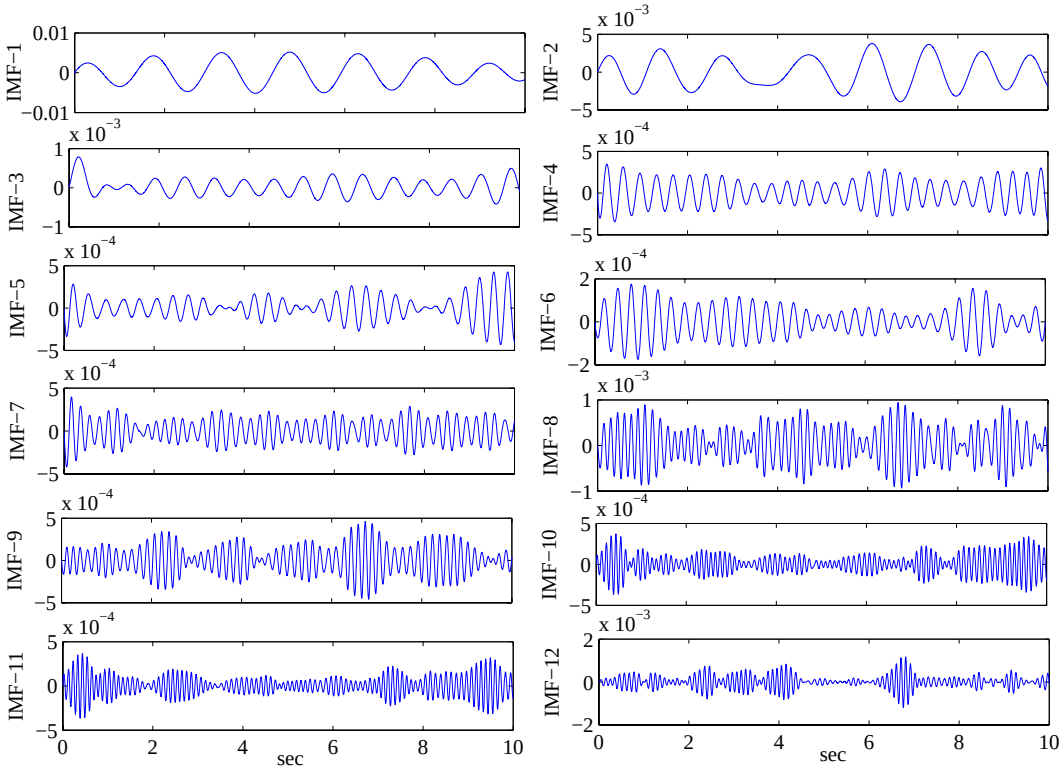

Figure 5.9: Intrinsic mode functions for a sample data-set

of data are considered and the mean and cov for the 12 identified modes are reported in Table. 5.4. The results assume measurements from 3 sensors (on the roof) and mean values for β. The dispersion in the identified frequencies and damping improve substantially for most of the modes when compared to the MCC method (Table 5.2). The convergence of the method, as evident from the steady-state average 2-norm of the error in Eq. 5.6, is shown in Fig. 5.10.

The availability of a high-fidelity FE model in this study allows a relatively straightforward means to select the appropriate frequency bands for processing the measurement data using EMD. It is likely that such accurate FE models or prior knowledge may not be available in many practical situations. A method to overcome this issue is proposed here. Contiguous frequency bands are selected from measurements from three sensors and the estimation is carried out using EMD-MCC for 100 non-overlapping data sets. The variation in the estimated frequencies and the average error in each contiguous band (given by elements of the vector $\boldsymbol{\gamma}$ in Eq.5.6) with a bandwidth of 0.5 Hz is shown in Fig. 5.11. It is clear that the average error is less corresponding to certain modal frequencies which correlate well to the presence of physical modes whereas, for frequency bands that do not contain physical modes, the average error is relatively large. Similar trends in the dispersion for the natural frequency estimates are also observed, but the results are not reported here for the sake of brevity. EMD allowed good delineation of closely-spaced modes in some frequency bands, which is an important result.

A short note on the main limitation of the proposed method. Motivated by the physical nature of the problem at hand, the issue of initial modal matrix estimate is overcome using shape functions that satisfy the essential boundary conditions, namely zero-displacement at the base of the structure. It is conceivable that such assumptions may not be possible for a large class of problems in the area of source separation, and hence no claims as to the efficacy of the proposed method are made in that regard. However, the results using

real-life measurement data do demonstrate the strength and usefulness of the proposed method in dealing with underdetermined problems in modal identification.

5.4 Summary

The MCC method is extended to handle the problem of underdetermined modal identification of structures. The underdetermined blind identification problem is solved by first using empirical mode decomposition (EMD) to generate the intrinsic mode functions (IMFs) and subsequently treating the IMFs as pseudo-sources in an iterative procedure within the framework of the MCC method. The capability of the method is demonstrated using actual measurements recently collected from the Apron Control Tower, located at the Pearson International airport in Mississauga, Canada. Results show that it is possible to estimate twelve dominant modes with the data obtained from as few as 3 sensors. Identification results show that the dispersion of the results for the natural frequencies is relatively small, indicating a good degree of confidence in the estimation procedure. The method is also shown to perform well under reduced number of sensors, which is clearly advantageous in dealing with situations involving limited sensors. The need for sensor measurements at the relevant degrees of freedom in order to identify the mode shapes is alleviated, which the main advantage of this method.

Although the proposed method is expected to perform well for a large class of ambient system identification problems, selecting the initial mixing matrix efficiently for general source separation problems still remains a challenge which is one of the shortcomings of the approach. Furthermore, this method fails to overcome the issue of identification due to the presence of very closely spaced modes with energy coupling, such as those found in structures equipped with TMDs. This issue is addressed in the next chapter in an alternate hybrid approach of combining EMD and MCC, which also exhibits the capability

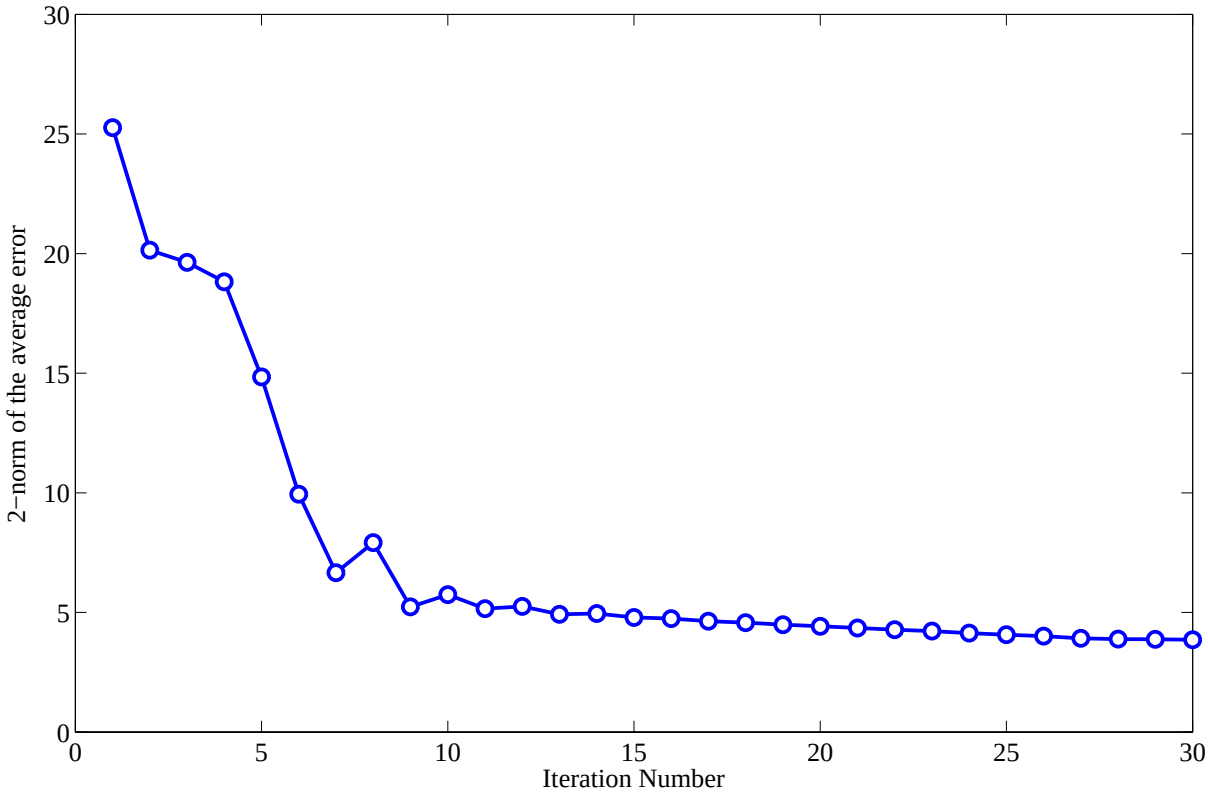

Figure 5.10: Convergence of the Emd-MCC method

to identify structures equipped with TMD.

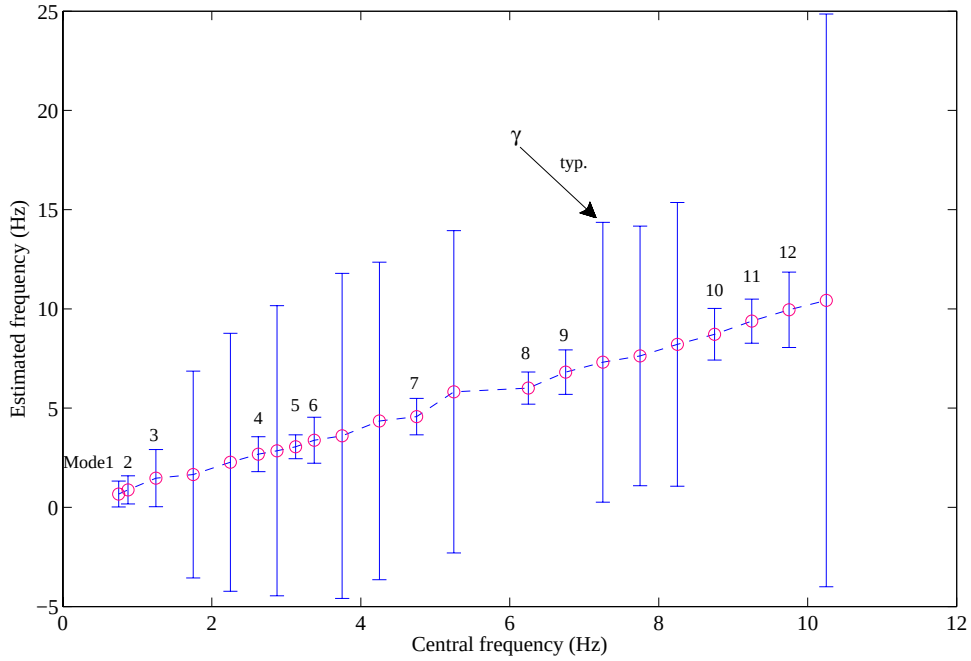

Figure 5.11: Convergence error for the case of contiguous frequency selection

Table 5.3: Performance of EMD-MCC method with reduced sensor density

Average MAC values						
Mode	No. of sensors					
#	1	2	3	4	5	6
1	0.99	0.99	0.99	0.99	0.99	0.99
2	0.98	0.98	0.98	0.98	0.98	0.98
3	0.97	0.98	0.98	0.98	0.98	0.98
4	0.98	0.98	0.98	0.98	0.98	0.98
5	0.97	0.98	0.98	0.97	0.97	0.98
6	-	0.97	0.98	0.97	0.97	0.98
7	0.97	0.98	0.98	0.98	0.98	0.98
8	0.99	0.98	0.98	0.98	0.98	0.98
9	0.97	0.98	0.98	0.98	0.98	0.98
10	-	0.95	0.97	0.98	0.98	0.98
11	-	-	0.98	0.98	0.98	0.98
12	-	-	0.98	0.97	0.98	0.98

Table 5.4: Statistics of identified frequencies (ω) and damping ($\zeta\%$) of the Apron Tower using EMD-MCC methods

Mode #	Model f(Hz)	ω (Hz)		ζ(%)		MAC
		Mean	Cov(%)	Mean	Cov(%)	
1	0.66	0.67	1.0	0.85	10.2	1
2	0.92	0.89	1.8	1.95	12.6	0.98
3	1.40	1.47	1.6	2.80	15.1	0.97
4	2.73	2.68	1.6	1.2	16.1	0.98
5	3.01	3.06	1.5	2.85	15.3	0.97
6	3.36	3.38	1.7	4.10	18.5	0.98
7	4.59	4.57	1.7	2.60	16.4	0.97
8	6.08	6.01	1.6	2.89	14.6	0.99
9	6.71	6.81	1.8	4.48	19.3	0.97
10	9.01	8.72	1.5	3.05	14.2	0.96
11	9.43	9.38	2.0	2.65	15.4	0.99
12	10.09	9.95	1.9	5.00	26.5	0.98

Chapter 6

Identification and Retuning of Inservice Tuned Mass Dampers

One of the main limitations of most time and frequency domain methods reviewed in chapter 2 is their inability to identify structures with relatively large damping and closely-spaced modes. Such instances occur, for example, in structures equipped with TMDs, which have become increasingly common [82, 51, 58, 53, 1]. To the knowledge of the knowledge of the author, this issue has not been addressed in the literature.

In this chapter, a novel hybrid time and time-frequency identification method, MCC-EMD, is introduced to address the problem of identification of structures with a TMD. The motivation to the identification of structures with TMD is provided first, followed by the description of the methodology. The re-tuning algorithms are presented next. The details of implementation, key results, and discussion are presented next. Experimental results for a two-story bench-scale model with a TMD are presented, followed by some important conclusions.

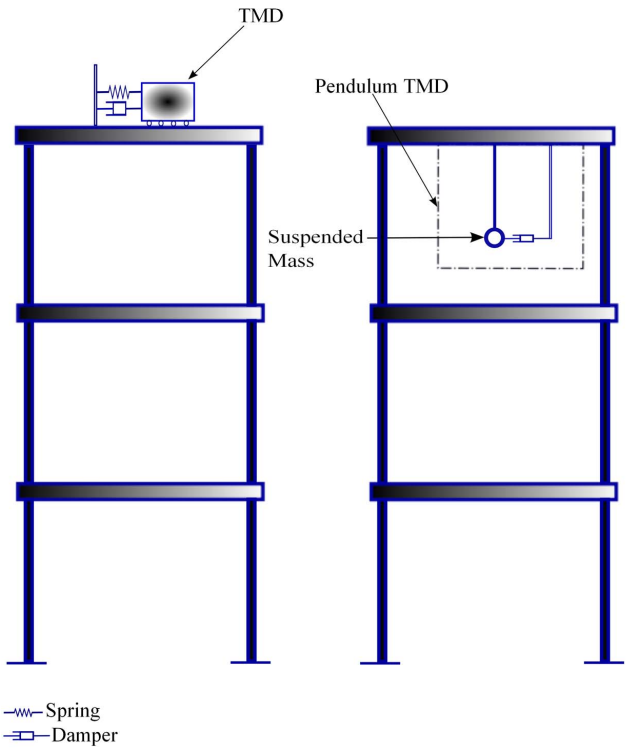

Figure 6.1: Multi-degree of freedom system with TMD

6.1 Motivation

Tuned mass dampers (TMD), are one of the most popularly deployed passive vibration energy dissipation devices in flexible structures [82, 51, 58, 53, 1]. Their performance is well documented in the literature, e.g., [26, 86, 74, 31]. Fig. 6.1 shows the two common types of TMD used in structures.

When tuned to the resonant mode of vibration of the primary structure, an optimally designed TMD adds significant damping in the dominant vibration modes, thereby reducing the overall vibration response of the structure. De-tuning, resulting from several

sources such as the alteration of the structural properties of the primary structure, deterioration of the TMD, in-correct design forecasts, etc., may lead to a significant loss in their performance. In order to re-tune the TMD, system identification of the primary structure while the TMD is in operation is often required, followed by an estimation of the modal properties of the bare-structure. In this chapter, a novel identification and re-tuning algorithm based on hybrid MCC and EMD method, is proposed. Using the proposed method, the system identification procedure and the steps necessary to re-tune a sub-optimal TMD using in-situ ambient vibration measurements are demonstrated.

Semi-active TMDs and multiple TMDs (MTMDs) are some examples of devices designed to overcome the problem of de-tuning in TMDs [69, 78, 52, 1, 18, 42]. These devices are fundamentally robust due to the nature of their design. For example, MTMDs feature several individual TMDs, each tuned to a distinct mode of vibration, while semi-active TMDs employ adaptive elements to respond to the changes in the operating environment. Many existing applications of TMDs feature a single TMD, either of translational or suspended type, with no provisions to adapt their intrinsic properties. Current practice to overcome the de-tuning problem in such traditional TMDs involves the determination of the modal properties of the primary structure while arresting the motion of the TMD [30]. Despite its simplicity, such an approach is both manually intensive and expensive. Alternatively, using the hybrid proposed here, the ambient vibrations measurements are used directly in the estimation and re-tuning process, without manual intervention.

There are two main difficulties that are overcome using the method proposed here. The first one is the difficulty introduced in the identification process due to the presence of closely spaced modes in the TMD-controlled structure, along with a relatively high damping in the fundamental mode(s) due to the TMD. The second difficulty is in the re-tuning procedure, wherein it is necessary to extract the modal properties of the bare-structure (without the effect of TMD) from the identified results of the structure with the TMD.

Extracting the modal properties of the bare structure is necessary because the optimal tuning parameters of the TMD are a function of the bare-structure modal properties. The application of time-domain methods such as NeXT-ERA, SSI, SOBI and MCC failed to identify the modal properties for a structure equipped with a TMD. Motivated by this, a new hybrid approach integrating the MCC and EMD procedures within the framework of blind identification is proposed.

Upon completion of the system identification procedure, there are two main tasks in the process of re-tuning the TMD. First, the fundamental frequency and the primary mode are estimated first using the measurement data obtained from the structure with a TMD. These estimates are then processed using a newly developed procedure to obtain the estimates for the optimal stiffness and the damping coefficients of the TMD. The methodology is validated using both numerical simulations and experimental tests. Although not pursued here, for the case of multiple TMDs tuned to different modes of the structure, more than one mode is required for re-tuning. Since the complete modal information is obtained from the system identification step, the extension of the proposed method to this case is expected to be straight-forward.

6.2 Modal Identification using MCC-EMD Method

The MCC method is unable to resolve sources with close spectral content, which is one its main drawbacks. This issue is of significance in the current study involving TMDs, as the presence of a TMD introduces an additional mode with relatively little separation from the structural mode of interest. In order to overcome this issue, the EMD method is integrated within the framework of the MCC method, called MCC-EMD method. The basic elements of the EMD signal processing technique has already been introduced in chapter 2. For the sake of completeness a brief description of EMD is presented first followed by the details of

the MCC-EMD method. To facilitate easy understanding of the material in the subsequent discussions a list of acronyms is provided in Table. 6.1.

Table 6.1: Important Acronyms

TMD	Tuned Mass Damper
EMD	Empirical Mode Decomposition
MCC	Modified Cross-Correlation
MTMD	Multiple Tuned Mass Damper
MDOF	Multi-Degrees-of-Freedom
SNR	Signal-to-Noise Ratio
MAC	Modal Assurance Criterion
RMS	Root-Mean-Square
PGA	Peak Ground Acceleration

The main purpose of EMD is to decompose a signal into intrinsic mode functions (IMF) that admit a well-behaved Hilbert transform [43]. For MDOF systems, the IMFs extracted from the free-vibration responses can be regarded as the modes of vibration [88]. An IMF is defined as a function that satisfies the following conditions: (i) it is mono-component and (ii) the mean values of the envelopes defined by the local maxima and the local minima are zero. The procedure of extracting an IMF is called sifting. Details of the shifting procedure have been explained in section 2.3.1 and are not repeated here.

Suitable band-pass filters need to be applied to the data to extract n IMFs, where n represents the number of desired modes [88]. For example, an acceleration response $\ddot{x}(t)$ can be decomposed into n IMFs according to:

$$\ddot{x}(t) \approx \sum_{j=1}^{n} x_j(t) + \epsilon(t) \tag{6.1}$$

where $\epsilon(t)$ represents the residual error.

Delineating modes containing high energy content in the spectrum is relatively straightforward. However, this exercise is difficult for modes with low energy content, reflected by their inconspicuous presence in the spectrum. This difficulty is overcome using the MCC-EMD method as explained next. In the proposed method, the first 2 closely spaced IMFs ($\Gamma_i, i = 1, 2$) of the structure (tuned to the first mode) are extracted using EMD according to:

$$\ddot{x} \approx \sum_{i=1}^{2} \Gamma_i(t) + \hat{\epsilon}(t) \tag{6.2}$$

Then, the auto-correlation of Γ_1 and Γ_2 for all time-lags is calculated and represented in a vector $\tilde{\mathbf{\Gamma}}$. Subsequently, the next $(n-2)$ modes are extracted from correlation of the responses ($\mathbf{r}$) using MCC according to:

$$\begin{aligned} \hat{\mathbf{A}}_r &= \mathbf{Q}^{-1}\mathbf{V}_{\bar{\mathbf{r}}} \\ \tilde{\mathbf{s}} &= \hat{\mathbf{A}}_r^{-1}\mathbf{r} \end{aligned} \tag{6.3}$$

Then, an augmented matrix $\mathbf{s}_e$ is constructed, expressed as:

$$\mathbf{s}_e = \left[\tilde{\mathbf{\Gamma}} \ \vdots \ \tilde{\mathbf{s}}\right] \tag{6.4}$$

The modal transformation matrix or the mixing matrix $\hat{\mathbf{A}}_e$ is estimated using the following least square estimator:

$$\hat{\mathbf{A}}_e = \left(\mathbf{s}_e^T\mathbf{s}_e\right)^{-1}\mathbf{s}_e^T \ \mathbf{r} \tag{6.5}$$

The natural frequencies and the corresponding damping estimates are calculated directly by applying Hilbert transform to the recovered sources, $\mathbf{s}_e$.

The MCC-EMD method is extended to the case when the number of sensors is less than the modes to be identified as follows. First, it is assumed that the mode-shapes of a flexural structure follows the deflected profile of the form $\hat{\phi}_i(\frac{x}{l})$ satisfying the zero displacement boundary condition at $x = 0$. These functions are used to approximate the mode shape coordinates at the degrees of freedom that are not instrumented ($\hat{\phi}_i(\frac{x}{l})$), and are given by:

$$\hat{\phi}_i(\frac{x}{l}) = \alpha_i \sin\left(([2i-1]+\beta_i)\,\frac{\pi x}{2l}\right); i = 1, 2, ..., n \tag{6.6}$$

where, x represents the sensor locations along the height of the structure having the overall height of l, and $\hat{\phi}_i$ is the estimated i^{th} mode of the mixing matrix $\hat{\mathbf{A}}_e$. The unknown coefficients α and β are estimated by minimizing the least-square error between the observed and the estimated values (using Eq. 6.6) of the mode-shape coordinates at the instrumented floor levels. Once α_i and β_i are estimated, the mode shape co-ordinates at the un-instrumented floor levels are obtained using Eq. 6.6.

6.3 Re-tuning

In order to derive the re-tuning algorithms, it is instructive to observe the equations of motion for a two-degree-of-freedom representation for the system shown below.

The equations of motion for the system in Fig. 6.2 can be written as:

$$\begin{aligned} M\ddot{X} + C\dot{X} + KX - \Big[k(x-X) + c(\dot{x}-\dot{X})\Big] &= w \\ m\ddot{x} + \Big[k(x-X) + c(\dot{x}-\dot{X})\Big] &= 0 \end{aligned} \tag{6.7}$$

where, $M,\ C,\ K$ are the mass, damping, and stiffness coefficients of the primary structure, and $m,\ c,\ k$ are the mass, damping, and stiffness coefficients of the TMD. w is the external excitation source, which is assumed to be Gaussian and white for the purposes of this study. Of particular interest is the case of TMD for a general N-degree primary structure. The

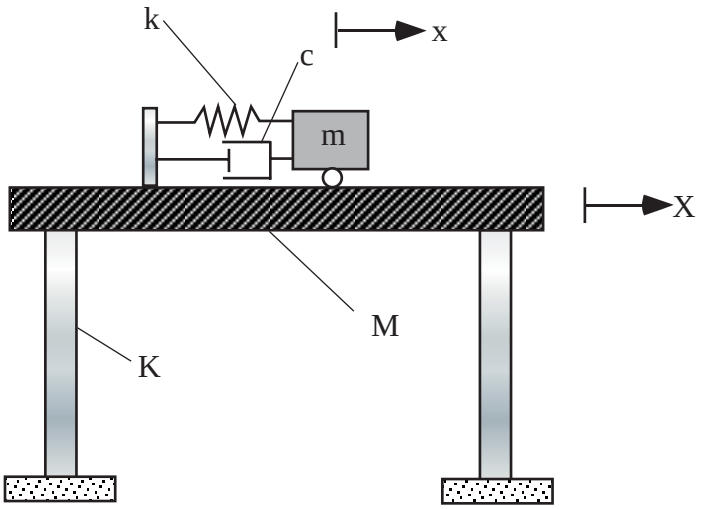

Figure 6.2: Two-degree of freedom model

equations of motion for the i^{th} mode when the TMD is present in the j^{th} floor level can be written as (assuming a proportionally damped system):

$$\begin{aligned} M_i\ddot{y}_i + C_i\dot{y}_i + K_i y_i - \phi_{ij}\left[k(x - X_j) + c(\dot{x} - \dot{X}_j)\right] &= w_i \\ m\ddot{x} + \left[k(x - X_j) + c(\dot{x} - \dot{X}_j)\right] &= 0 \end{aligned} \tag{6.8}$$

where, the quantities $M_i,\ C_i,\ K_i,\ w_i$ should be interpreted as corresponding to the i^{th} mode. From Eq. 6.7 and Eq. 6.8 one can readily observe that as long as ϕ_{ij} is normalized such that its value is 1 for the j^{th} location, the TMD design quantities obtained using Eq. 6.7 can be used directly to design a TMD corresponding to the i^{th} mode [74].

With this background, the optimal design TMD parameters are calculated for the system described in Fig. 6.2. The optimal TMD parameters are specified by its optimum mass ratio (μ_{opt}), optimum frequency ratio (f_{opt}), and optimum damping ratio (ξ_{opt}). These quantities represent the ratio of the TMD parameters to the corresponding primary structure parameters. Since it is the issue of re-tuning that is dealt with here, μ_{opt} is assumed to be according to the as-built system, i.e., $\mu_{opt} = \mu$, the mass ratio of the existing structure. Hence, f_{opt} and ξ_{opt} are determined as a function of the mass ratio and primary structure

damping ratio (ζ_p) using the procedure described next.

There are two main approaches to calculate the optimal tuning parameters of the TMD. In the first method, analytical formulae are developed by minimizing the Root-Mean-Square (RMS) acceleration (displacement) response of the primary mass. Such formulae have been well-documented in the literature for various types of excitations [86, 74, 31, 62, 60, 61]. The second approach is a numerical search, where the optimal values are determined using simulations. In this approach, many limitations that exist in the analytical methods such as the nature of disturbance, type of damping, etc., do not exist. The main idea here is to simulate the response quantity of interest, say the acceleration of the main mass, for various values of the frequency ratio (f) and TMD damping ratio (ζ_s) with a given mass ratio. This procedure is repeated for several mass ratios for a given ζ_p. The optimal values of frequency ratio and TMD damping ratio, f_{opt} and ζ_{opt} respectively, are obtained by minimizing the mean-square maximum floor acceleration divided by the mean-square of the excitation. This is repeated for different levels of ζ_p and the combination of f_{opt} and ζ_{opt} in each case are used to develop regression relationships for the optimal tuning parameters.

Fig. 6.3 shows the plots of f_{opt} and ζ_{opt} with respect to μ, for $\zeta_p = 2\%$ and 5% respectively. The results obtained using the procedure described above are processed using standard curve-fitting techniques. It is seen that the ζ_{opt} is insensitive to the value of ζ_p, whereas f_{opt} depends on ζ_p and thus, f_{opt} is further regressed over ζ_p. The final relationships so obtained (Fig. 6.9) are as follows:

$$\begin{aligned} \xi_{opt} &= 2.5\mu\,(1.0 - 3.25\mu) \\ f_{opt} &= \beta\mu^2 - 1.8\mu + 1.0 \end{aligned} \tag{6.9}$$

where, $\beta = 16.7e^{-60\zeta_p}$ and $0\% \leq \zeta_p \leq 5\%$. The optimal parameters valid for mass ratios in the range $0 - 0.15$ as described in Eq. 6.9, are illustrated in Fig. 6.4. An important observation to be noted from Fig. 6.4 is that for mass ratios less than 5%, the effect

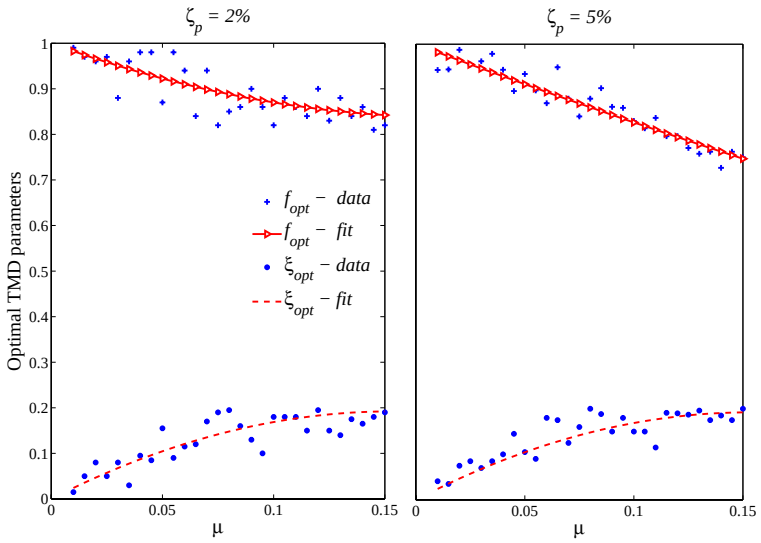

Figure 6.3: Optimal TMD parameters for various values of ζ_p

of primary structure damping ζ_p on the optimal frequency ratio f_{opt} is not significant. Similarly, the effect of ζ_p on ξ_{opt} is minimal for the range of values considered here. For the current study, ζ_p is assumed to be 2% in the fundamental mode.

The main issue in extending the expressions in Eq. 6.9 to a general $N-DOF$ system, whose i^{th} mode is described by Eq. 6.8, is the calculation of the modal mass ratio $\mu_i = \frac{m}{\phi_i^T \mathbf{M} \phi_i}$, and the corresponding frequency in the i^{th} mode. This means that the i^{th} mode and frequency of the $N-DOF$ primary structure is to be estimated-assuming the mass distribution of the structure is known-using the measurements obtained from the structure with the TMD. The procedure to determine ϕ_i is described next. Once ϕ_i is estimated, the optimal parameters of the TMD can be calculated using:

$$\begin{aligned} k_{opt} &= f_{opt}^2 \Omega^2 m \\ c_{opt} &= 2\xi_{opt} f_{opt} \Omega m \end{aligned} \tag{6.10}$$

where Ω is the natural frequency of the primary system to which the TMD is tuned.

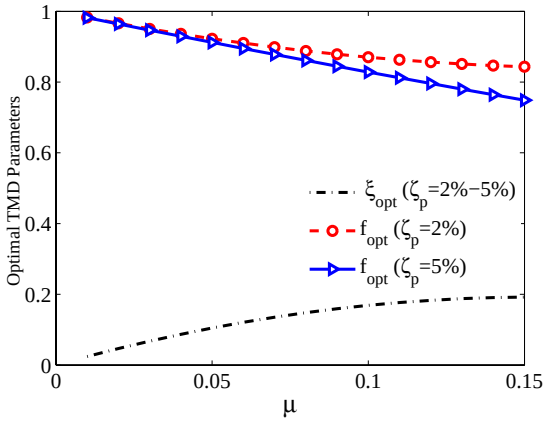

Figure 6.4: Regression models for optimal parameters of the TMD

6.3.1 Modal estimation of the primary structure and re-tuning

For the ensuing discussions and results, the TMD is assumed to be connected to the roof, i.e., the DOF represented by N. The estimates for the modal properties (size, $N+1$) using the MCC-EMD method for the structure with the TMD cannot be directly utilized for re-tuning, since they represent the TMD-controlled structure, not the bare structure. The estimates are updated to estimate the modal matrix of the bare structure as follows. To begin the re-tuning process, Ω, which is the fundamental frequency of the primary structure, is approximated by the arithmetic mean of the two lowest frequencies (ω_1 and ω_2) of the structure with the TMD according to:

$$\hat{\Omega} \approx \frac{\omega_1 + \omega_2}{2} \tag{6.11}$$

The modal parameters including ω_1 and ω_2 are determined using the MCC-EMD method described earlier. The columns of the estimated modal matrix $\tilde{\Phi}_{N+1\times N+1}$ corresponding to the two frequencies ω_1 and ω_2 are averaged, followed by an elimination of the row corresponding to $N+1$ DOF, resulting in the estimate, $\hat{\Phi}_{N\times N}$. This is motivated by the observation that the amplitude of the TMD motion is maximum in the neighborhood

of the tuned frequency, and minimum in the remaining ones. Once $\hat{\Phi}$ and $\hat{\Omega}$ are estimated, the optimal parameters of the TMD are calculated according to Eq. 6.9 and Eq. 6.10. The TMD is re-tuned using $\hat{\Phi}$ and $\hat{\Omega}$. The process is repeated until the difference in magnitude of the energy content in the frequencies ω_1 and ω_2 of the controlled structure reaches a specified tolerance, ϵ. This is given by:

$$\frac{\tilde{s}_e^k(\omega_1) - \tilde{s}_e^k(\omega_2)}{\tilde{s}_e^k(\omega_2)} \leq \varepsilon \tag{6.12}$$

where $\tilde{s}_e(\omega)$ is the magnitude of the Fourier transform of $\tilde{\mathbf{s}}_e(t)$, and k represents the iteration step.

The re-tuning method proposed above requires that the TMD be successively re-tuned at the end of each iteration step. Where this is not possible (due to practical or other limitations), two methods for re-tuning the TMD which do not involve iterative procedures are proposed. In the first method, the optimal frequency ratio, damping ratio, and the fundamental frequency are calculated according to:

$$\begin{aligned} \tilde{\Omega} &= E[\Omega] \\ \tilde{f}_{opt} &= E[f_{opt}] \\ \tilde{\xi}_{opt} &= E[\xi_{opt}] \end{aligned} \tag{6.13}$$

where $E[\cdot]$ denotes the expectation operator, which is the sample mean for the purposes of this study. These values are then used to calculate the TMD parameters according to Eq. 6.10. This method is referred to as *mean-level* re-tuning. In the second method, the optimal frequency ratio, damping ratio, and the fundamental frequency are calculated according to:

$$\begin{aligned}
\tilde{\Omega} &= E[\Omega] + \sigma_{\Omega} \\
\tilde{f}_{opt} &= E[f_{opt}] + \sigma_{f_{opt}} \\
\tilde{\xi}_{opt} &= E[\xi_{opt}] + \sigma_{\xi_{opt}}
\end{aligned} \tag{6.14}$$

where, σ denotes the standard deviation of the corresponding quantity. Re-tuning according to Eq. 6.14 is referred to as $mean + \sigma$ level re-tuning. In both these methods, the only requirement is the availability of multiple observations to allow for a statistically meaningful analysis. This could be, for example, in the form of a relatively long observation period to allow for segmentation of the data into several non-overlapping windows of data.

6.4 Numerical Simulation

6.4.1 Numerical Model

A 5−storey structure model with a TMD at the top floor [62] is simulated to demonstrate the methodology, and to present the key results for the proposed algorithm. The state-space model for this system system subjected to an external disturbance vector, $\mathbf{w}$ is given by:

$$\begin{aligned}
\dot{\mathbf{x}} &= \mathbf{A}\mathbf{x} + \mathbf{E}\,\mathbf{w} \\
\mathbf{y} &= \widetilde{\mathbf{C}}\mathbf{x}
\end{aligned} \tag{6.15}$$

Here, the vector $\mathbf{x}$ is a vector of states, and the vector $\mathbf{y}$ represents the output vector, which is governed by the $\widetilde{\mathbf{C}}$ matrix. The matrix, $\mathbf{E}$ governs the location of the excitation on the structure. The system matrix, $\mathbf{A}$ is constructed using the mass, stiffness and damping properties, whose structure are shown below:

$$\mathbf{M} = \begin{bmatrix} M[\mathbf{I}]_{5\times5} & [\mathbf{0}]_{5\times1} \\ [\mathbf{0}]_{1\times5} & m \end{bmatrix}$$

$$\mathbf{K} = \begin{bmatrix} [\mathbf{K}_s]_{5\times5} & [\mathbf{0}]_{5\times1} \\ [\mathbf{0}]_{1\times5} & [0]_{1\times1} \end{bmatrix} + \begin{bmatrix} [\mathbf{0}]_{4\times4} & [\mathbf{0}]_{4\times2} \\ [\mathbf{0}]_{2\times4} & k\begin{bmatrix} 1 & -1 \\ -1 & 1 \end{bmatrix} \end{bmatrix} \tag{6.16}$$

$$\mathbf{C} = \begin{bmatrix} [\mathbf{C}_s]_{5\times5} & [\mathbf{0}]_{5\times1} \\ [\mathbf{0}]_{1\times5} & [0]_{1\times1} \end{bmatrix} + \begin{bmatrix} [\mathbf{0}]_{4\times4} & [\mathbf{0}]_{4\times2} \\ [\mathbf{0}]_{2\times4} & c\begin{bmatrix} 1 & -1 \\ -1 & 1 \end{bmatrix} \end{bmatrix}$$

where, $\mathbf{K}_s$, $\mathbf{C}_s$, k, c stands for superstructure, and TMD stiffness and damping coefficients, respectively. For the bare structure, the weight of each floor is assumed to be 19.2 kN, and the natural frequencies are 0.91, 3.37, 7.11, 10.66, and 12.73 Hz. The damping is assumed to be 2% critical in all modes. The weight of the TMD is 2.74 kN, $k = 77.8$ N/cm, and $c = 3.72$ N.s/cm. The mode shape matrix for the bare structure is given by [62]:

$$\begin{bmatrix} 1.00 & 1.00 & 1.00 & 1.00 & 1.00 \\ 3.02 & 2.12 & 0.92 & -0.33 & -1.21 \\ 5.27 & 1.89 & -0.64 & -0.63 & 1.12 \\ 7.31 & 0.18 & -0.96 & 0.88 & -0.70 \\ 8.96 & -2.09 & 0.74 & -0.35 & 0.21 \end{bmatrix} \tag{6.17}$$

Two kinds of excitations are considered for this study: stationary un-correlated white noise generated from a Gaussian distribution, and earthquake (El Centro ground motion, PGA of $0.3g$) excitation. Results for the case of availability of measurements at all the degrees of freedom, and partial availability of measurements (accelerations at the 1^{st}, 3^{rd},

the roof, and the TMD level) are studied. To investigate the sensitivity of noise on the performance of the proposed method, limiting cases of 0% and 20% Signal-to-Noise Ratio (SNR) are considered. The correlation between the theoretical structural modes and the identified modes is performed using the Modal Assurance Criterion (MAC)[65].

6.4.2 Identification Results

The results of identification of the structure with the TMD using the MCC-EMD method is presented in this section. In this approach, the first two closely spaced modes are extracted by decomposing the acceleration signal obtained from the higher floors using EMD, followed by the application of suitable intermittency criteria. Then, the remaining 4 well-spaced modes are separated by first eliminating the 2 modes extracted using EMD through suitable high pass filters, followed by the application of MCC method to the residual signal.

The identification results from traditional SOBI and MCC methods are relatively poor in the presence of a well-tuned TMD. This is evident from the simulation results presented in Table 6.2. Table 6.2 shows the correlation of the predicted and theoretical modes as a function of tuning ratio (α), defined as:

$$\alpha = \frac{f}{f_{opt}} \tag{6.18}$$

where f stands for tuning frequency. $\alpha = 1$, implies an optimally designed TMD, whereas other values correspond to de-tuned cases. It is evident from the results that as α approaches 1, SOBI and MCC methods are unable to provide reliable estimates for the two dominant modes. The performance deteriorates further in the presence of measurement noise (results not shown).

The results presented next are for the case of the structure with TMD using the MCC-EMD method. The process of sifting to delineate the two closely-spaced modes using

Table 6.2: Results from the SOBI and MCC methods in terms of MAC as a function of the tuning ratio (α)

	SOBI						MCC					
α	Mode						Mode					
	1	2	3	4	5	6	1	2	3	4	5	6
4.0	0.99	0.99	0.99	0.99	0.99	0.99	0.99	0.99	0.99	0.99	0.99	0.99
3.0	0.99	0.99	0.99	0.99	0.99	0.99	0.99	0.99	0.99	0.99	0.99	0.99
2.5	0.99	0.99	0.99	0.99	0.99	0.99	0.99	0.99	0.99	0.99	0.99	0.99
2.0	0.98	0.98	0.99	0.99	0.99	0.99	0.99	0.99	0.99	0.99	0.99	0.99
1.5	0.95	0.97	0.98	0.99	0.99	0.99	0.98	0.98	0.99	0.99	0.99	0.99
1.2	0.92	0.96	0.98	0.98	0.98	0.99	0.95	0.96	0.99	0.99	0.99	0.99
1.1	0.89	0.93	0.98	0.98	0.98	0.99	0.91	0.94	0.99	0.99	0.99	0.99

EMD is shown in Fig. 6.5. The effect of adding noise is studied next, and the results are presented in Table 6.3. When the accelerations at all the floor locations are available, the MCC-EMD method is able to identify the modes of the structure well. The results hold true for the case of SNR=20% as well, and the mode shapes are presented in fig. 6.6. The average frequencies and damping ratios for 50 trials using monte-carlo simulation, and the absolute values of percentage errors with respect to their theoretical values are presented in Tables 6.4 and 6.5. From these results, it can be seen that the results of identification are accurate for all the modes, for both stationary and earthquake cases. The error in the damping estimates is within 5%, which is slightly more than the frequency estimates

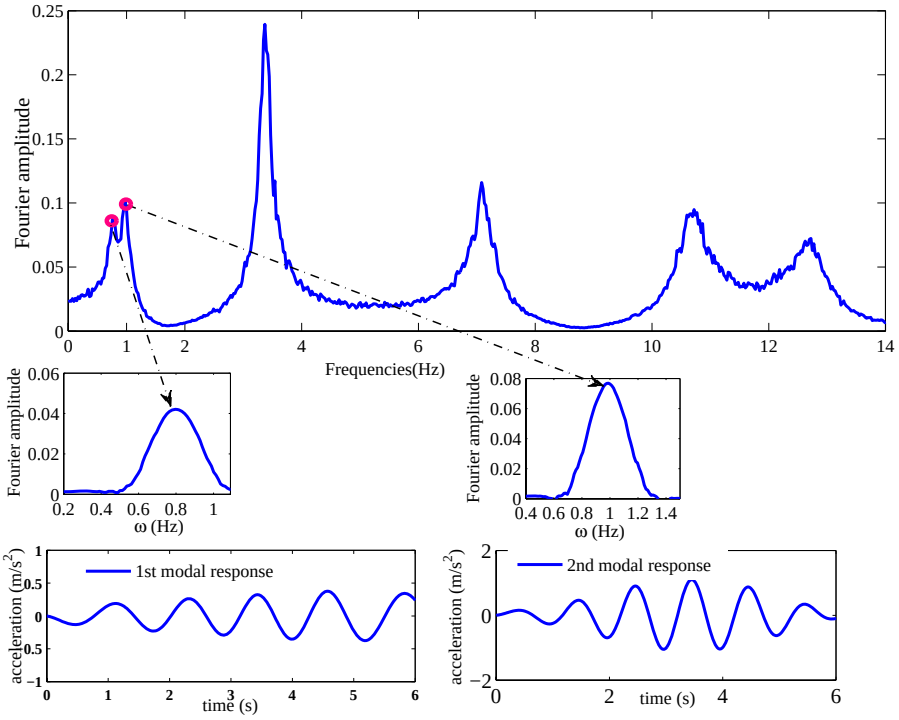

Figure 6.5: Delineation of closely spaced modes using EMD

(within 2.6%). The presence of the TMD results in relatively large values of damping-more than 7% critical-for the two lowest modes.

The MCC-EMD method is then used to identify the TMD controlled system when only partial floor acceleration measurements are available, and the results are presented in Tables 6.3, 6.4 and 6.5 alongside the full response cases. To obtain the mode shapes, a least square error minimization procedure between the observed and the estimated mode shape coordinates is adopted as explained previously. The unknown coefficients α_i and β_i are estimated by minimizing the least square error between the observed and the estimated values (using Eq. 6.6) of the mode-shape coordinates at the 1^{st}, 3^{rd}, 5^{th} floor levels. Once α_i and β_i are estimated, obtaining the mode shape co-ordinates at the 2^{nd} and 4^{th} floor levels for the four modes becomes a relatively straightforward task. Estimating the 6^{th} mode by the application of Eq. 6.6 is difficult due to a large change in the curvature. The

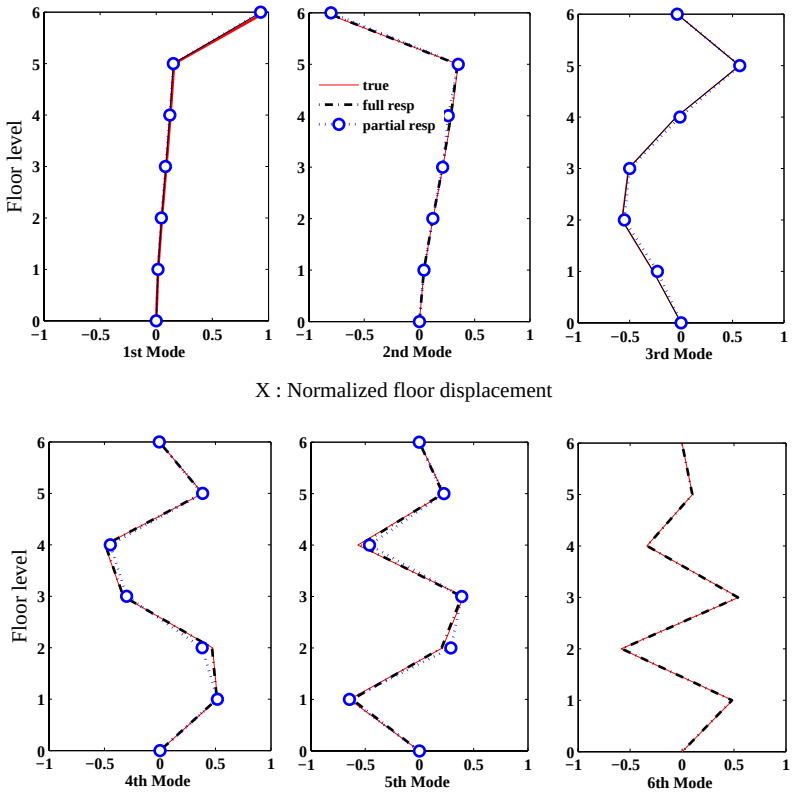

Figure 6.6: Identified Mode-shapes

identified values of frequencies and damping ratios are reasonably accurate for the first 5 modes. Compared to the frequency estimates, the absolute values of percentage errors in the damping estimates is slightly higher. The normalized mode shapes for the first 5 modes are shown in Fig. 6.6. It can be observed from Fig. 6.6 that the method fails to estimate the 6^{th} mode shape for the reason stated earlier. However, the frequencies and damping for all the 6 modes are identified with sufficient accuracy, even in the presence of measurement noise, which is an important result.

Table 6.3: Results of identification for two values of signal-to-noise ratio (SNR)

Mode No	White Noise				Earthquake			
	SNR=0%		SNR=20%		SNR=0%		SNR=20%	
	Full	Partial	Full	Partial	Full	Partial	Full	Partial
1	0.97	0.96	0.97	0.95	0.97	0.95	0.96	0.95
2	0.99	0.99	0.98	0.98	0.99	0.97	0.98	0.97
3	0.99	0.99	0.99	0.98	0.99	0.98	0.99	0.98
4	0.99	0.99	0.99	0.99	0.99	0.99	0.99	0.98
5	0.99	0.99	0.98	0.99	0.99	0.98	0.99	0.97
6	0.99	-	0.99	-	0.99	-	0.98	-

6.4.3 Re-tuning Results

The mode-shape and the fundamental frequency estimates for a single iteration cycle for the 6-DOF structure (given in Eq. 6.15 and Eq. 6.16), for various levels of de-tuning, are presented in Table 6.6. A parameter λ is used to vary the TMD stiffness of the controlled system (i.e, $k_{tmd} = \lambda k_{opt}$). From the results it can be concluded that the mode-shapes of the 5-DOF system can be identified with a high degree of confidence, as reflected by their MAC values, using the procedure outlined earlier. However, a single iteration consistently under-estimates the fundamental frequency Ω. Furthermore, the accuracy tends to decrease as λ is in the neighborhood of 1.0, which is the optimal value.

To assess the effectiveness of the *mean-level* and the *mean+σ* level re-tuning algorithms, 50 trials of simulations are performed, and the identification is carried out using the proce-

Table 6.4: Identified frequencies, modal damping ratio, and the error (*in parentheses*) of the structure with the TMD for the broad-band excitation case with SNR = 20%

Mode No	ω (Hz)			ζ(%)		
	True	Full	Partial	True	Full	Partial
1	0.78	0.79	0.79	7.67	7.93	7.99
		(1.28%)	(1.28%)		(3.12%)	(3.9%)
2	0.99	1.00	1.01	7.20	7.00	6.96
		(1%)	(2%)		(2.78%)	(3.33%)
3	3.38	3.40	3.41	2.16	2.10	2.08
		(0.59%)	(0.89%)		(2.78%)	(3.70%)
4	7.10	7.08	7.07	2.032	1.98	1.96
		(0.28%)	(0.42%)		(2.56%)	(3.54%)
5	10.66	10.67	10.68	2.007	1.96	1.94
		(0.09%)	(0.19%)		(2.34%)	(3.34%)
6	12.73	12.50	12.48	2.001	1.99	1.96
		(1.81%)	(1.96%)		(0.55%)	(2.05%)

dures described in the previous section. A parameter λ is used to vary the TMD stiffness of the controlled system (i.e, $k_{tmd} = \lambda k_{opt}$). The values of λ are considered between 0.75-1.25, to reflect various levels of de-tuning. The cases where λ varies between 0.75-0.9 refer to an *under-tuned* system, whereas the same between 1.00 - 1.25 refers to an *over-tuned* system. To verify the accuracy of the iterative re-tuning method, the algorithm is implemented on a single set of data, unlike the multiple sets necessary for the *mean-level* and the *mean+σ* level re-tuning algorithms. These are shown in Figs. 6.7 to 6.9.

Table 6.5: Identified frequencies and MAC values of 5 storey TMD system using $El-Centro$ ground motion response with SNR = 20%

Mode No	ω (Hz)			ζ(%)		
	True	Full	Partial	True	Full	Partial
1	0.78	0.79	0.80	7.67	7.97	8.00
		(1.28%)	(2.56%)		(3.64%)	(4.03%)
2	0.99	1.00	1.01	7.20	6.99	6.95
		(1%)	(2%)		(2.92%)	(3.47%)
3	3.38	3.40	3.42	2.16	2.09	2.07
		(0.59%)	(1.18%)		(3.24%)	(4.17%)
4	7.10	7.06	7.03	2.032	1.96	1.94
		(0.56%)	(0.99%)		(3.54%)	(4.53%)
5	10.66	10.70	10.74	2.007	1.95	1.92
		(0.38%)	(0.75%)		(2.84%)	(4.33%)
6	12.73	12.49	12.47	2.001	1.97	1.95
		(1.89%)	(2.04%)		(1.55%)	(2.55%)

From Fig. 6.7, it is evident that as λ approaches 0.9, the performance of *mean*-level re-tuning deteriorates compared to the other three methods. This observation is consistent with the results in Table 6.6, where the error in the estimate of Ω increases as λ approaches 1. The *mean*+σ-level re-tuning provides more reliable estimates of the optimal TMD parameters, which is clear from the Fourier amplitudes corresponding to the closely-spaced modes. The results of re-tuning using the iterative method is comparable to *mean*+σ-level re-tuning. Observations along similar lines can be drawn for the case of an over-tuned system as evidenced by Fig. 6.8.

Table 6.6: Identification of the primary structure from the controlled structure

λ	MAC values					Ω	$\hat{\Omega}$	%error
	1	2	3	4	5	true	est	
0.75	0.99	0.99	0.99	0.99	0.99	0.91	0.88	3.30
0.90	0.99	0.99	0.99	0.99	0.99	0.91	0.86	5.49
1.00	0.99	0.99	0.99	0.99	0.99	0.91	0.87	4.40
1.10	0.98	0.99	0.99	0.99	0.99	0.91	0.89	2.20
1.25	0.98	0.99	0.98	0.99	0.99	0.91	0.88	3.30

The average of the error given by Eq. 6.12, for 50 simulation trials is shown in Fig. 6.9 as a function of the p, which is the ratio of the TMD mass to the total structure mass, for the under-tuned case. It can be seen that the iterative method of re-tuning converges close to the optimally tuned condition rapidly (i.e., within 2 iterations). Similar results are observed for the over-tuning case as well, but they are not included here due to space limitations.

6.5 Experimental Study

In order to demonstrate the practical applicability of the proposed identification and re-tuning methods, the algorithms are implemented using acceleration data acquired from a bench-scale two-story model with a pendulum TMD as shown in Fig. 6.10. The structural model consists of two floor weights, 140 N each. Flexural stiffness is provided by four 1.30 cm aluminum equal angles, 130 cm tall and 0.17 cm thick. The identified lateral

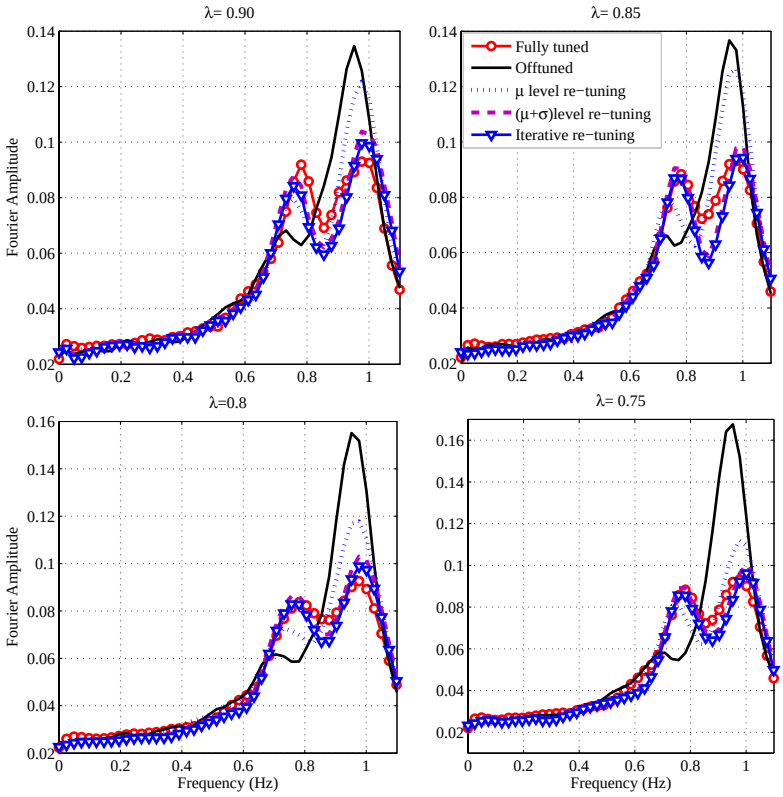

Figure 6.7: Results for re-tuning for an under-tuned system

frequencies of this system are approximately 2.65 Hz. The identified structural damping in both the lateral directions is approximately 2% critical. The suspended mass is 1.5 kg, which corresponds to a mass ratio of approximately 5%. The position of a tuning frame as it slides inside a rail provides a simple means to adjust the natural frequency of the pendulum. An air-damper is connected between the suspended mass and the rail assembly to provide a small amount of damping to the pendulum TMD. A broad-band excitation is commanded to an actuator (shaker shown in Fig. 6.11)connected to the first floor level, and the accelerations are recorded using low-frequency accelerometers at both the floor levels, in both directions. The theoretically calculated optimal length of the pendulum

for the set-up in Fig. 6.10 (and Fig. 6.11) using the expressions given in Eq. 6.10 is 44 mm, which will serve as a base-line to compare the re-tuned length. The mode shape and frequency for this purpose was obtained by constructing a finite-element model of the model, and conducting an eigen-value analysis of the system.

The tuning frame is adjusted first to a de-tuned configuration with an effective length of 35 mm, and the acceleration response data are collected for the broad-band excitation case. The sampling frequency is set to 100 Hz throughout the experiment. The excitation is connected to the lower floor. The MCC-EMD method, along with the re-tuning algorithms are implemented on the measured data. The optimal length as calculated using *mean*-level and *mean*+σ level algorithms are 41.1 mm and 44.6 mm, respectively. A total of 20 time-segments were used for the calculations, and the structure was excited for a total of 5 minutes. The magnitude of the transfer function between the roof acceleration and the command force is shown in Fig. 6.12, for three cases: de-tuned, mean and mean+σ-level re-tuning. The advantage of re-tuning is clearly evident from the transfer function plot. As was previously observed from the simulation results, the mean+σ level re-tuning provides good estimates for the optimal length, and the mean-level re-tuning results in lower estimates. The iterative re-tuning provided identical values of the optimal length as the mean+σ-level re-tuning, and are hence not shown.

6.6 Summary

A novel hybrid time and time-frequency identification algorithm based on blind source separation principles, called the MCC-EMD method, is proposed for structures equipped with TMDs. This method is then extended to re-tune TMDs using ambient vibration measurements. The proposed algorithm uses empirical mode decomposition (EMD) to separate the closely spaced modes, followed by the application of the MCC method to

resolve the remaining well-separated modes. It is shown that the identification method is robust to relative high levels of noise, of the order of 20%, and can be extended to the case of partial measurements as well. Furthermore, it is shown that the new method to re-tune TMDs is effective for a range of conditions, and is capable of handling practical situations as evidenced from the experimental results involving ambient measurements.

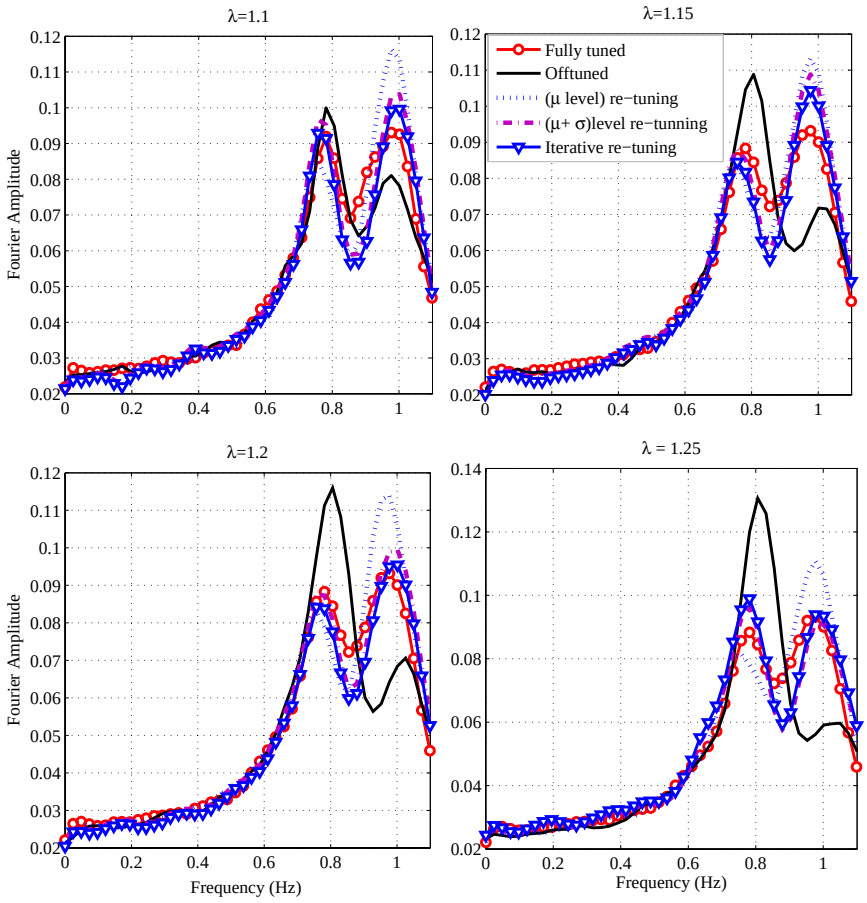

Figure 6.8: Results for re-tuning for an over-tuned system

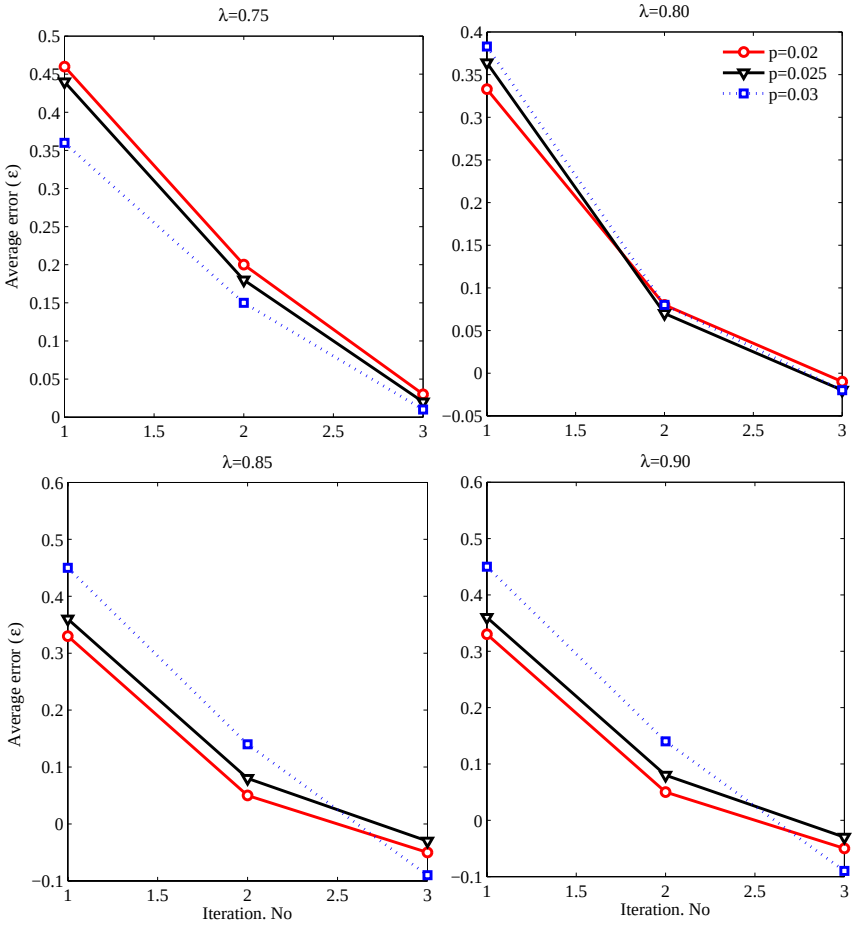

Figure 6.9: Convergence of the iterative re-tuning method, under-tuned case

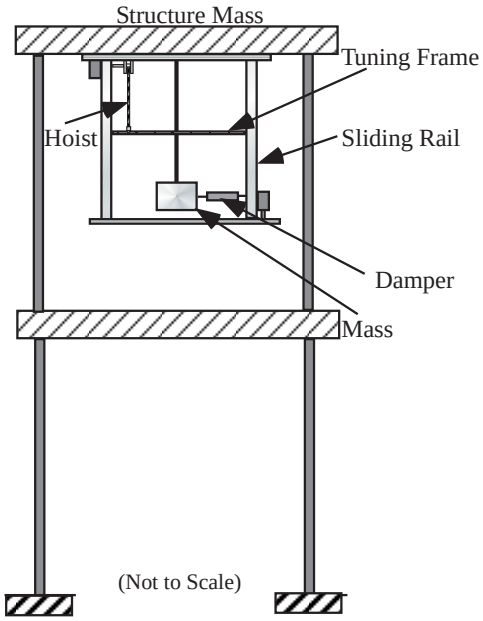

Figure 6.10: Schematic of the experiment to validate the identification and re-tuning algorithms

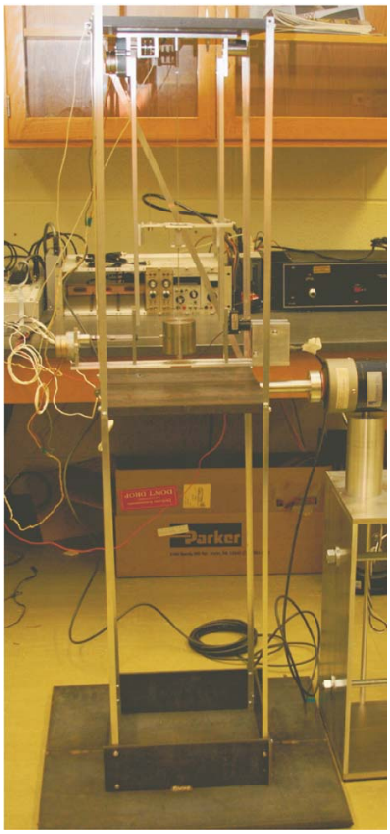

Figure 6.11: Experimental set-up and instrumentation details

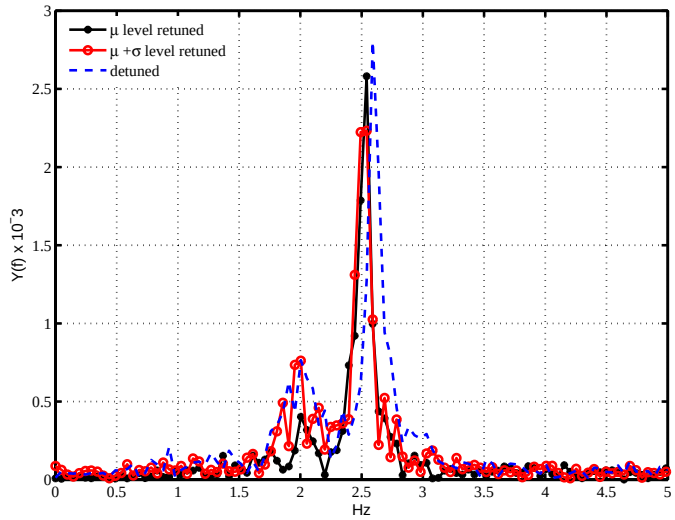

Figure 6.12: Magnitude of the transfer function for the tuned and the de-tuned cases

Chapter 7

Conclusions and Recommendations

An extensive study of blind identification techniques has been undertaken in this dissertation, with special emphasis on amalgamating the time domain and time frequency domain techniques, to develop a set of new hybrid time and time-frequency source separation methods. En-route, several milestones have been achieved in the context of blind identification of structures. The key contributions of this research are briefly summarized as follows:

1. A new blind identification has been developed in time domain called modified cross correlation method (MCC). This method extends the ideas of SOBI to address modal identification of full-scale structures subjected to ambient vibrations. Specifically, the issue of estimating damping and the presence of noise is addressed in this framework.

2. A hybrid time and time-frequency method extending the concepts of MCC to the wavelet domain utilizing stationary wavelet transforms has been introduced.

3. A novel hybrid algorithm, called EMD-MCC to address the case of under-determined blind identification of full-scale structures has been developed. This method utilizes the concepts of a time-frequency decomposition, known as empirical mode decomposition, and forms a hybrid approach within the framework of BSS.

4. The concept of hybrid time and time-frequency integration is extended to address the issue of identification of structures with large amount of damping in the primary modes, specifically for the case of structures equipped with TMDs. The methodology is then extended to re-tune in-service TMDs.

5. Contributions listed in items 1 and 2 have already been accepted in reputed international journals [37, 35]. Contribution listed in item 2 was selected as a featured article by the Journal Smart Materials and Structures. Contributions listed in items 3 and 4 are currently under review in reputed international journals [39, 38].

7.1 Conclusions

Having highlighted the significant contributions of this dissertation, the central conclusions in this dissertation are summarized as follows:

1. Most existing methods to perform BSS such as ICA and SOBI, fail to perform adequately in the presence of even relatively small amounts of damping. In this regard, the MCC method, which is an extension of the traditional SOBI technique, performs better than SOBI under non-stationary excitations and moderate amount of damping. MCC outperforms SOBI for very high levels of damping under stationary excitations .

2. WMCC performs better than its time domain counterparts, MCC and SOBI, in identifying full-scale structures under both ambient and earthquake excitation cases. Case studies have shown that the method is more equipped compared to SOBI and MCC methods when the number of sensors used to acquire data is reduced, which is clearly an advantage while dealing with practical economics of health monitoring and modal identification of real full-scale structures.

3. EMD-MCC is shown to identify real full-scale structures with several degrees of freedom using a relatively few sensor measurements. The need for sensor measurements at all relevant degrees of freedom in order to identify the mode shapes is alleviated, which is the main advantage of this method. The method is expected to perform well for a large class of structural and mechanical system identification problems, provided the initial mixing matrix is selected efficiently based on the dynamic behavior of the given structure.

4. A novel identification algorithm based on hybrid time and time frequency blind source separation principles, called the MCC-EMD method has been developed to identify structures equipped with TMDs. The method is then extended to re-tune TMDs using ambient vibration measurements. It is shown that the identification method is robust to relative high levels of noise, of the order of 20%, and can be extended to the case of partial measurements as well. Furthermore, it is shown that the new method is effective to re-tune TMDs for a range of conditions, and is capable of handling practical situations as evidenced from the experimental results involving ambient measurements.

7.2 Recommendations for future study

In course of the dissertation work, many facets of blind identification using the principles of BSS have been unraveled. Some of the possible extensions of the current work can be summarized as under:

1. Extension of the current algorithms to handle systems whose dynamic properties (eg., stiffness) change with time, or track abrupt changes in stiffness that may occur when a structure sustains damage. Presently all the algorithms operate in a batch

mode. These algorithms could potentially be equipped to operate in an adaptive framework.

2. The present hybrid methods could also be made more robust to investigate the problem of blind identification of structures under wide variety of non-stationary excitations.

3. The problem of under-determined BSS could be generalized for a wide class of structures by relaxing the requirement of initial mode shape.

4. Presently none of the BSS methods are equipped to identify structures with complex modes, a case commonly encountered in structures with non-proportional damping. The current methods could be extended to identify complex modes.

5. The hybrid algorithms could be replaced by a set of algorithms utilizing the principles of sub-band decomposition, operating completely under the framework of BSS. Such algorithms have the potential to address the issue of under-determined source separation as well as to tackle identification under extremely narrow-band excitations.

6. Extension of the MCC-EMD method, to identify structures equipped with TMDs, in an adaptive manner. Re-tuning of TMDs could also be accomplished in an adaptive manner, implemented real-time.

APPENDICES

Appendix A

State Space Models

State space models are a way of representing the second order dynamic system models, in the form of first order differential equations. Consider the equation of motion of a n degree of freedom linear, time invariant system, in the second order form :

$$\mathbf{M}\ddot{\mathbf{x}}(t) + \widetilde{\mathbf{C}}\dot{\mathbf{x}}(t) + \mathbf{K}\mathbf{x}(t) = \mathbf{u}(t) \tag{A.1}$$

where $\mathbf{M}$, $\widetilde{\mathbf{C}}$ and $\mathbf{K}$ are $n \times n$ matrices defining the mass, damping, and stiffness of the structure, $\mathbf{x}(t)$ and $\mathbf{u}(t)$ are $n \times 1$ vectors describing the displacement and excitation, respectively. Denoting the displacements and the velocities at various degrees of freedom by $x_1(t),\ x_2(t),\ .....,x_n(t)$ and $\dot{x}_1(t),\ \dot{x}_2(t),\ .....,\dot{x}_n(t)$ respectively, the state vector $\mathbf{x}(t)$ is defined as:

$$\mathbf{x}(t) = [x_1(t),\ x_2(t),\ .....,x_n(t),\ \dot{x}_1(t),\ \dot{x}_2(t),\ .....,\dot{x}_n(t)]^T \tag{A.2}$$

The second order equation can now be replaced by the state-space form according to :

$$\begin{aligned} \dot{\mathbf{x}}(t) &= \mathbf{A}\mathbf{x}(t) + \mathbf{B}\,\mathbf{u}(t) \\ \mathbf{y}(t) &= \mathbf{C}\mathbf{x}(t) \end{aligned} \tag{A.3}$$

Here, the vector $\mathbf{y}$ represents the output vector, which is governed by the $\mathbf{C}$ matrix. The system matrix, $\mathbf{A}$, and the excitation matrix $\mathbf{B}$ are given by :

$$\begin{aligned} \mathbf{A} &= \begin{bmatrix} [\mathbf{0}]_{n\times n} & [\mathbf{I}]_{n\times n} \\ -\mathbf{M^{-1}K} & -\mathbf{M^{-1}}\widetilde{\mathbf{C}} \end{bmatrix} \\ \mathbf{B} &= \left[[0,0,0,.....,0]_{1\times n}\,,\ \left[-\frac{1}{m}, -\frac{1}{m}, -\frac{1}{m}, ..., -\frac{1}{m} \right]_{1\times n} \right]^T \end{aligned} \tag{A.4}$$

where m is the mass lumped at each floor level (i. e. $\mathbf{M} = diag(m)$). For sampled data systems with discrete sampling intervals $0,\ \Delta t,\ 2\Delta t, ..., (k+1)\,\Delta t, ..., n\Delta t$, Eq. A.3 can be expressed as:

$$\begin{aligned} \mathbf{x}(k+1) &= \bar{\mathbf{A}}\mathbf{x}(k) + \bar{\mathbf{B}}\,\mathbf{u}(k) \\ \mathbf{y}(k) &= \mathbf{C}\mathbf{x}(k) \end{aligned} \tag{A.5}$$

Eq. A.5 is called discrete state space form. The matrices $\bar{\mathbf{A}}$ and $\bar{\mathbf{B}}$ are related to the continuous time state matrices $\mathbf{A}$ and $\mathbf{B}$ according to :

$$\bar{\mathbf{A}} = e^{\mathbf{A}\,(k\Delta t)}, \qquad \bar{\mathbf{B}} = \int_0^{\Delta t} e^{\mathbf{A}\,\tau}\,\mathbf{B}\,d\tau \tag{A.6}$$

Appendix B

Markov Parameters

The response of a linear system in discrete time (Eq. A.5), to unit pulse input is often referred to as markov parameters. The unit pulse input to the system given by Eq. A.5 can be represented as :

$$\begin{aligned} &u(k) = 1 \\ &u(k-1) = u(k-2) = u(k-3) =, \ldots\ldots\ldots\ldots = u(k-p) = 0 \\ &u(k+1) = u(k+2) = u(k+3) =, \ldots\ldots\ldots\ldots = u(k+s-1) = 0 \end{aligned} \tag{B.1}$$

Solving for the output $\mathbf{y}(k)$, by substituting the Eq. B.1 into the Eq. A.5 with zero initial condition yields:

$$\begin{aligned} &\mathbf{x}(k) = 0 && \Rightarrow && \mathbf{y}(k) = 0 \\ &\mathbf{x}(k+1) = \bar{\mathbf{B}} && \Rightarrow && \mathbf{y}(k+1) = \mathbf{C}\bar{\mathbf{B}} \\ &\mathbf{x}(k+2) = \bar{\mathbf{A}}\bar{\mathbf{B}} && \Rightarrow && \mathbf{y}(k+2) = \mathbf{C}\bar{\mathbf{A}}\bar{\mathbf{B}} \\ &: && && : \\ &: && && : \\ &\mathbf{x}(k+s-1) = \bar{\mathbf{A}}^{s-2}\bar{\mathbf{B}} && \Rightarrow && \mathbf{y}(k+s-1) = \mathbf{C}\bar{\mathbf{A}}^{s-2}\bar{\mathbf{B}} \end{aligned} \tag{B.2}$$

The constant matrices:

$$\mathbf{C}\bar{\mathbf{B}},\ \mathbf{C}\bar{\mathbf{A}}\bar{\mathbf{B}},\ .....,\mathbf{C}\bar{\mathbf{A}}^{s-2}\bar{\mathbf{B}} \tag{B.3}$$

are called system markov parameters or, in short, markov parameters. The markov parameters are commonly used as the basis for identifying mathematical models for linear dynamical systems.

Appendix C

SOBI in the presence of additive measurement noise

Consider the static mixture of sources mixed with noise below:

$$\mathbf{x}(k) = \mathbf{A}\mathbf{s}(k) + \boldsymbol{\nu}(k) \tag{C.1}$$

Under the assumption that the sources, $\mathbf{s}$ are uncorrelated with unit variance, and the noise is uncorrelated white with a variance σ^2, the main steps in SOBI are as follows. The covariance matrices for zero and non-zero time-lags are given by:

$$\hat{\mathbf{R}}_x(0) = \mathbf{A}\mathbf{R}_{\mathbf{s}}(0)\mathbf{A}^T + \sigma^2\mathbf{I} \tag{C.2}$$

$$\hat{\mathbf{R}}_{\mathbf{x}}(p) = \mathbf{A}\mathbf{R}_s(p)\mathbf{A}^T \tag{C.3}$$

The standard whitening is realized by a linear transformation expressed as under:

$$\bar{\mathbf{x}}(k) = \mathbf{Q}\mathbf{x}(k) = \boldsymbol{\Lambda}_{\mathbf{x}}^{-\frac{1}{2}}\mathbf{V}_{\mathbf{x}}^T\mathbf{x}(k) \tag{C.4}$$

The whitened correlation matrix is given by

$$\mathbf{R}_{\bar{\mathbf{x}}}(p) = \mathbf{QAR}_s(p)\mathbf{A}^T\mathbf{Q}^T \tag{C.5}$$

If the diagonal matrix $\mathbf{\Lambda}_{\bar{\mathbf{x}}}$ has distinct eigen-values, then the mixing matrix can be estimated uniquely by the following equation:

$$\hat{\mathbf{A}} = \mathbf{Q}^{-1}\mathbf{V}_{\bar{\mathbf{x}}} = \mathbf{V}_{\mathbf{x}}\mathbf{\Lambda}_{\mathbf{x}}^{1/2}\mathbf{V}_{\bar{\mathbf{x}}} \tag{C.6}$$

Appendix D

ARMA model for wind Excitation

The longitudinal and lateral components of the turbulent wind is modeled using an ARMA model representing a Gaussian stochastic process [77, 17] at each spatial location, $V(t)$, where $V(t)$ has zero mean, unit variance and is stationary over time. Assuming the order of the moving average and the autoregressive parts as (q), the vector ARMA process is then given by

$$V(t) = \sum_{i=1}^{q} A_i V\left(t - i\Delta t\right) + \sum_{i=0}^{q} B_i \Psi\left(t - i\Delta t\right) \tag{D.1}$$

where $\Psi(t)$ is the vector of white noise at time t. The first step is to choose a model for the cross correlation matrix $\mathbf{C}_V(t)$ between $V(s)$ and $V(s+t)$. The resulting correlation matrix is then used to determine the coefficient matrices in Eq. D.1 [77, 17]. The components of the cross-correlation matrix $\mathbf{C}_V(t)$ is given by $P_{ij}(t)$which is the cross-correlation between the i^{th} and j^{th} locations at times s and $s+t$, respectively. If (y_i, z_i) denotes the i^{th} spatial location, then $P_{ij}(t)$ is assumed to be:

$$P_{ij}(t) = \int_0^{\infty} \sqrt{S_i(n) S_j(n)} coh(y_i, z_i, y_j, z_j, n) \cos(2\pi n t) dn \tag{D.2}$$

where $S_i(n)$ is the power spectral density function at location i and $coh(y_i, z_i, y_j, z_j, n)$ is

the coherence at frequency n. The Kaimal spectrum [50] is used as the basis for generating the turbulent fluctuations and is given by the following equation:

$$\frac{nS_i(n)}{u_*^2} = \frac{105f}{(1+33f)^{5/3}} \tag{D.3}$$

where u_* is the friction velocity, and $f(n,z) = \frac{nz_i}{U(z_i)}$ is the reduced frequency. Spatial coherence is modeled using Davenport's approximation:

$$coh(y_i, z_i, y_j, z_j, n) = \exp\left[-\frac{n\left[c_z^2\left(z_i - z_j\right)^2 + c_y^2\left(y_i - y_j\right)\right]^{1/2}}{\frac{1}{2}\left[U\left(z_i\right) + U\left(z_j\right)\right]}\right] \tag{D.4}$$

where the constants c_y and c_z describe the relative effect of separation in the y (lateral) and z (height) directions respectively and U being the mean wind velocity. The cross-correlation matrices for each time are then combined to form a complete correlation matrix $\mathbf{C}$ for the process $V(t)$. In the next step the matrix $\mathbf{C}$ is used to calculate the coefficient matrices of the ARMA process ($\mathbf{A}_i$ and $\mathbf{B}_i$).

For the lateral component of turbulence, the following (kaimal) spectrum is used:

$$\frac{nSi(n)}{u_*^2} = \frac{17f}{(1+9.5f)^{5/3}} \tag{D.5}$$

The component due to vortex shedding is developed in a similar manner with the underlying spectrum given by [85] :

$$S(n) = \frac{C_s^2}{2B\pi^{3/2}f_s}\exp\left[-\left(\frac{1-n/2\pi f_s}{B}\right)^2\right] \tag{D.6}$$

where f_s =shedding frequency; B =spectral bandwidth and C_s = is the fluctuating wake coefficient.

Appendix E

Joint Diagonalization

In order to derive the expression of the jacobi angle for joint diagonalization, it is instructive to consider the ordinary diagonalization of a simple 2×2 real symmetric matrix.

Consider a 2×2 real symmetric matrix of the form,

$$\mathbf{M} = \begin{bmatrix} a_k & b_k \\ b_k & d_k \end{bmatrix} \tag{E.1}$$

The transformation matrix parameterized by θ is of the form:

$$\mathbf{V} = \begin{bmatrix} \cos\theta & -\sin\theta \\ \sin\theta & \cos\theta \end{bmatrix} \tag{E.2}$$

The diagonalizing transformation is given by the quadratic:

$$\mathbf{\Lambda} = \mathbf{\Phi^T M \Phi} \tag{E.3}$$

where, the angle,

$$\tan 2\theta = \frac{2b_k}{a_k - d_k} \tag{E.4}$$

and Λ, $\mathbf{\Phi}$ are the diagonal matrix of eigenvalues and orthonormal eigenvectors respectively [33, 68].

Consider, the case of multiple matrices which are stacked one after another as for example:

$$\mathbf{R} = \left[\left[\begin{array}{cc} a_k & b_k \\ b_k & d_k \end{array} \right] \left[\begin{array}{cc} e_k & f_k \\ f_k & g_k \end{array} \right] \left[\begin{array}{cc} m_k & n_k \\ n_k & p_k \end{array} \right] ..... \left[\begin{array}{cc} x_k & y_k \\ y_k & z_k \end{array} \right] \right] \tag{E.5}$$

Such matrices can be jointly diagonalized by first forming a 2×2 matrix G and then calculating the rotation angle θ which depends on the *on* and *off* diagonal terms of the matrix G . The matrix G is given by [81]:

$$\mathbf{G} = \left[\begin{array}{ccccc} a_k - d_k & e_k - g_k & m_k - p_k & ... & ... \\ 2b_k & 2f_k & 2n_k & ... & ... \end{array} \right] \left[\begin{array}{ccccc} a_k - d_k & e_k - g_k & m_k - p_k & ... & ... \\ 2b_k & 2f_k & 2n_k & ... & ... \end{array} \right]^T \tag{E.6}$$

The diagonalizing transformation is given by the quadratic form according to Eq. E.3. The angle $\tan 2\theta$ is given by:

$$\tan 2\theta = \frac{t_{off}}{t_{on} + (t_{on}^2 + t_{off}^2)^{1/2}} \tag{E.7}$$

where $t_{on} = \mathbf{G}(1,1) - \mathbf{G}(2,2)$ and $t_{off} = \mathbf{G}(1,2) + \mathbf{G}(2,1)$

Appendix F

Time Invariance of SWT

To observe this important property of the SWT, if we consider the shifted version of the signal $x(t-\tau)$ and substitute it in Eq. 4.5 the following expressions are obtained :

$$\begin{aligned} d_k^j\{x(t-\tau)\} &= 2^{-j/2} \int_{-\infty}^{\infty} x(t-\tau)\, \psi(2^{-j}t - 2^{-j}k)\, dt \\ &= 2^{-j/2} \int_{-\infty}^{\infty} x(t')\, \psi(2^{-j}t' + 2^{-j}\tau - 2^{-j}k)\, dt' \ ; \text{ where } t' = t-\tau; \\ &= 2^{-j/2} \int_{-\infty}^{\infty} x(t')\, \psi\left(\frac{t' - \{k-\tau\}}{2^j}\right) dt' \\ &= 2^{-j/2} \int_{-\infty}^{\infty} x(t)\, \psi\left(\frac{t - \{k-\tau\}}{2^j}\right) dt \\ &= d_{k-\tau}^j\{x(t)\} \end{aligned} \tag{F.1}$$

This equation shows that the coefficients of a delayed signal are a time shifted version of those of the original signal.

Appendix G

Hilbert Transform

Hilbert Transform (HT) plays a significant role in time-frequency analysis of non-stationary signals. The HT ($\tilde{y}(t)$) of a real-valued function, $y(t)$ in the range $-\infty < t < \infty$, is defined as :

$$\tilde{y}(t) = H[y(t)] = \int_{-\infty}^{\infty} \frac{y(u)}{\pi(t-u)} du \tag{G.1}$$

Where H denotes the HT operator. HT can be used to identify the natural frequency and damping of freely vibrating single-degree-of-freedom (SDOF) systems [27] by first applying the transform to the decaying response to form an analytic signal $z(t)$, and then determining the amplitude envelop and the time dependent phase according to,

$$z(t) = y(t) + i\tilde{y}(t) = A(t)e^{i\theta(t)}$$

$$A(t) = |z(t)| = \sqrt{y^2(t) + \tilde{y}^2(t)}$$

$$\theta(t) = \arg(z(t)) = \tan^{-1}[\frac{\tilde{y}(t)}{y(t)}] \tag{G.2}$$

(G.3)

where, $A(t)$ and $\theta(t)$ are defined as the amplitude envelop and instantaneous phase angle of $y(t)$ respectively. The natural frequency ω can be determined by the simple relation:

$$\omega(t) = \frac{d\theta(t)}{dt} \tag{G.4}$$

The damping can be determined by observing the slope of $\ln A(t)$ versus time.

For example, let us consider a single degree of freedom system according to,

$$x(t) = Ae^{-\zeta\omega t} \sin(\omega_d t + \phi) \tag{G.5}$$

where $\omega_d = \omega\sqrt{1-\zeta^2}$ is the damped natural frequency. The analytic signal can be approximated as :

$$z(t) = A(t)e^{j\phi(t)} \approx \left(Ae^{-\zeta\omega t}\right) e^{-j\left(\omega_d t + \phi - \pi/2\right)} \tag{G.6}$$

Since $\ln A(t) \approx \ln A - \zeta\omega t$, the damping ratio ζ can be estimated from the slope of the plot of $\ln A(t)$ versus time, once ω is estimated according to Eq. G.4.

Bibliography

[1] M. Abe and Y. Fujino. Dynamic characterization of multiple tuned mass dampers and some design formulas. *Earthquake Engineering and Structural Dynamics*, 23:813–835, 1994. 118, 119, 120

[2] M. Abe and T. Igusa. Tuned mass dampers for structures with closely spaced natural frequencies. *Earthquake Engineering and Structural Dynamics*, 24(2):247–261, 1994.

[3] R.J. Allemang and D.L. Brown. A unified matrix polynomial approach to modal identification. *Journal of Sound and Vibration*, 211(3):301–322, 1998. 9

[4] S. Amari, T.P. Chen, and A. Cichocki. Non-holonomic constraints in learning algorithm for blind source separation. *Neural Computation*, 12:1463–1484, 2000. 39

[5] S. Amari and A. Cichocki. Adaptive blind signal processing-neural network approaches. *Proceedings of the IEEE*, 86, 1998.

[6] J. Antoni. Blind separation of vibration components: Principles and demonstrations. *Mechanical Systems and Signal Processing*, 19:1166–1180, 2005. 95

[7] I. Y. Bar-Itzhack. Matrix symmetrization. *Journal of Guidance, Control, and Dynamics*, 21(1):178–179, 1998. 52

[8] B. Basu, S. Nagarajaiah, and A. Chakraborty. Online identification of linear time-varying stiffness of structural systems by wavelet analysis. *Structural Health Monitoring*, 7(1):21–36, 2008. 70

[9] A. Belouchrani, K. Abed-Meraim, J.F. Cardoso, and E. Moulines. Second -order blind separation of temporally correlated sources. *in Proc. Int. Conf. on Digital Sig. Proc.*, 1993.

[10] A. Belouchrani, K. Abed-Meraim, J.F. Cardoso, and E. Moulines. A blind source separation technique using second-order statistics. *IEEE Transactions on signal processing*, 45(2):434–444, 1997. 3, 39, 52

[11] J. S. Bendat and A. G. Piersol. *Random data: Analysis and measurement procedures*. Wiley, New York, 2000. 14, 24

[12] Rune. Brincker, Carlos. E. Ventura, and Palle. Anderson. Damping estimation by frequency domain decomposition. In *Proceedings of SPIE, the International Society for Optical Engineering*, volume 4359, pages 698–703, 2001. 10

[13] Rune. Brincker, Lingmi. Zhang, and Palle. Anderson. Modal identification from ambient responses using frequency domain decomposition. In *Proceedings of the International Modal Analysis Conference(IMAC)*, San Antonio, Texas, USA, 2000. 10, 25

[14] J.M.W. Brownjohn. Ambient vibration studies for system identification of tall buildings. *Earthquake Engineering and Structural Dynamics*, 32(1):71, 2003.

[15] J. M. Caicedo, S. J. Dyke, and E. A. Johnson. Natural excitation technique and eigensystem realization algorithm for phase i of the iasc-asce benchmark problem: Simulated data. *J. Engrg. Mech.*, 130(1):49–60, Jan 2004.

[16] J. F. Cardoso and B. H. Laheld. Equivariant adaptive source separation. *IEEE Trans. Signal Processing*, 44, December 1996. 38, 39

[17] M. T. Chay, F. Albermani, and R. Wilson. Numerical and analytical simulation of downburst wind loads. *Engineering Structures*, 28:240–254, 2006. 64, 159

[18] Genda. Chen and Jingning. Wu. Experimental study on multiple tuned mass dampers to reduce seismic responses of a three-storey building structure. *Earthquake Engineering and Structural Dynamics*, 32(5):793–810, 2003. 120

[19] A. Cichocki and S. Amari. *Adaptive Blind Signal and Image Processing*. John Wiley and Sons, Ltd, 2003. 30, 38, 39

[20] A. Cichocki and R. Unbehauen. Robust neural networks with on-line learning for blind identification and blind separation of sources. *IEEE Trans. Circuits and Systems I: Fundamentals Theory and Applications*, 43, Nov 1996. 38, 39

[21] A. Cichocki, R. Unbehauen, and E. Rummert. Robust learning algorithm for blind separation of signals. *Electronics Letters*, 30, August 1994. 38, 39

[22] P. Comon. Independent component analysis: a new concept? *Signal Processing*, 36:287–314, 1994. 30, 34, 35

[23] T. Correa-Kijewski and D.J. Pirnia. Dynamic behaviour of tall buildings under wind: Insights from full-scale monitoring. *Struc. Design Tall Spec. Build.*, 16:471–486, 2007.

[24] S. Cruces, L. Castedo, and A. Cichocki. Novel blind source separation algorithms using cumulants. *In proceedings of ICASSP'2000*, pages 3152–3155, June 2000. 38, 39

[25] S. Cruces, A. Cichocki, and L. Castedo. An iterative inversion approach to blind source separation. *IEEE Trans. On Neural Networks*, 11, 2000. 38

[26] J.P. DenHartog. *Mechanical Vibration*. McGraw-Hill, New York, 1956. 119

[27] M Feldman. Non-linear system vibartion analysis using hilbert transform-i. free vibration analysis method 'freevib'. *Mechanical Systems and Signal Processing*, 8(2):119–127, 1994. 164

[28] J.E. Fowler. The redundant discrete wavelet transform and additive noise. *Signal Processing Letters*, 12(9):629 – 632, September 2005. 73

[29] Y. Fujino, M. Abe, H. Shibuya, M. Yanagihara, M. Sato, S. Nakamura, and Y. Sakamoto. Forced and ambient vibration tests and vibration monitoring of hakucho suspension bridge. *Journal of the Transportation Research Board*, 1696:57–63, 2000.

[30] S Gamble. Private communication. 2009. 120

[31] R.R. Gerges and B.J. Vickery. Optimum design of pendulum-type tuned mass dampers. *The Structural Design Of Tall And Special Buildings*, 14(4):353–368, 2005. 119, 126

[32] R. Ghanem and F. Romeo. A wavelet based approach for the identification of linear time-varying dynamical systems. *Journal of Sound and Vibration*, 234(4):555–576, 2000. 70

[33] G. H Golub and C.F.V. Loan. *Matrix Computations*. Johns Hopkins Univ. Press, 1989. 80, 162

[34] M. Gul and F. N. Catbas. Ambient vibration data analysis for structural identification and global condition assessment. *J. Engrg. Mech.*, 134(8):650–662, 2008.

[35] B. Hazra and S. Narasimhan. Wavelet-based blind identification of the UCLA Factor building using ambient and earthquake responses. *Smart Materials and Structures*, 19(2):doi:10.1088/0964–1726/19/2/025005, 2010. 149

[36] B. Hazra, A. J. Roffel, S. Narasimhan, and M. D. Pandey. Blind identification of civil-structures. In *SEI-Structures Congress*, Austin, Texas, USA, 2009.

[37] B. Hazra, A. J. Roffel, S. Narasimhan, and M. D. Pandey. Modified cross-correlation method for the blind identification of structures. *Journal of Engineering Mechanics*, in press, 2010. 149

[38] B. Hazra, A. Sadhu, R. Lourenco, and S. Narasimhan. Re-tuning tuned mass dampers using ambient vibration measurements. *Smart Materials and Structures*, in review, 2010. 149

[39] B. Hazra, A. Sadhu, A. J. Roffel, P. E. Paquet, and S. Narasimhan. Under-determined blind identification of structures using the modified cross-correlation method. *Journal of Engineering Mechanics*, in review. 149

[40] X. He, B. Moaveni, J. P. Conte, A. Elgamal, and S. F. Masri. Modal identification study of vincent thomas bridge using simulated wind-induced ambient vibration data. *Computer-Aided Civil and Infrastructure Engineering*, 23(5):373–388, 2008.

[41] A. Hera and Z. Hou. Application of wavelet approach for asce structural health monitoring benchmark studies. *J. Engrg. Mech*, 130(1):96–104, 2004. 70

[42] Nam. Hoang and Pennung. Warnitchai. Design of multiple tuned mass dampers by using a numerical optimizer. *Earthquake Engineering and Structural Dynamics*, 34(2):125–144, 2004. 120

[43] N.E. Huang *et. al.* The empirical mode decomposition for the hilbert spectrum for nonlinear and non-stationary time series analysis. *Proceedings of Royal Society of London Series*, pages 903–95, 1998. 27, 28, 96, 97, 122

[44] A. Hyvarinen, J. Karhunen, and E. Oja. *Independent Component Analysis*. John Wiley, New York, 2001. 3, 30, 38

[45] S.R. Ibrahim and E.C. Mikulcik. A time domain modal vibration test technique. *Shock and Vibration Bulletin*, 43(4):21–37, 1973. 2, 9, 21

[46] G.H. James, T.G. Carne, and J.P. Lauffer. The natural excitation technique (net) for modal parameter extraction from operating structures. *Modal Analysis*, 10:260–277, 1995. 2, 9, 13, 29, 41, 45, 46, 75

[47] J.N. Juang and R.S. Pappa. An eigen system realization algorithm for modal parameter identification and model reduction. *Journal of Guidance, Control and Dynamics*, 8(5):620–627, 1985. 2, 9, 10, 75

[48] J.N. Juang and Minh.Q. Phan. *Identification and Control of Mechanical Systems*. Cambridge University Press, Cambridge, UK, 2006. 10, 12

[49] C. Jutten and J. Herault. Blind separation of sources: 1. an adaptive algorithm based on neuromimetic architecture. *Signal Processing*, 24:1–10, 1991. 30, 34

[50] J.C. Kaimal, J.C. Wyngaard, Y. Izumi, and O.R. Cote. Spectral characteristics of surface-layer turbulance. *Quaterly Journal of the Royal Meteorological Society*, 98:563–589, 1972. 160

[51] A. Kareem and T. Kijewski. Mitigation of motions of tall buildings with specific examples of recent applicaitons. *Wind and Structures*, 2(3):201–251, 1999. 118, 119

[52] Ahsan Kareem and Samuel Kline. Performance of multiple mass dampers under random loading. *Journal of Structural Engineering*, 121(2):348–361, February 1995 1995. 120

[53] Lari Kela and Pekka Vahaoja. Recent studies of adaptive tuned vibration absorbers/neutralizers. *Applied Mechanics Reviews*, 62(6):060801, November 2009 2009. 118, 119

[54] G. Kerschen, F. Poncelet, and J.C. Golinval. Physical interpretation of independent component analysis in structural dynamics. *Mechanical Systems and Signal Processing*, 21:1561–1575, 2007. 33, 34, 41, 44, 46, 57, 95

[55] T. Kijewski and A. Kareem. Wavelet transforms for system identification in civil engineering. *Computer-Aided Civil and Infrastructure Engineering*, 18(5):339–355, 2003. 70

[56] P. Kisilev, M. Zibulevsky, and Y.Z. Yehoshua. Multiscale framework for blind separation of linearly mixed signals. *Journal of Machine Learning Research*, 1(1):1–25, 2003. 42, 76, 95

[57] M.D. Kohler, M.P Davis, and E. Safak. Earthquake and ambient vibration monitoring of the steel-frame ucla factor building. *Earthquake Spectra*, 21(3):1–22, 2005. 82, 85

[58] K. C. S. Kwok and B. Samali. Performance of tuned mass dampers under wind loads. *Engineering Structures*, 17(9):655–667, 1995. 118, 119

[59] J. Lardies and S. Gouttebroze. Identification of modal parameters using the wavelet transform. *International Journal of Mechanical Science*, 44:2263–2283, 2002. 70

[60] C. L. Lee, Y. T. Chen, L. L. Chung, and Y. P. Wang. Optimal design theories and applications of tuned mass dampers. *Engineering Structures*, 28:43–53, 2006. 126

[61] C. C. Lin, C. M. Hu, J. F. Wang, and R. Y. Hu. Vibration control effectiveness of passive tuned mass dampers. *Journal of the Chinese Institute of Engineers*, 17:367–376, 1994. 126

[62] C. C. Lin, J. F. Wang, and J.M. Ueng. Vibration control identification of seismically excited m.d.o.f. structure-ptmd systems. *Journal of Sound and Vibration*, 240(1):87–115, 2001. 126, 130, 131

[63] S. Lin, J. N. Yang, and N. Huang. Damage identification of a benchmark building for structural health monitoring. *Smart materials and structures*, 14(3):162–169, 2005.

[64] H. Lus, R Betti, and R.W. Longman. Identification of linear structural systems using earthquake-induced vibration data. *Earthquake Engrg. and Struct. Dyn.*, 28(11):1449–67, 1999.

[65] N. M. M. Maia *et. al. Theoretical and Experimental Modal Analysis*. Research Studies Press, Taunton, Somerset, UK, 1997. 9, 10, 56, 132

[66] S. G. Mallat. *A Wavelet Tour of Signal Processing*. Academic Press, San Diego, 1998. 71, 72, 73

[67] S. I. McNeill and D.C. Zimmerman. A framework for blind modal identification using joint approximate diagonalization. *Mechanical Systems and Signal Processing*, 22:1526–1548, 2008.

[68] L. Meirovitch. *Principles and Techniques of Vibrations*. Prentice Hall, New Jersey, 1997. 98, 162

[69] S. Nagarajaiah and N. Varadarajan. Semi-active control of wind excited building with variable stiffness tmd using short-time fourier transform. *Journal of Engineering Structures*, 27:431–441, 2005. 120

[70] G.P. Nason and B.W. Silverman. The stationary wavelet transform and some statistical applications. *Lecture Notes in Statistics*, Feb 1995. 73

[71] R. D. Nayeri, S. F. Masri, R.G. Ghanem, and R. L. Nigbor. A novel approach for the structural identification and monitoring of a full-scale 17-story building based on ambient vibration measurements. *Smart Materials and Structures*, 17(2):1–19, April 2008. 82, 83, 85, 87

[72] R.D Nayeri, S.F Masri, and A.G. Chassiakos. Application of structural health monitoring techniques to track structural changes in a retrofitted building based on ambient vibration. *Journal of Engineering Mechanics*, 133(12):1311–25, 2007. 105

[73] J. O'Callahan, P. Avitabile, and R. Riemer. System equivalent reduction expansion process (serep). In *7th International Modal Analysis Conference*, pages 29–37, Las Vegas, Nevada, USA, 1989. 63

[74] R. Rana and T.T. Soong. Parametric study and simplified design of tuned mass dampers. *Engineering Structures*, 20(3):193–204, 1998. 119, 125, 126

[75] M.H. Richardson and D.L. Formenti. Parameter estimation from frequency response measurements using rational fraction polynomials. *Proceedings of 1st IMAC Conference, Orlando, Florida*, 1982. 9

[76] G. Rilling, P. Flandrin, and P. Goncalves. On empirical mode decomposition and its algorithms. *IEEE-EURASIP workshop on nonlinear signal and image processing*, 2003. 28

[77] E. Samras, M. Shinozuka, and A. Tsurui. Arma representation of random processes. *Journal of Engineering Mechanics*, 111(3):449–461, 1985. 64, 159

[78] Mehdi Setareh, John K. Ritchey, Thomas M. Murray, Jeong-Hoi Koo, and Mehdi Ahmadian. Semiactive tuned mass damper for floor vibration control. *Journal of Structural Engineering*, 133(2):242–250, February 2007. 120

[79] Dan Simon. *Optimal State Estimation*. Wiley-Interscience, New Jersey, 2006. 18

[80] D. Skolnik, Y. Lei, E. Yu, and J. Wallace. Identification, model updating, and response prediction of an instruemented 15-story steel-frame building. *Earthquake Spectra*, 22(3):781–802, 2006. 26, 82, 83, 85

[81] A. Souloumiac and J.F. Cardoso. Jacobi angles for simultaneous diagonaliation. *SIAM Journal of Matrix Analysis and Applications*, 17(1):161–164, Jan 1996. 162

[82] B. F. Spencer and S. Nagarajaiah. State of the art of structural control. *J. of Struc. Eng.*, 129(7):845–856, 2003. 118, 119

[83] P. VanOverschee and B. De Moor. N4sid: numerical algorithms for state space subspace system identification. *Proceedings of the IFAC World Congress*, pages 361–364, 1993. 2, 9, 14, 56

[84] P. VanOverschee and B. De Moor. *Subspace identification for linear systems: Theory, Implementation, Applications*. Dordrecht, Netherlands, 1996. 9, 14

[85] B.J. Vickery and A.W. Clark. Lift or across-wind response to tapered stacks. *J. Struct. Div.*, 98(1):1–20, 1972. 160

[86] G. W. Warburton. Optimum absorber parameters for various combinations of response and excitation parameters. *Earthquake Engrg. and Struct. Dyn.*, 10(3):381–401, 1982. 119, 126

[87] J. N. Yang, Y. Lei, S. Lin, and N. Huang. Identification of natural frequencies and dampings of in situ tall buildings using ambient wind vibration data. *Journal of Engineering Mechanics*, 130(5):570–577, 2004. 27, 96

[88] J. N. Yang, Y. Lei, S. Pan, and N. Huang. System identification of linear structures based on hilbert huang spectral analysis. part 1: normal modes. *Earthquake Engng Struct. Dyn.*, 32(9):1443–67, 2003. 27, 28, 29, 96, 97, 98, 122

[89] J. N. Yang, S. Pan, and S. Lin. Least-squares estimation with unknown excitations for damage identification of structures. *Journal of Engineering Mechanics*, 133(1):12–21, 2007.

[90] L. Zhang, H. Kanda, L. Brown, D, and J. Allemang, R. Frequency domain poly reference method for modal analysis. *Journal of Applied Mechanics, ASME*, 106(85), 1985. 10

[91] Min Zheng, Fan Shen, Yuping Dou, and Xiaoyan Yan. Modal identification based on hilbert-huang transform of structural response with svd preprocessing. *Acta Mechanica Sinica*, 25(5):883–888, 2009.

[92] Wanliang. Zhou and David. Chelidze. Blind source separation based vibration mode identification. *Mechanical Systems and Signal Processing*, 21:3072–3087, 2007. 34, 41, 44, 95

[93] B.A. Zibulevsky and B.A. Pearlmutter. Blind source separation by sparse decomposition. *Neural Computations*, 13(4):863, 2001. 95